Chapter 15
Corrosion and Stress Corrosion Cracking Fundamentals

Corrosion can be broadly described as the destruction or deterioration of a metal or alloy by way of a chemical or electrochemical reaction with its environment. It can be considered as extractive metallurgy in reverse, or the process by which a metal is returned to its natural state—an oxide. Corrosion can occur in wet (aqueous) environments and also in dry (gaseous) environments, and can occur at a high rate or a very slow rate. It can also take many forms, as discussed in the next section.

Nearly, all metallic corrosion processes involve the transfer of electronic charge in aqueous solutions. Consider the corrosion of zinc in hydrochloric (HCl) acid. Zinc reacts with the acid to form soluble zinc chloride and liberates hydrogen bubbles at the surface. It occurs by two reactions. The first is the oxidation of Zn to Zn^{++} and the liberation of 2 electrons, and the second is the combination of the two electrons with 2 hydrogen ions to yield 2 hydrogen atoms or H_2. The reactions are as follows:

$$Zn \rightarrow Zn^{++} + 2e^{-} \tag{15.1}$$

$$2H^{+} + 2e^{-} \rightarrow H_2, \tag{15.2}$$

for a total reaction described by:

$$Zn + 2HCl \rightarrow ZnCl_2 + H_2 \tag{15.3}$$

or in ionic form:

$$Zn + 2H^{+} + 2Cl^{-} \rightarrow Zn^{++} + 2Cl^{-} + H_2. \tag{15.4}$$

The reaction in Eq. (15.1) is the anodic, or oxidation reaction in which the valence of Zn increases from 0 to +2 and liberates electrons. The reaction in Eq. (15.2) is the cathodic, or reduction reaction in which the oxidation state of H decreases from +1 to 0 by consuming electrons. Water is the carrier of ions, or the electrolyte. Note that the reactions shown in Eqs. (15.1) and (15.2) can occur simultaneously on the surface of a piece of Zn immersed in HCl. These reactions involve the transfer of charge or current. The relationship between current and mass of the reacting metal, *M*, is given by Faraday's law:

G.S. Was, *Fundamentals of Radiation Materials Science*,
DOI 10.1007/978-1-4939-3438-6_15

$$M = kIt, \tag{15.5}$$

where I is the current (amperes, A), t is the time (s), and k is the electrochemical equivalent (g/Coulomb or g/C) given by:

$$k = A/nF, \tag{15.6}$$

where A is the atomic weight, n is the number of equivalents exchanged, and F is Faraday's constant (96,500 C/eq). Recall that a Coulomb is the amount of charge transferred by a current of one ampere for 1 s. Hence, the corrosion rate of a metal is directly related to its reaction rate with the environment.

This chapter will focus on the fundamentals of aqueous corrosion by virtue of its importance in water reactor systems, and provide a foundation for understanding the interplay between corrosion and irradiation in the degradation of metals and alloys treated in Chap. 16. It begins with a description of the various forms of corrosion followed by the thermodynamics of corrosion including the use of potential–pH or Pourbaix diagrams, kinetics of corrosion, passivity, crevice corrosion, and then stress corrosion cracking. The latter two topics provide a basis for understanding the processes of irradiation accelerated corrosion (IAC) and irradiation-assisted stress corrosion cracking (IASCC).

15.1 Forms of Corrosion

While corrosion is most often envisioned as the loss of metal from a surface exposed to the electrolyte, corrosion can take many forms as summarized in Fig. 15.1. The eight forms of corrosion include uniform corrosion, crevice corrosion, pitting, intergranular attack, selective leaching or dealloying, erosion corrosion, stress corrosion cracking, and hydrogen damage.

Uniform corrosion

Uniform corrosion is characterized by a reaction that proceeds uniformly over the entire surface of the component, e.g., rusting of iron or tarnishing of silver. Various units are used to describe the uniform removal of metal, such as the thinning rate in mm/yr or the mass loss per unit area in g/m^{2}yr. Uniform corrosion is not really uniform on a microscopic level. In fact, the orientation of grain faces on the surface will determine which corrodes the fastest. As grains dissolve away, preferential sites for attack will alternate. All other forms of corrosion can be broadly classified as localized corrosion.

Crevice corrosion

Crevice corrosion is characterized by intense localized corrosion that occurs most frequently within crevices or shielded areas on metal surfaces exposed to corrosives. The attack is usually associated with small volumes of stagnant solution.

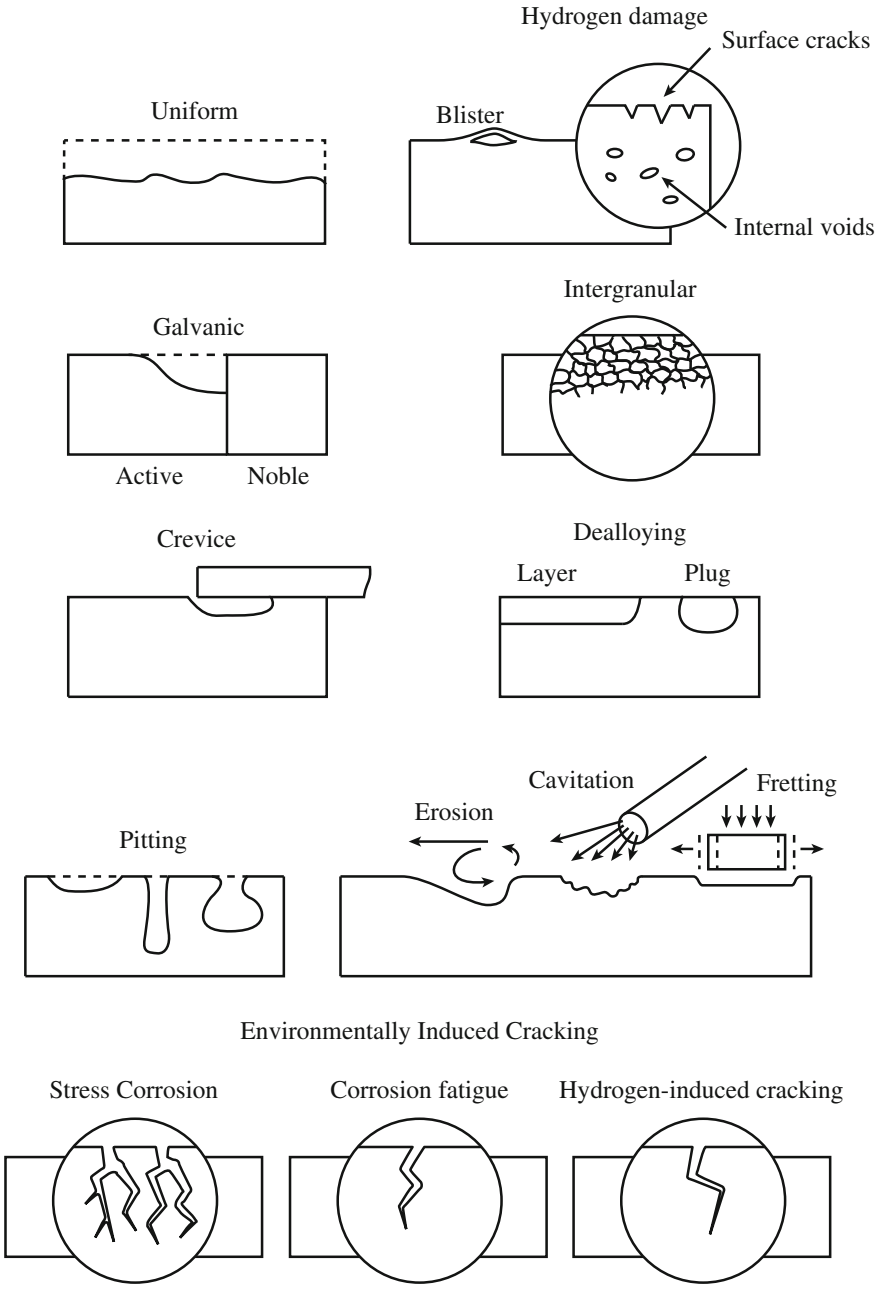

Fig. 15.1 Eight forms of corrosion (after [2])

To function as a corrosion site, a crevice must be wide enough to permit liquid entry, but sufficiently narrow to maintain a stagnant zone. For this reason, crevice corrosion usually occurs in openings of width $\leq$0.1 mm. In tight cracks, the gap may be as small as 10–100 nm.

Although crevice corrosion can result from a difference in metal ion and oxygen concentration between the crevice and the outside (oxygen cell), more processes are involved. Initially, oxidation and reduction occur uniformly over the entire metal surface, and charge is conserved. But after a short time, oxygen in the crevice is depleted because of restricted access, so the reduction reaction cannot occur in the crevice. Corrosion can continue if the reduction reaction occurs on the external surface. After awhile, the excess positive charge in the crevice due to continued metal dissolution will drive Cl^- migration into the crevice to balance the overall charge. The increased metal chloride concentration hydrolyzes the water producing an insoluble hydroxide (MOH) and a free acid. The pH in the crevice drops and metal dissolution is accelerated, thus increasing Cl^- migration into the crevice. The process is autocatalytic and rapidly accelerating.

Pitting corrosion

Pitting is a form of extremely localized corrosion that results in holes in the metal. Pits are often very small in diameter ($\sim$ 10–1000 μm) and can be either high or low density. The surface of a component undergoing pitting may show little or no attack away from the pits themselves.

Pitting is autocatalytic in nature in that the corrosion processes within a pit produce conditions that are both stimulating and necessary for continued pit activity. Say, for example, that a metal M is undergoing pitting in an aerated NaCl solution. Metal dissolution occurs within the pit, while oxygen reduction occurs outside the pit on adjacent surfaces. The excess positive charge in the pit induces Cl^- migration into the pit producing a high concentration of metal chlorides, MCl, and hydrogen ions as a result of the hydrolysis of water. Since both hydrogen ions (low pH) and Cl^- stimulate the dissolution of metal, the process accelerates with time. Since the solubility of oxygen in concentrated solutions is very small, no oxygen reduction occurs in the pit. Instead, oxygen is reduced on adjacent surfaces, and this tends to suppress corrosion on the exposed surface by a sort of cathodic protection. Further, since the pit area is much smaller than the unpitted area, to maintain charge conservation ($I_{\text{oxidation}} = I_{\text{reduction}}$), then $i_{\text{anode}} \gg i_{\text{cathode}}$, where I is current and i is current density.

The pitting process resembles quite closely that of crevice corrosion. In fact, practically all systems that show pitting attack are susceptible to crevice corrosion. However, the reverse is not always true. It is the self-initiating characteristic of pitting that makes it unique. Unfortunately, the mechanism of pit initiation is not well understood. It is believed that pits probably nucleate at weak points in the surface film that can be attacked by ions such as Cl^-, causing a defect and initiating the localized corrosion process.

Intergranular corrosion

Localized attack of grain boundary regions can result in a loss of strength and/or disintegration of the region. The grain boundary itself is only slightly more reactive than the matrix and generally will not cause problems. However, in cases where there is a change in composition or phase, then severe intergranular corrosion can occur. Some examples are the segregation or depletion of alloying elements. Fe in Al will segregate to the grain boundary and cause intergranular corrosion (IGC), as does depletion of Cr at the grain boundaries in stainless steel and nickel-base austenitic alloys.

Selective leaching or dealloying

Selective leaching or dealloying is the preferential removal of one element from a solid alloy by corrosion. The most common example is the selective removal of zinc in brass. The overall dimension of the part does not change, but it becomes considerably weaker and permeable due to its porous nature. The color also changes to a red or copper color. This mechanism is known to occur in other systems such as Cu–Ni alloys and is also referred to as "dezincification." The process occurs by either a layer-type or plug-type mechanism. In the case of brass, both Zn and Cu dissolve into solution, but while the Zn ions stay in solution, the Cu plates back onto the structure. When oxygen is present, the copper often appears as a copper oxide on the surface.

Erosion corrosion

Erosion corrosion is the acceleration or increase in the rate of deterioration or attack of a metal because of the relative movement between a corrosive fluid and the metal surface. The metal is removed as the dissolved ions or solid corrosion products are swept away. Mechanical wear and abrasion are often involved in the process.

Corrosion is characterized by a grooved, scalloped, or scooped out appearance of the surface. Metals that depend on a surface film (passive layer) for protection are damaged when the protective layer is worn away. Soft metals such as copper or lead are readily damaged or worn mechanically. If the flow rate over the metal surface is high enough, cavitation can occur. Cavitation is damage to the metal caused by collapse of bubbles on the metal surface (tube wall). The pounding causes cavity formation. Examples of cavitation damage include ship propellers and pump impellers.

Stress corrosion cracking

Stress corrosion cracking (including stress-assisted corrosion and corrosion fatigue) is the premature failure of an alloy or metal in the presence of a tensile stress and an aggressive environment. Examples include stainless steels in Cl^- and OH^-, aluminum alloys in halides (Cl^-, Br^-, etc.), carbon steel in OH^- and NO_3^-, α-brass in NH_4^+, and stainless steels and nickel-base alloys in high-temperature water. In stress corrosion cracking, the metal or alloy is virtually unattacked over most of its

surface, while fine cracks pass through it. Cracks can be either transgranular or intergranular. In the past, it was believed that only alloys were susceptible to SCC, but recent evidence shows that pure metals can also fail by this process.

Hydrogen (embrittlement) damage

Hydrogen damage can take many forms. One is blistering in which penetration of hydrogen results in the formation of high-pressure bubbles which then deform the surface and can lead to exfoliation if the metal between the bubble and the surface is thin enough. Hydrogen attack involves the reaction of hydrogen with a component of the alloy. For example, the reaction of hydrogen with carbon in steel to form methane can cause damage to the metal. Hydrogen also causes embrittlement by either directly affecting the strength of atom bonds in the matrix or grain boundary, or by enhancing localized plasticity, resulting in failure that resembles brittle fracture.

Understanding the various forms of corrosion requires an understanding of the driving force for corrosion described by thermodynamics, as well as the kinetics of corrosion. Combined, they provide the foundation for understanding the various ways in which metals and alloys behave in aqueous environments and exposed to ionizing radiation.

15.2 Thermodynamics of Corrosion

15.2.1 The Driving Force for Corrosion

The tendency for corrosion to occur is determined by thermodynamics. The corrosion reaction can be written as follows:

$$(-v_A)A + (-v_B)B + (-v_C)C + \cdots = v_M M + v_N N + v_O O + \cdots, \tag{15.7}$$

where v_i are stoichiometric coefficients for substances, *A, B, C*, etc., and their sign is positive for products and negative for reactants. Equation (15.7) states that $(-v_A)$ particles (molecules, atoms, ions) of substance *A*, $(-v_B)$ particles of substance *B*, etc., react to form v_M particles of *M*, v_N particles of *N*, etc. The electrochemical potential, $\tilde{\mu}_k$, of a species *k* can be defined as the partial molar Gibbs energy of this species:

$$\tilde{\mu}_k \equiv \left(\frac{\partial G}{\partial n_k}\right)_{P,T,n_{j\neq k}}, \tag{15.8}$$

where $\tilde{\mu}_k$ denotes the change in the Gibbs energy of the system, *G*, upon addition of a differential amount of the species *k* normalized to a one mole change in *k*. The change in Gibbs energy for this reaction is as follows:

$$\Delta G = v_M \tilde{\mu}_M + v_N \tilde{\mu}_N + \cdots - [(-v_A)\tilde{\mu}_A + (-v_B)\tilde{\mu}_B + \cdots] = \sum_k v_k \tilde{\mu}_k. \quad (15.9)$$

Actually, the electrochemical potential is composed of "chemical" and "electrical" parts such that:

$$(\tilde{\mu}_k)_x = (\mu_k)_x + nFE_x \quad (15.10)$$

$(\tilde{\mu}_k)_x$ is the electrochemical potential of the kth particle type in phase x, and $(\mu_k)_x$ is the chemical potential of the kth particle type in phase x. The term nFE_x is the work to transfer n charges from infinite separation to the inside of the phase, E_x, and is the Galvani or electrochemical potential in the phase under consideration. For example, consider the reaction of pure metallic zinc in HCl:

$$(\mathrm{Zn})_\mathrm{m} + 2(\mathrm{H}^+)_\mathrm{l} \rightarrow (\mathrm{Zn}^{2+})_\mathrm{l} + (\mathrm{H}_2)_\mathrm{g}, \quad (15.11)$$

where subscripts m, l, and g denote metal, liquid, and gas, respectively. From the above, the Gibbs energy of the reaction is as follows:

$$\Delta G = (\tilde{\mu}_{\mathrm{Zn}^{2+}})_\mathrm{l} + \left(\mu_{\mathrm{H}_2}\right)_\mathrm{g} - 2(\tilde{\mu}_{\mathrm{H}^+})_\mathrm{l} - (\mu_{\mathrm{Zn}})_\mathrm{m}, \quad (15.12)$$

and using Eq. (15.10), we can write:

$$\Delta G = (\mu_{\mathrm{Zn}^{2+}})_\mathrm{l} + \left(\mu_{\mathrm{H}_2}\right)_\mathrm{g} - 2(\mu_{\mathrm{H}^+})_\mathrm{l} - (\mu_{\mathrm{Zn}})_\mathrm{m} + 2FE_\mathrm{l} - 2FE_\mathrm{l}. \quad (15.13)$$

However, since the electrical work terms always exactly cancel, the Gibbs energy of the reaction is determined solely by the chemical potentials:

$$\Delta G = \sum_k v_k (\mu_k)_x. \quad (15.14)$$

The chemical potential of each species can be written as follows:

$$\mu_k = \mu_k^0 + RT \ln a_k, \quad (15.15)$$

where μ_k^0 is the standard chemical potential and the activity is $a_k = \gamma_k C_k$, where γ_k is the activity coefficient and C_k is the concentration of species k. Substituting into Eq. (15.14) gives:

$$\Delta G = \sum v_k \mu_k^0 + RT \ln \Pi a_k^{v_k}, \quad (15.16)$$

where $\sum v_k \mu_k^0 = \Delta G^0$ is the standard Gibbs reaction energy, yielding:

$$\Delta G - \Delta G^0 = RT \ln \Pi a_k^{v_k} = RT \ln \frac{a_M^{v_M} . a_N^{v_N} \ldots}{a_A^{-v_A} \cdot a_B^{-v_B} \ldots} = RT \ln \frac{a_{\text{product}}}{a_{\text{reactant}}}. \tag{15.17}$$

If an electrochemical cell is operated under reversible conditions, the charge, nF, passed reversibly at equilibrium through a potential E corresponds to the free energy change, ΔG. That is, $|\Delta G|$ = charge passed · potential difference = work (energy) to transfer n charges from infinite separation to the inside of the phase:

$$|\Delta G| = nF.|E|, \tag{15.18}$$

where n is the number of electrons involved in the reaction and E is the cell potential. According to sign convention:

$$\Delta G = -nFE, \quad \text{and} \quad \Delta G^0 = -nFE^0. \tag{15.19}$$

Substituting into Eq. (15.17) gives:

$$E - E^0 = -\frac{RT}{nF} \ln \left[\frac{a_{\text{prod}}}{a_{\text{react}}}\right] = -\frac{2.3RT}{nF} \log \left[\frac{a_{\text{prod}}}{a_{\text{react}}}\right]. \tag{15.20}$$

This is the Nernst equation, which expresses the exact electromotive force (EMF) of a cell in terms of the activities of products and reactants of the cell. The equation applies equally well to a single electrode or the total reaction. For Zn immersed in water at 25 °C (298 K):

Anodic reaction: $Zn \rightarrow Zn^{++} + 2e^-$

$$E_{Zn} = E^0_{Zn} - \frac{0.0257}{2} \ln \left[\frac{a_{Zn^{++}}}{a_{Zn}}\right] = E^0_{Zn} - \frac{0.0257}{2} \ln a_{Zn^{++}}, \quad \text{since } a_{Zn} = 1.$$

Cathodic reaction: $2H^+ + 2e^- \rightarrow H_2$

$$E_{H_2} = E^0_{H_2} - \frac{0.0257}{2} \ln \left[\frac{p_{H_2}}{a^2_{H_2}}\right],$$

where p_{H_2} is the hydrogen gas pressure. The total reaction is as follows: $Zn + 2H^+ \rightarrow Zn^{++} + H_2$, and the EMF of the cell is as follows:

$$E_{\text{cell}} = E_{Zn} + E_{H_2} = E^0_{Zn} + E^0_{H_2} - \frac{0.0257}{2} \ln [a_{Zn^{++}}] - \frac{0.0257}{2} \ln \left[\frac{p_{H_2}}{a^2_{H^+}}\right].$$

E_0 is the standard potential or *standard single electrode potential* (SSEP). This refers to the reactants and products in the standard state. E is the single electrode potential, or *equilibrium standard electrode potential* (ESEP), and refers to the reactants and products in any state.

We now pose a fundamental question: What is the tendency for metals to corrode? The real measure of whether a metal will corrode is whether its actual single electrode potential is above or below its equilibrium single electrode potential (ESEP). For example, the reaction $M = M^{n+} + ne^-$ will proceed to the right if the measured single electrode potential (MSEP) is greater than the equilibrium single electrode potential, MSEP > ESEP. However, if MSEP < ESEP, the reaction will proceed to the left. The problem is that we cannot measure potentials or voltages of a single electrode without another electrode being present. But we may try to build separate cells to physically separate the anode from the cathode.

In the cell shown in Fig. 15.2, the Pt electrode serves only as a site for the reduction of hydrogen and is physically separated from the Zn electrode. Pt does not participate in the reaction. As before:

$$E_{\mathrm{Zn}} = E^0_{\mathrm{Zn}} - \frac{0.0257}{2} \ln a_{\mathrm{Zn}^{++}},$$

and

$$E_{\mathrm{H_2}} = E^0_{\mathrm{H_2}} - \frac{0.0257}{2} \ln \left[\frac{p_{\mathrm{H_2}}}{a^2_{\mathrm{H_2}}} \right].$$

To measure E^0_{Zn}, we must establish a reference. We arbitrarily let this reference be $E^0_{\mathrm{H_2}} \equiv 0$. This is the SSEP for the reduction of hydrogen. Fixing $p_{\mathrm{H_2}} = 1$ atm and $a_{\mathrm{H}^+} = 1$, then $E_{\mathrm{H_2}} = 0$. Therefore:

$$E_{\mathrm{cell}} = E_{\mathrm{Zn}} = E^0_{\mathrm{Zn}} - \frac{RT}{2F} \ln a_{\mathrm{Zn}^{++}}.$$

If we want to find the value of E^0_{Zn}, then setting $a_{\mathrm{Zn}^{++}} = 1$ gives $E_{\mathrm{cell}} = E^0_{\mathrm{Zn}}$. Hence, the half-cell potential for any electrode is equal to the EMF of a cell with the standard hydrogen electrode (SHE) as the other electrode.

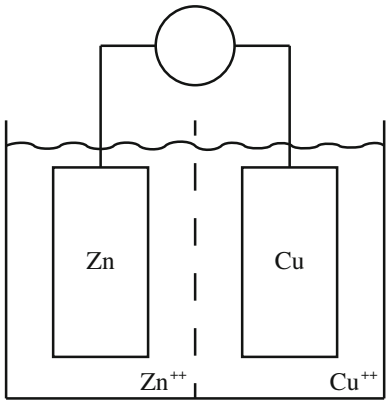

Fig. 15.2 A Zn–Cu electrochemical cell

15.2.2 EMF Series and Sign Conventions

Since the equilibrium cell voltage of a cell consisting of an electrode X and the normal hydrogen electrode is the equilibrium electrode potential, E_X of the X electrode, an orderly arrangement can be constructed of the standard potentials of all metals. This arrangement is termed the EMF series or potential series and is shown in Table 15.1. The position in the EMF series is determined by the equilibrium potential of a metal in contact with its ions at a concentration equal to unit activity. Notice that the equilibrium potential (by definition) for H_2/H^+ is 0. Metals with positive potentials are more noble than hydrogen, while those with negative values are less noble, or active with respect to hydrogen. Thus, the direction of increasingly positive values is the noble direction, whereas the direction of increasingly negative values is the active direction.

Table 15.1 Standard electromotive force potentials (reduction potentials) (after [2])

	Reaction	Standard potential, E^0 (volts vs. SHE)
Noble	$Au^{3+} + 3e^- = Au$	+1.498
↑	$Cl_2 + 2e^- = 2Cl^-$	+1.358
	$O_2 + 4H^+ + 4e^- = 2H_2O$ (pH 0)	+1.229
	$Pt^{3+} + 3e^- = Pt$	+1.2
	$O_2 + 2H_2 + 4e^- = 4OH^-$ (pH 7)[a]	+0.82
	$Ag^+ + e^- = Ag$	+0.799
	$Hg_2^{2+} + 4e^- = 2Hg$	+0.788
	$Fe^{3+} + e^- = Fe^{2+}$	+0.771
	$O_2 + 2H_2O + 4e^- = 4OH^-$ (pH 14)	+0.401
	$Cu^{2+} + 2e^- = Cu$	+0.337
	$Sn^4 + 2e^- = Sn^{2+}$	+0.15
	$2H^+ + 2e^- = H_2$	0.000
	$Pb^{2+} + 2e^- = Pb$	−0.126
	$Sn^{2+} + 2e^- = Sn$	–0.136
	$Ni^{2+} + 2e^- = Ni$	–0.250
	$Co^{2+} + 2e^- = Co$	−0.277
	$Cd^{2+} + 2e^- = Cd$	−0.403
	$Fe^{2+} + 2e^- = Fe$	–0.440
	$Cr^{3+} + 3e^- = Cr$	−0.744
	$Zn^{2+} + 2e^- = Zn$	−0.763
	$2H_2O + 2e^- = H_2 + 2OH^-$	−0.828
↓	$Al^{3+} + 3e^- = Al$	−1.662
	$Mg^{2+} + 2e^- = Mg$	–2.363
	$Na^+ + e^- = Na$	–2.714
Active	$K^+ + e^- = K$	–2.925

[a]Not a standard state

Unfortunately, a problem arises with differences in convention for the sign of the E^0 values. In one convention we have zinc-minus, copper-plus such that the values of E^0 for the Zn/Zn^{++} and the Cu/Cu^{++} electrodes are -0.76 and $+0.34$ V, respectively, for a Zn electrode in a solution of unit activity of Zn^{++} and a Cu electrode in a solution of unit activity of Cu^{++}. The other convention is zinc-plus and copper-minus. The proper convention is determined as follows:

1. Set up a cell consisting of an SHE on the left side and another electrode on the right side.
2. Measure the open-circuit potential of the cell by applying a potential difference exactly equal and opposite in sign to that produced by the cell itself. This is done by adjusting a potentiometer until the reading on the galvanometer is zero (no current flowing).
3. The potentiometer reading gives the magnitude of the potential difference across the cell as well as the sign of the charge on the electrode.

For example, the following cell
$Pt/H_2[1\ \text{atm}],\ H^+[a_{H^+} = 1]//Zn^{++}[a_{Zn^{++}} = 1]/Zn$ gives:

1. A magnitude of $E^0_{Zn/Zn^{++}}$ of 0.76 V,
2. The zinc electrode is negative.

For Pt/H_2 [1 atm], $H^+[a_{H^+} = 1]//Cu^{++}[a_{Cu^{++}} = 1]/Cu$ we have:

1. The magnitude of $E^0_{Cu/Cu^{++}}$ is 0.34 V,
2. The copper electrode is positive.

By affixing to the measured magnitude of $E^0_{Zn/Zn^{++}}$ for a Zn/Zn^{++} electrode the same sign as the observed polarity of the zinc electrode, we have: $E^0_{Zn/Zn^{++}} = -0.76$ V and $E^0_{Cu/Cu^{++}} = 0.34$ V. As a rule, if charge transfer reactions are written as reductions (electronations), e.g., $Zn^{++} + 2e^- \rightarrow Zn$, the sign of the electrode potential as derived from the free energy change comes out in agreement with that indicated by the observed polarity of the electrode: $\Delta G = -nFE$ or $E = -\Delta G/nF$.

Based on a 1953 meeting of the International Union of Pure and Applied Chemistry (IUPAC) in Stockholm, the following decisions were made that reinforce the rule given above:

1. The cell implicit in the measurement of a standard electrode potential should be arranged so that the hydrogen electrode is on the left:

$$Pt/H_2[1\ \text{atm}],\ H^+[a_{H^+} = 1]//M^{++}/M.$$

2. The measured potential difference across such a cell furnishes the magnitude of the standard electrode potential.
3. The polarity of the electrode on the right, i.e., the sign of the charge on the M electrode, serves to define the sign that is affixed to the E^0 value.
4. The charge transfer reaction implicit in the statement of a standard potential of an M/M^+ electrode is a reduction reaction $M^{n+} + ne^- \rightarrow M$.

For a cell with two electrodes, neither of which are H_2, how does one determine which is the anode (where oxidation occurs) and which is the cathode (where reduction occurs)? There are two conventions for making this determination: the American (or sign bivariant) convention and the European (or sign invariant) convention.

American (sign bivariant) convention

Write the reaction as either an oxidation reaction or a reduction reaction:

$$\text{Oxidation:} \quad \text{Zn} \rightarrow \text{Zn}^{++} + 2\text{e}^- \quad E^0 = +0.76 \text{ V}$$
$$\text{Reduction:} \quad \text{Zn}^{++} + 2\text{e}^- \rightarrow \text{Zn} \quad E^0 = -0.76 \text{ V}$$

Using the Nernst equation for these two equations:

$$E = E^0 - \frac{RT}{nF} \ln \frac{a_\text{p}}{a_\text{r}}, \tag{15.21}$$

Oxidation:

$$E_\text{Zn} = E^0_\text{Zn} - \frac{RT}{nF} \ln a_{\text{Zn}^{++}} = 0.76 - \frac{RT}{2F} \ln a_{\text{Zn}^{++}}$$

Reduction:

$$E_\text{Zn} = E^0_\text{Zn} - \frac{RT}{2F} \ln \frac{1}{a_{\text{Zn}^{++}}} = 0.76 - \frac{RT}{2F} \ln a_{\text{Zn}^{++}}$$

1. Write the reaction as either an oxidation or reduction reaction.
2. Use the corresponding oxidation or reduction potentials.
3. Identify the products and reactants from the reaction.

In the American convention, the sign on the EMF is an indication of the thermodynamic tendency for the reaction to proceed as written.

$E_\text{Zn} = +0.76$ V(oxidation) $\Rightarrow \Delta G < 0$: reaction proceeds spontaneously
$E_\text{Zn} = -0.76$ V(reduction) $\Rightarrow \Delta G > 0$: reaction won't go

Notice that $E^{\text{oxidation}}_\text{Zn} = -E^{\text{reduction}}_\text{Zn}$.

European (sign invariant) convention

Write the reaction as a reduction reaction:

$$Zn^{++} + 2e^{-} \rightarrow Zn$$

The Nernst equation is written as follows:

$$E = E^0 + \frac{RT}{nF} \ln \frac{a_A}{a_D}, \tag{15.22}$$

where A = electron acceptor or the oxidized specie (ion) and D = electron donor or the reduced specie (metal), giving:

$$E_{Zn} = E^0_{Zn} + \frac{RT}{2F} \ln a_{Zn^{++}} = -0.76 + \frac{RT}{2F} \ln a_{Zn^{++}}.$$

The sign on the EMF in the European convention arises because negatively charged electrons are liberated at the zinc electrode. This convention is implemented as follows:

1. Subtract the standard potential of the electrode on the left from that on the right.
2. The sign of the potential difference across the cell corresponds to the polarity of the electrode on the right.

For an electrochemical cell in which two different metals are coupled, the rules are then applied as follows:

American convention

- Guess at reactions (oxidation/reduction).
- Adjust the sign on E^0 according to the direction of the reaction.
- Use $E = E^0 - \frac{RT}{nF} \ln \frac{a_p}{a_r}$.
- Compare the sign on E_{cell} to determine the direction in which the reaction will go.

$$\begin{pmatrix} E_{cell} < 0 \rightarrow \Delta G > 0, \text{ no} \\ E_{cell} > 0 \rightarrow \Delta G < 0, \text{ yes} \end{pmatrix}$$

European convention

- Fix the electrode locations.
- Write both reactions as either oxidation or reduction.
- Use $E = E^0 + \frac{RT}{nF} \ln \frac{a_A}{a_D}$.
- $E_{cell} = E_{RHS} - E_{LHS}$.

- Sign applies to RHS. If $<0 \rightarrow$ anode
  If $>0 \rightarrow$ cathode

The two conventions can be used to determine the EMF of the cell shown in Fig. 15.2. Under the American convention, we guess at the reactions and write:

$$\mathrm{Zn} \rightarrow \mathrm{Zn}^{++} + 2\mathrm{e}^- \quad E_{\mathrm{Zn}} = E^0_{\mathrm{Zn}} - \frac{RT}{2F} \ln a_{\mathrm{Zn}^{++}}$$

$$\mathrm{Cu}^{++} + 2\mathrm{e}^- \rightarrow \mathrm{Cu} \quad E_{\mathrm{Cu}} = E^0_{\mathrm{Cu}} - \frac{RT}{2F} \ln \frac{1}{a_{\mathrm{Cu}^{++}}}$$

$$\text{Adding gives: } E_{\mathrm{cell}} = E_{\mathrm{Zn}} + E_{\mathrm{Cu}} = 0.76\ \mathrm{V} + 0.34\ \mathrm{V} - \frac{RT}{2F} \ln \frac{a_{\mathrm{Zn}^{++}}}{a_{\mathrm{Cu}^{++}}}.$$

For unit activities, $a_{\mathrm{Cu}^{++}} = a_{\mathrm{Zn}^{++}} = 1$, giving $E_{\mathrm{cell}} = 1.1$ V, $\Delta G < 0$, and the reaction proceeds as written. Note that if it was assumed instead that Cu was the anode and Zn the cathode, then the following would occur:

$$\text{Anode :} \quad \mathrm{Cu} \rightarrow \mathrm{Cu}^{++} + 2\mathrm{e}^- \quad E_{\mathrm{Cu}} = E^0_{\mathrm{Cu}} - \frac{RT}{2F} \ln a_{\mathrm{Cu}^{++}}$$

$$\text{Cathode :} \quad \mathrm{Zn}^{++} + 2\mathrm{e}^- \rightarrow \mathrm{Zn} \quad E_{\mathrm{Zn}} = E^0_{\mathrm{Zn}} - \frac{RT}{2F} \ln \frac{1}{a_{\mathrm{Zn}^{++}}}$$

Adding gives: $E_{\mathrm{cell}} = E_{\mathrm{Zn}} + E_{\mathrm{Cu}} = -0.34\ \mathrm{V} - 0.76\ \mathrm{V} = -1.1\ \mathrm{V}$, $E_{\mathrm{cell}} < 0$, $\Delta G > 0$, and the reaction as written would not go. Rather it will proceed in the opposite direction.

Following the European convention, both reactions are written as reduction reactions:

$$\mathrm{Zn}^{++} + 2\mathrm{e}^- \rightarrow \mathrm{Zn} \quad \text{and} \quad \mathrm{Cu}^{++} + 2\mathrm{e}^- \rightarrow \mathrm{Cu}$$

Subtract the RHS from the LHS to give:

$$\begin{aligned} \mathrm{E}_{\mathrm{cell}} = \mathrm{E}_{\mathrm{Zn}} - \mathrm{E}_{\mathrm{Cu}} = E_{\mathrm{Zn}} &= E^0_{\mathrm{Zn}} + \frac{RT}{2F} \ln a_{\mathrm{Zn}^{++}} - E^0_{\mathrm{Cu}} - \frac{RT}{2F} \ln a_{\mathrm{Cu}^{++}} \\ &= E^0_{\mathrm{Zn}} - E^0_{\mathrm{Cu}} + \frac{RT}{2F} \ln \frac{a_{\mathrm{Zn}^{++}}}{a_{\mathrm{Cu}^{++}}}. \end{aligned}$$

For unit activities, $E_{\mathrm{cell}} = -1.1$ V, which says that the zinc electrode is negative with respect to the Cu electrode, so zinc is the anode and Cu is the cathode.

Of two metals composing a cell, the anode is the more active in the EMF series provided that the ion activities in equilibrium are both unity. Since unit activity corresponds in some cases to impossible concentrations of metal ions because of restricted solubility of metal salts, it is obvious that the EMF series has only limited utility for predicting which metal is anodic to another. In practice, the actual activities of ions in equilibrium with a given metal vary greatly with the environment. So two approaches are taken. One is to use a more reasonable activity of, say,

Table 15.2 Galvanic series in seawater

Cathodic (noble)
↑
platinum
gold
graphite
titanium
silver
zirconium
AISI Type 316, 317 stainless steels (passive)
AISI Type 304 stainless steel (passive)
AISI Type 430 stainless steel (passive)
nickel (passive)
copper-nickel (70-30)
bronzes
copper
brasses
nickel (active)
naval brass
tin
lead
AISI Type 316, 317 stainless steels (active)
AISI Type 304 stainless steel (active)
cast iron
steel or iron
aluminum alloy 2024
cadmium
aluminum alloy 1100
zinc
magnesium and magnesium alloys
↓
Anodic (active)

10^{-6} mol/kg such that $a_{M^{2+}} \simeq C_{M^{2+}}$. This is the approach followed in the discussion of stability (Pourbaix) diagrams in Sect. 15.2.3. The second is to arrange the metals and alloys in accord with their actual measured potentials in a given environment, such as seawater. An example is shown in Table 15.2.

15.2.3 Stability (Pourbaix) Diagrams

The stability of a metal in an aqueous solution can be represented by an E-pH, or Pourbaix diagram [1]. These diagrams are graphical representations of the domains of stability of metals, metal ions, oxides, and other species in solution. The diagrams are based on thermodynamic computations for a number of selected chemical species and the possible equilibria between them. It is possible to predict from an E-pH diagram if a metal will corrode or not. It is *not* possible to determine how fast it will corrode.

The stability diagram is analogous to the equilibrium phase diagram in that it portrays phase equilibria between metal, metal ions, and metal oxide all at 25 °C in aqueous solutions, much as the equilibrium phase diagram portrays phase equilibrium in a binary alloy as in Fig. 15.3(a). We can write equations for phases of iron that might form in aqueous solutions and then do tests to find regions of validity or applicability. For example, consider the line labeled ① in Fig. 15.3(a):

$$e^- + Fe^{3+} = Fe^{2+} \quad E_{Fe^{3+}/Fe^{2+}} = E^0_{Fe^{3+}/Fe^{2+}} + \frac{RT}{F}\ln\left[\frac{a_{Fe^{3+}}}{a_{Fe^{2+}}}\right]$$
$$= 0.77 + 0.0257\ln\left[\frac{a_{Fe^{3+}}}{a_{Fe^{2+}}}\right].$$

Choosing a metal ion activity of 10^{-6} mol/kg, then $a_{Fe^{3+}} = a_{Fe^{2+}} = 10^{-6}$, so $E = 0.77$ V.

Consider next, line ② in Fig. 15.3(a):

$$2e^- + Fe^{2+} = Fe \quad E_{Fe^{2+}/Fe} = E^0_{Fe^{2+}/Fe} + \frac{RT}{F}\ln a_{Fe^{2+}},$$

and for an activity of 10^{-6},

$$E_{Fe^{2+}/Fe} = -0.44 + \frac{0.059}{2}(-6)$$
$$= -0.62 \text{ V}.$$

These are examples of a particular type of reaction known as pure charge transfer reactions. These electrochemical reactions involve only electrons and the reduced and oxidized species. They do not have protons (H^+) as reacting particles and so are not influenced by pH; hence, they represent horizontal lines in the stability diagram. In our example, we selected a single activity for the reaction. However, stability

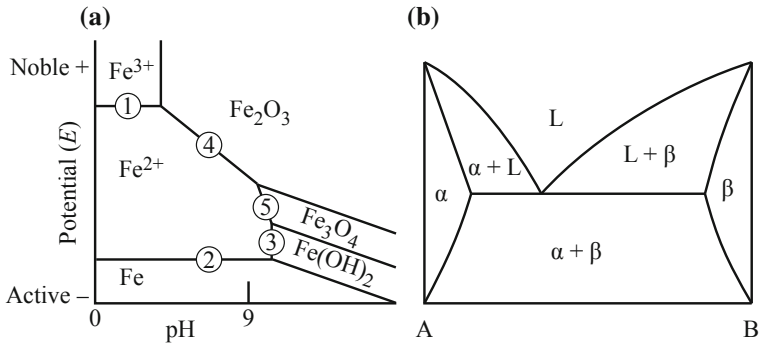

Fig. 15.3 Comparison of (**a**) a Pourbaix diagram with (**b**) a phase diagram. Both diagrams describe regions in which the various phases are thermodynamically stable

diagrams are often drawn for several activities. In the case of line ② in the iron stability diagram:

$$\begin{aligned} E_{Fe^{2+}/Fe} &= -0.44 \text{ V}, a = 1 \text{ mol/kg} \\ &= -0.50 \text{ V}, a = 10^{-2} \text{ mol/kg} \\ &= -0.56 \text{ V}, a = 10^{-4} \text{ mol/kg} \\ &= -0.62 \text{ V}, a = 10^{-6} \text{ mol/kg} \end{aligned}$$

as shown in Fig. 15.4. For any activity of Fe^{2+} in the solution, a horizontal line represents the equilibrium potential, that is, the potential at which Fe^{2+} ion and Fe metal can coexist. Above the line is the region of stability of Fe^{2+}; iron metal at these potentials will tend to corrode and produce Fe^{2+} as the stable species. Below the line, Fe metal is stable, and iron in these conditions will not corrode.

Consider next, line ③, which is a vertical line described by the reaction:

$$Fe^{2+} + 2H_2O = Fe(OH)_2 + 2H^+, \text{ or equivalently, } Fe^{2+} + 2OH^- = Fe(OH)_2.$$

Note that there is no charge transfer in this reaction. Iron is in the +2 valence state on both sides, and there is no change in the oxidation state. This is called an acid–base reaction. Since no charge is transferred, the reaction is independent of potential, hence a vertical line in the stability diagram. The pH is found as follows. Recall that:

$$\Delta G^0 = \sum \nu_p \mu_p^0 - \sum \nu_r \mu_r^0 = -RT \ln \frac{a_p}{a_r} \sum \nu_r \mu_r^0 = -2.3RT \log \frac{a_p}{a_r}. \quad (15.23)$$

Applying this equation to the reaction describing line ③ gives:

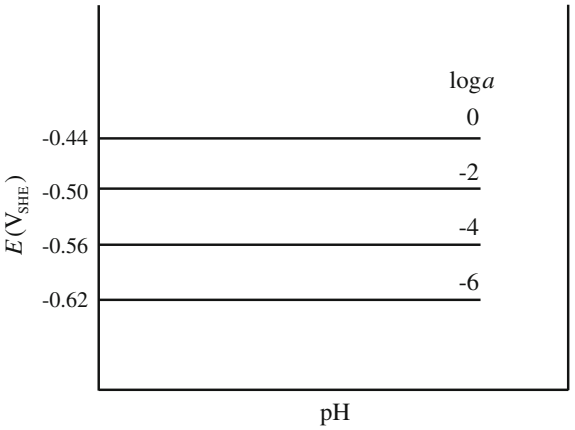

Fig. 15.4 Potential–pH diagram showing the equilibrium for the reaction $Fe = Fe^{++} + 2e^-$ at Fe^{++} activities from 10^{-6} to 1.0

$$\frac{\mu^0_{Fe^{2+}} + 2\mu^0_{H_2O} - \mu^0_{Fe(OH)_2} - 2\mu^0_{H^+}}{2.3RT} = \log \frac{a_{Fe(OH)_2} a^2_{H^+}}{a_{Fe^{2+}} a^2_{H_2O}}. \tag{15.24}$$

Note that there is no acceptor/donor or oxidized/reduced species in this reaction, so we use product/reactant. But since this appears on both sides of the equation, the choice is arbitrary. From the Atlas of Electrochemical Equilibria [1], we find that:

$$\begin{aligned} \mu^0_{H^+} &= 0 \\ \mu^0_{H_2O} &= -56{,}690\,\text{cal/mol} \\ \mu^0_{Fe^{2+}} &= -20{,}310\,\text{cal/mol} \\ \mu^0_{Fe(OH)_2} &= -115{,}586\,\text{cal/mol} \end{aligned}$$

R = 1.986 cal/mole K (8.31 J/mole K). For an iron ion activity, $a_{Fe^{2+}} = 10^{-6}$ mol/kg, substitution of the values for the chemical potentials in Eq. (15.24) into Eq. (15.23) yields pH = 9.65.

A third type of reaction involves both electrons and H^+ and is represented by sloping lines as, for example, lines ④ and ⑤ in Fig. 15.3(a). The reaction for line ④ is given by:

$$Fe_2O_3 + 6H^+ + 2e^- = 2Fe^{2+} + 3H_2O.$$

The sloping line indicates both pH and potential dependence. The potential for line ④ is written as follows:

$$E_{Fe_2O_3/Fe^{2+}} = E^0_{Fe_2O_3/Fe^{2+}} + \frac{RT}{2F} \ln \frac{a_{Fe_2O_3} a^6_{H^+}}{a^2_{Fe^{2+}} a^3_{H_2O}}.$$

Taking $a_{Fe_2O_3} = a_{H_2O} = 1$ mol/kg, we have:

$$\begin{aligned} E_{Fe_2O_3/Fe^{2+}} &= 0.73 - \frac{RT}{2F} \ln a^2_{Fe^{2+}} + \frac{RT}{2F} \ln a^6_{H^+} \\ &= 0.73 - \frac{RT}{F} \ln a_{Fe^{2+}} + \frac{3RT}{F} \ln a_{H^+} \\ &= 0.73 - 0.059 \ln a_{Fe^{2+}} + 3(0.059) \ln a_{H^+} \\ &= 0.73 - 0.059 \ln a_{Fe^{2+}} - 0.177\text{pH}. \end{aligned}$$

Note that the slope of the line is −0.177.

The reaction for line ⑤ is written as follows:

$$Fe_3O_4 + 8H^+ + 2e^- = 3Fe^{2+} + 4H_2O.$$

Assuming unit activities, the potential for line ⑤ is written as follows:

$$E_{Fe_3O_4/Fe^{2+}} = E^0_{Fe_3O_4/Fe^{2+}} + \frac{0.059}{2}\log\frac{a^8_{H^+}}{a^3_{Fe^{2+}}}$$
$$= 0.98 - 0.236\text{pH} - 0.88\ \log\ a_{Fe^{2+}}.$$

Note that the factor in front of the pH term is larger than for line ④ and is reflected in the steeper slope of line ⑤.

We still need to determine E^0. Recall from Eq. (15.19) that:

$$\Delta G^0 = -nFE^0, \quad \text{or} \quad E^0 = -\frac{\Delta G^0}{nF}, \tag{15.25}$$

and from Eq. (15.16):

$$E^0 = \frac{\sum \nu_{ox}\mu^0_{ox} - \sum \nu_{red}\mu^0_{red}}{nF}. \tag{15.26}$$

Applying Eq. (15.26) to reaction ⑤ gives:

$$E^0_{Fe_3O_4/Fe^{2+}} = \frac{\left[\mu^0_{Fe_3O_4} + 8\mu^0_{H^+}\right] - \left[3\mu^0_{Fe^{2+}} - 4\mu^0_{H_2O}\right]}{2F}$$

By convention, $\mu^0_{H^+} = \mu^0_{H_2} = 0$, and

$$\mu^0_{Fe^{2+}} = -20{,}310 \text{ cal/mole},$$
$$\mu^0_{H_2O} = -56{,}690 \text{ cal/mole},$$
$$\mu^0_{Fe_3O_4} = -242{,}400 \text{ cal/mole},$$

and substituting in for F = 96,500 C/eq = 23,060 cal/eq yields $E^0_{Fe_3O_4/Fe^{2+}} = 0.98$ V.

Our diagram so far represents only the anodic half-cell of iron in water. We have not yet considered the cathodic half-cell. Consider the reaction between hydrogen gas and an acid solution:

$$2H^+ + 2e^- = H_2.$$

An equivalent reaction in neutral or alkaline solutions is as follows:

$$2H_2O + 2e^- = H_2 + 2OH^-.$$

Thus, at higher pH where OH^- is predominant over H^+, the second equation is the more appropriate reaction. However, because the two are equivalent (add OH^- to both sides), then:

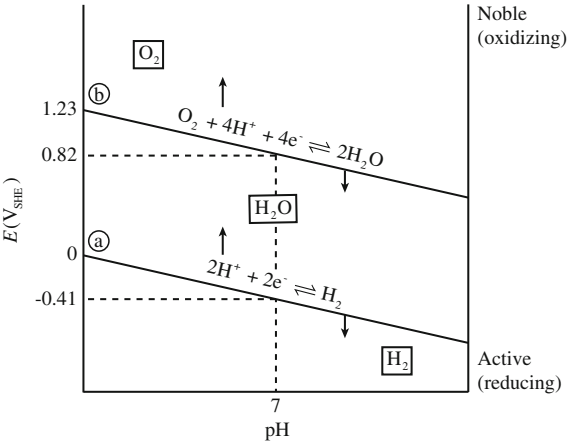

Fig. 15.5 E-pH diagram for water

$$2H^+ + 2e^- = H_2 \qquad ⓐ$$

represents the pH dependence of the half-cell electrode for both. Plotted on a potential–pH diagram shows that $E_{H^+/H_2} = 0$ at pH = 0 ($a_{H^+} = 1$) with a slope of −0.059 V as in Fig. 15.5. For a potential more active than E_{H^+/H_2}, hydrogen is evolved and water is thermodynamically unstable and will decompose. Below the ⓐ line, water is unstable and will decompose to H_2 gas. Above the ⓐ line, water is stable and H_2 (if present) is oxidized to H^+ or H_2O.

As the potential becomes more noble (positive), the oxidation of water becomes thermodynamically feasible:

$$O_2 + 4H^+ + 4e^- = 2H_2O\,(\text{acid})$$

or

$$O_2 + H_2O + 4e^- = 4OH^-(\text{neutral, alkaline})$$

and

$$O_2 + 4H^+ + 4e^- = 2H_2O, \quad \text{or} \quad O_2 + 2H_2O + 4e^- = 4OH^- \qquad ⓑ$$

$$\begin{aligned} E_{O_2/H_2O} &= E^0_{O_2/H_2O} + \frac{0.059}{4}\log\frac{[H^+]^4 p_{O_2}}{a^2_{H_2O}} \\ &= 1.23 - 0.059\,\text{pH}. \end{aligned} \qquad (15.27)$$

For $p_{O_2} = 1$ atm, $E_{O_2/H_2O} = E^0 - 0.059\,\text{pH}$. For pH = 0, $E = E^0 = 1.226$ V (for unit activity of OH^-). For pH = 14, $E = 0.401$ V. At potentials noble to E_{O_2/H_2O} at any pH, water is unstable and is oxidized to O_2. Below E_{O_2/H_2O}, water is stable and

dissolved oxygen is reduced to water. Note that the two equations are represented by the lines ⓐ and ⓑ, respectively, on the E-pH diagram for water and have the same slope as in Fig. 15.5. Below line ⓐ, the reaction $2H^+ + 2e^- = H_2$ proceeds to the right reducing hydrogen to form hydrogen gas. Above line ⓑ, water is oxidized to form gaseous oxygen and the reaction described by line ⓑ proceeds to the left. Between the lines, the stable form of water is H_2O. So the potential–pH diagram is divided into three regions:

Top: Water is oxidized to form O_2 gas.
Middle: Water is stable and cannot be electrolyzed.
Bottom: H^+ is reduced to form H_2 gas.

The potential–pH diagram in Fig. 15.6 shows the conditions under which corrosion will cause H_2 evolution or will reduce dissolved O_2. Note that when pressure is increased, line ⓑ moves up and line ⓐ moves down, expanding the domain over which water is stable. The superposition of the water E-pH diagram onto the E-pH diagram for iron is shown in Fig. 15.7.

The E-pH diagram can be divided into corrosion, immunity, and passivation domains as in Fig. 15.8. The immunity domain is that in which iron metal is stable in water. The passivation domain is one in which an oxide, hydroxide, hydride, or salt is the solid stable form, but not the metal. The corrosion domain is the one in which the metal ion is the stable form. Consider the anodic and cathodic reactions occurring at points ①, ②, and ③ along the vertical dotted line in Fig. 15.7. Fe^{2+} is stable at point ①, and only one reduction reaction (reduction of oxygen) is possible. Given this situation, some specific corrosion control strategies are implied. First, if the cell is deaerated, thus removing oxygen, then the reduction reaction is suppressed and the anodic reaction cannot proceed. A second strategy is anodic protection in which the potential is increased into the passive region in which the

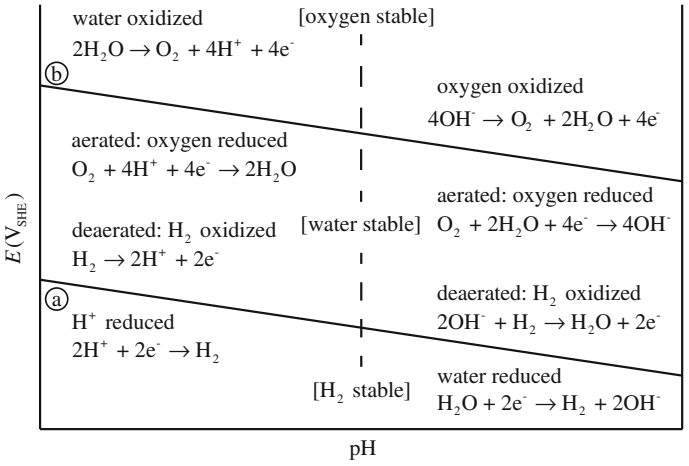

Fig. 15.6 Reactions in the various regions of E-pH diagram for water

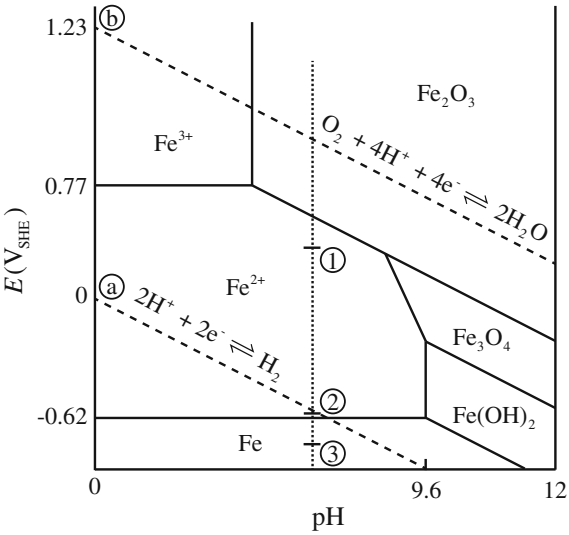

Fig. 15.7 Superposition of E-pH diagram for water onto that for iron

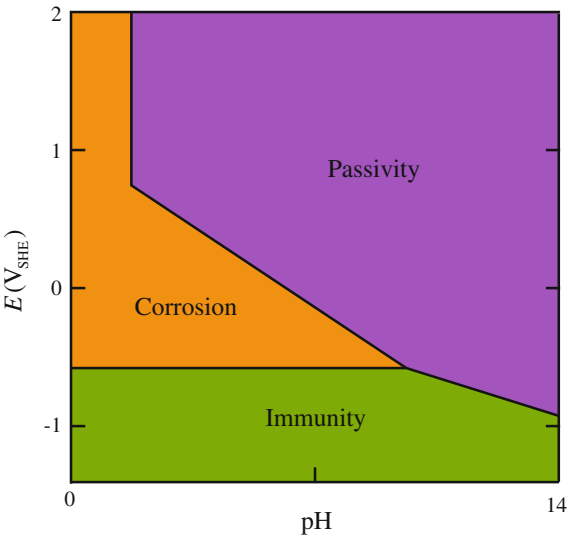

Fig. 15.8 Division of E-pH diagram into domains

passive film will suppress the dissolution of Fe to Fe^{2+}. A third option is to raise the pH into the passive region, achieving the same result as option 2. For point ②, there are two possible reduction reactions, so deaeration would not work in this case. Corrosion control strategies for point ② include increasing the pH, increasing the potential (anodic protection), and decreasing the potential (cathodic protection). Note that decreasing the potential is the better strategy since the magnitude of the decrease is small, compared to a very large increase required to achieve anodic protection. Point ③ is in the stable Fe region so no control measures need to be taken to prevent corrosion of Fe.

While E-pH diagrams are extremely useful for determining the stability of metals in aqueous solutions, they have limitations. These include the following:

- E-pH diagrams are *equilibrium* diagrams, so they tell us nothing about the kinetics of corrosion.
- They are constructed for pure metals. (However, they can be superimposed for approximation of the behavior of alloys.)
- They are dependent on temperature and are useful only at the temperature at which they are constructed.
- It is not always true that when a film forms, it is protective. A protective film must be a poor ionic conductor. So the passive region does not guarantee protection of the underlying metal.
- Most practical corrosion problems involve not only water, but anions such as Cl^- and $SO_4^=$. These must be accounted for separately.
- The pH value indicated in the diagram is that of the solution in direct contact with the metal and is not necessarily that of the bulk solution.

15.3 Kinetics of Corrosion

Imagine the immersion of a metal electrode M into an electrolyte containing M^+ ions, e.g., a Ag electrode in a silver nitrate solution, $AgNO_3$. At the instant of immersion, the metal is electroneutral (uncharged), $q_m = 0$. Since the interface region must then be electroneutral, there must be no net charge on the solution side, $|q_m| = |q_s| = 0$. There is zero potential difference and zero electric field in the interphase region, so there are no electrical effects and no electrochemistry.

Consider the one-step reduction reaction consisting of electron acceptance by an electron acceptor ion, A^+:

$$A^+ + e^- \rightarrow D.$$

Whether this will occur spontaneously will be determined by thermodynamics, in particular,

$$\tilde{\mu}_{A^+} + \mu_{A^+} + FE. \tag{15.28}$$

Since there is no field, FE is zero so $\tilde{\mu}_{A^+} = \mu_{A^+}$, and the interface is at equilibrium only if the chemical potential of A^+ is the same on both sides of the interface. If not, then the gradient of chemical potential acts as the driving force for diffusion.

Consider the movement of the positive ion A^+ from the solution side of the interface to the metal surface (a few tenths of a nm away). As the ion moves from solution to electrode, its potential energy changes. The positive ion must have a certain activation energy for the charge transfer reaction to occur. The process of an ion jumping from solution site to metal site is similar to lattice diffusion where

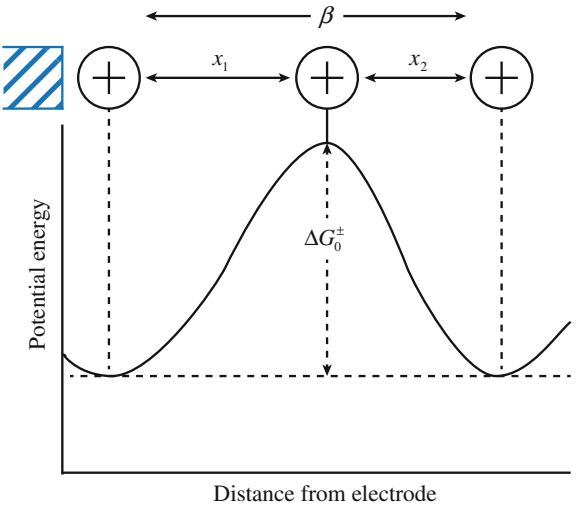

Fig. 15.9 Variation of potential energy with distance from the electrode surface

potential energy barriers must also be overcome as in Fig. 15.9. The frequency with which an ion successfully jumps the energy barrier for diffusion (jump frequency) is as follows:

$$k_{\mathrm{c}}^{\mathrm{r}} = \frac{kT}{h} \mathrm{e}^{-\frac{\Delta G_{\mathrm{cr}}^{0\pm}}{RT}}, \tag{15.29}$$

where subscript, c, refers to the chemical driving force (no electric field) and the superscript, *r*, refers to the reduction reaction. The pre-exponential term is the vibrational frequency, where *k* is Boltzmann's constant, *h* is Planck's constant, and *T* is temperature. The exponential term is the probability, and $\Delta G_{\mathrm{cr}}^{0\pm}$ is the standard free energy of activation, or the change in free energy required to climb to the top of the barrier ($\pm$) when there is zero electric field acting on the ion. The rate of the reduction reaction under zero electric field is the product of the jump frequency and the concentration of electron-acceptor ions, A^+, on the solution side of the interface:

$$v_{\mathrm{c}}^{\mathrm{r}} = k_{\mathrm{c}}^{\mathrm{r}} C_{\mathrm{A}^+}. \tag{15.30}$$

Hence, under zero-field conditions, the electron transfer reaction is given by purely chemical kinetics considerations.

The transfer of an electron from the electrode to the electron acceptor has left the metal positively charged (poorer in negative charges) and the solution negatively charged (poorer in positive charges). Charge separation at the interface has created an electrified interface, an electrical field, and a potential difference across the

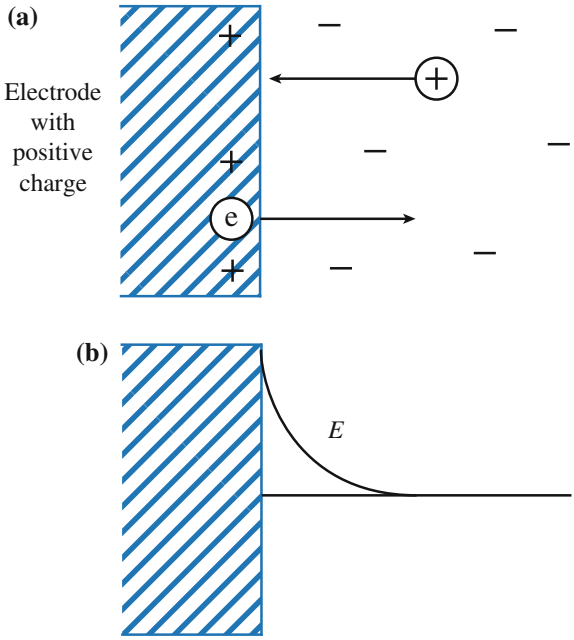

Fig. 15.10 The buildup of positive charge on the electrode surface (**a**) reduces an electric field (**b**) which generates a potential that makes addition of positive charge or removal of electrons more difficult (**c**)

interface. How is the rate of subsequent electron transfer affected by the creation of the electric field? The next electron and next ion must move against the field to react as in Fig. 15.10(a). Clearly, work must be done by the positive ion in order to climb the potential energy barrier as in Fig. 15.10(b). Thus, the reduction reaction consists of moving the ion from its initial state *across* the interface to its final position on the metal. The work in activating this ion is the charge times the potential difference through which the ion is moved to reach the top of the barrier. The total potential difference through which the ion passes is E, but of the contribution of electrostatic work to the standard free energy of activation for the reduction reaction, only a part of E is important. It is that part through which the ion passes to reach the peak of the energy barrier and is described by the symmetry factor, β:

$$\beta = \frac{\text{distance across the double layer to the summit}}{\text{distance across the whole double layer}} \equiv \text{symmetry factor} \qquad (15.31)$$

The electrical contribution to the free energy of activation for the reduction reaction is $+\beta FE$ as shown in Fig. 15.11(a). In a field, the total free energy of activation for reduction is the chemical free energy of activation, $\Delta G_{cr}^{0\pm}$, plus the electrical contribution βFE, yielding:

$$\Delta G_{r}^{0\pm} = \Delta G_{cr}^{0\pm} + \beta FE. \qquad (15.32)$$

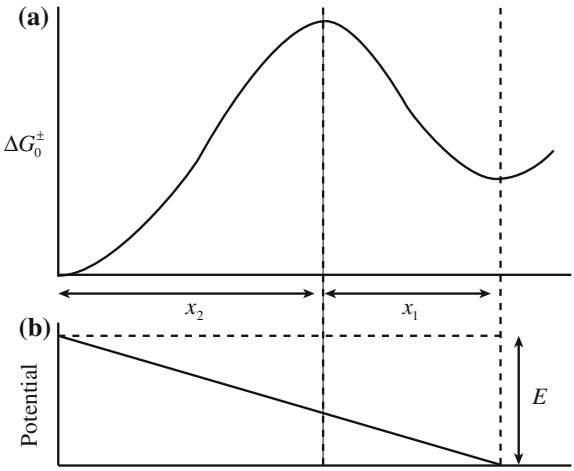

Fig. 15.11 (**a**) Variation of free energy change with distance from the electrode and (**b**) the contribution of the potential at the surface to the magnitude of the energy barrier

The rate of the reduction reaction under an electric field is then as follows:

$$\begin{aligned} v_{\mathrm{e}}^{\mathrm{r}} &= C_{\mathrm{A}^+}\frac{kT}{h}\mathrm{e}^{-\Delta G_{\mathrm{r}}^{0\pm}/RT} \\ &= C_{\mathrm{A}^+}\frac{kT}{h}\mathrm{e}^{-\Delta G_{\mathrm{cr}}^{0\pm}/RT}\mathrm{e}^{-\beta FE/RT} \\ &= k_{\mathrm{c}}^{\mathrm{r}} C_{\mathrm{A}^+}\mathrm{e}^{-\beta FE/RT}. \end{aligned} \tag{15.33}$$

$v_{\mathrm{e}}^{\mathrm{r}}$ has units of moles of positive ions reacting per second by crossing a unit area of the interface, and the subscript, e, denotes the reaction under an electric field. Multiplying by charge per mole, F, gives the current density:

$$\begin{aligned} i_{\mathrm{r}} &= F v_{\mathrm{e}}^{\mathrm{r}} \\ &= F k_{\mathrm{c}}^{\mathrm{r}} C_{\mathrm{A}^+}\mathrm{e}^{-\beta FE/RT}, \end{aligned} \tag{15.34}$$

in units of A/cm^2. Equation (15.34) shows the link between the electric field and the rate of electron transfer across the interface. Small changes in E produce large changes in i. For example, for $\beta \sim 1/2$, a potential change of 0.12 V produces a change in i by a factor of 10. Thus, if a metal is not connected to any other source of charge, every reduction of A^+ ions:

- Charges the metal more positively and the solution more negatively,
- Increases the potential difference and the field across the interface,
- Increases the electrical work of activating an ion to the top of the barrier,
- Decreases the electrical factor $\mathrm{e}^{-\beta FE/RT}$, and
- Reduces the rate of the reduction reaction.

According to this picture, charge leakage should stop after some time due to the buildup of such a large potential difference. But this does not happen. We have not considered the reverse reaction, oxidation:

$$D \rightarrow A^{+} + e^{-}.$$

If the directed field hinders the ion transfer from solution to electrode because the ion is moving against the field, then it helps the reverse reaction because the positive ion moves with the field which acts to reduce the work required to move it. If the positive ion has to be activated through a potential difference of βE in the forward direction (solution to metal) (Fig. 15.12(a)), it has to be activated through the remainder $(1 - \beta)E$ in the oxidation reaction as in Fig. 15.12(b). So the electrical work of activation for oxidation is $F[(1 - \beta)E]$, and the rate of oxidation is as follows:

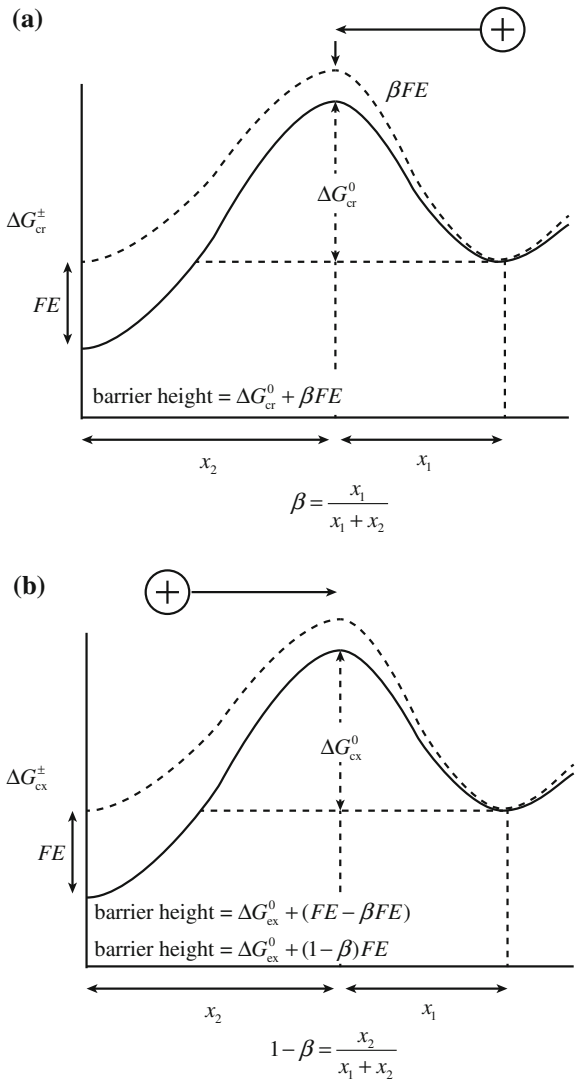

Fig. 15.12 Contribution of the potential to the energy barrier for (**a**) reduction and (**b**) oxidation

$$v_{\mathrm{e}}^{\mathrm{x}} = k_{\mathrm{c}}^{\mathrm{x}} C_{\mathrm{D}} \mathrm{e}^{(1-\beta)FE/RT}, \tag{15.35}$$

and the current density is as follows:

$$\begin{aligned} i_{\mathrm{x}} &= F v_{\mathrm{e}}^{\mathrm{x}} \\ &= F k_{\mathrm{c}}^{\mathrm{x}} C_D \mathrm{e}^{(1-\beta)FE/RT}. \end{aligned} \tag{15.36}$$

So, as the excess positive charge on the metal builds up and decreases the reduction rate, the reverse reaction rate increases by pumping electrons into the metal, decreasing the positive charge, and negating the tendency to stop the reduction reaction. If no external current source is applied, the reactions will just balance. The potential at which the currents become equal and the charges on the metal and in solution become constant (as well as the electric field) is the equilibrium (reversible) potential, E^{e}. At equilibrium, the oxidation and reduction reactions continue to occur, but at the same rate, the currents are equal in magnitude and opposite in direction:

$$i_{\mathrm{r}} = F k_{\mathrm{c}}^{\mathrm{r}} C_{\mathrm{A}^+} \mathrm{e}^{-\beta FE^{\mathrm{e}}/RT} = i_{\mathrm{x}} = F k_{\mathrm{c}}^{\mathrm{x}} C_{\mathrm{D}} \mathrm{e}^{(1-\beta)FE^{\mathrm{e}}/RT}. \tag{15.37}$$

Since the oxidation and reduction rates are equal, the magnitude can be designated by a single term, the *equilibrium exchange current density*, i_0, such that:

$$i_0 = i_{\mathrm{r}} = F k_{\mathrm{c}}^{\mathrm{r}} C_{\mathrm{A}^+} \mathrm{e}^{-\beta FE^{\mathrm{e}}/RT} = i_{\mathrm{x}} = F k_{\mathrm{c}}^{\mathrm{x}} C_{\mathrm{D}} \mathrm{e}^{(1-\beta)FE^{\mathrm{e}}/RT}. \tag{15.38}$$

The exchange current density reflects the kinetic properties of the particular interfacial system and can vary from one reaction to another and from one electrode to another by orders of magnitude. It cannot be measured directly because there is no *net* current to measure. A net flow (or drift) of electrons is produced only when the interface is no longer at equilibrium. The non-equilibrium drift current density is the difference between reduction and oxidation currents:

$$i = i_{\mathrm{x}} - i_{\mathrm{r}} = F k_{\mathrm{c}}^{\mathrm{x}} C_{\mathrm{D}} \mathrm{e}^{(1-\beta)FE/RT} - F k_{\mathrm{c}}^{\mathrm{r}} C_{\mathrm{A}^+} \mathrm{e}^{-\beta FE/RT}, \tag{15.39}$$

where $E \neq E^{\mathrm{e}}$ and is the potential difference across the interface. We can write E as follows:

$$E = E_{\mathrm{e}} + \Delta E = E^{\mathrm{e}} + \eta, \tag{15.40}$$

where η is the overpotential, which is a measure of the departure from equilibrium potential. For an externally driven electrochemical cell, the overpotential is the potential difference that drives the current; it is the current-producing potential. But if the system is a self-driven cell, then the current driven through the external load generates an excess potential; this is the current-produced potential. The term overpotential is used to refer to both the current-producing potential in a driven

system and to the current-produced potential in a self-driving cell. The net current density is then as follows:

$$i = \left\{ Fk_c^x C_D e^{(1-\beta)FE^e/RT} \right\} e^{(1-\beta)F\eta/RT} - \left\{ Fk_c^r C_{A^+} e^{-\beta FE^e/RT} \right\} e^{-\beta F\eta/RT} \quad (15.41)$$

But the terms inside the brackets are the expressions for the equilibrium exchange current density, i_0. Therefore:

$$i = i_0 \left[e^{(1-\beta)F\eta/RT} - e^{-\beta F\eta/RT} \right]. \quad (15.42)$$

This is the Butler–Volmer equation. It shows how the current density across a metal–solution interface depends on the difference η between the actual non-equilibrium and equilibrium potentials as in Fig. 15.13. Note that small changes in η produce large changes in i.

There are several special cases that result in more simplified forms of this equation. If we let the symmetry factor $\beta = 1/2$, then Eq. (15.42) becomes:

$$i = i_0 \left[e^{F\eta/2RT} - e^{-F\eta/2RT} \right], \quad (15.43)$$

and since $\frac{e^x - e^{-x}}{2} = \sinh x$ then $i = i_0 \sinh \frac{F\eta}{2RT}$ and a plot of i versus η yields a symmetric curve as in Fig. 15.14(a), where oxidation and reduction reactions proceed at equal rates (currents) for equal overpotentials. The practical significance

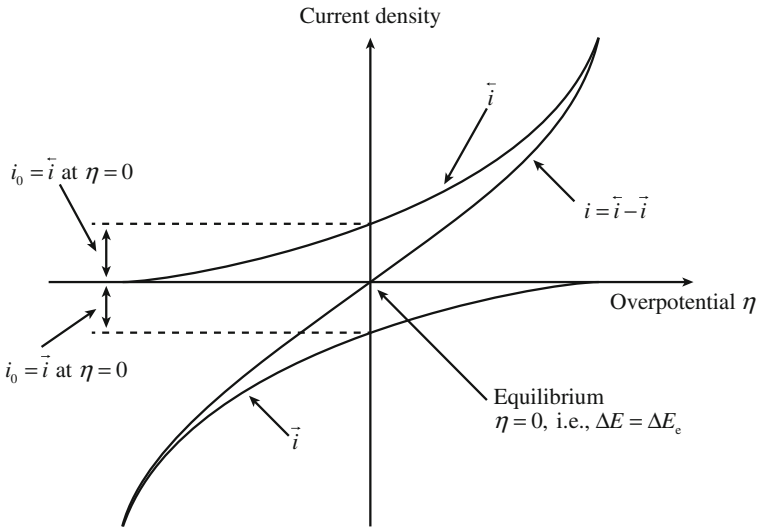

Fig. 15.13 Current density versus overpotential showing that the point of zero overpotential corresponds to zero current and occurs when the surface electrode is at equilibrium (after [2])

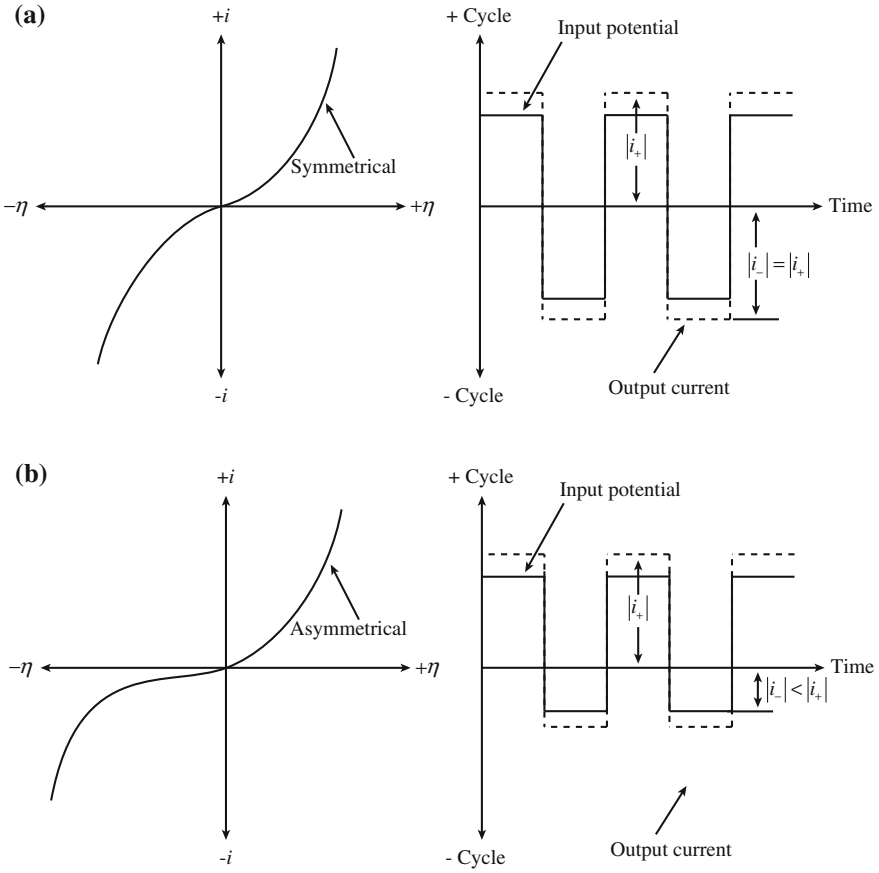

Fig. 15.14 (**a**) When the i versus η relation is perfectly symmetrical ($\beta = 1/2$), the interface cannot rectify the current responding to a periodically varying potential. (**b**) When the symmetry factor $\beta \neq 1/2$, the i versus η curve is asymmetrical and there is a Faradaic rectification effect or a periodically varying potential (after [2])

of this behavior is that the interface can only be rectifying if the symmetry factor $\beta \neq ½$ as in Fig. 15.14(b).

We now consider two limiting cases of the Butler–Volmer equation; one in which the overpotential is large and one in which the overpotential is small. When η is large positive, $e^{(1-\beta)F\eta/RT} \gg e^{-\beta F\eta/RT}$ and the corrosion current, i, is as follows:

$$i \simeq i_x = i_0 e^{(1-\beta)F\eta/RT}. \tag{15.44}$$

Taking the natural log of both sides yields:

$$\eta = -\frac{RT}{(1-\beta)F}\ln i_0 + \frac{RT}{(1-\beta)F}\ln\, i. \tag{15.45}$$

If η is large negative:

$$i \simeq i_r = -i_0 e^{-\beta F\eta/RT}, \quad \text{and} \quad \eta = \frac{RT}{\beta F}\ln i_0 - \frac{RT}{\beta F}\ln i. \tag{15.46}$$

The case with $\eta > 0$ is termed anodic polarization, and η is the anodic overpotential, η_A. The case with $\eta < 0$ is cathodic polarization, and η is the cathodic overpotential, η_C. We can write the anodic and cathodic overpotentials as Tafel equations:

$$\begin{aligned} \eta_A &= A + B\ln i_A \\ \eta_C &= A' + B'\ln i_C, \end{aligned} \tag{15.47}$$

where

$$\begin{aligned} A &= \frac{-RT}{(1-\beta)F}\ln i_0; \quad & B &= \frac{RT}{(1-\beta)F} \\ A' &= \frac{RT}{\beta F}\ln i_0; & B' &= \frac{-RT}{\beta F}. \end{aligned} \tag{15.48}$$

Hence, at large $|\eta|$ ($\geq$ 0.12 V), the overpotential is proportional to ln i as in Fig. 15.15. Note also that back extrapolation of the Tafel equations yields the exchange current density, i_0. The Tafel equations are central kinetic expressions in electrochemistry.

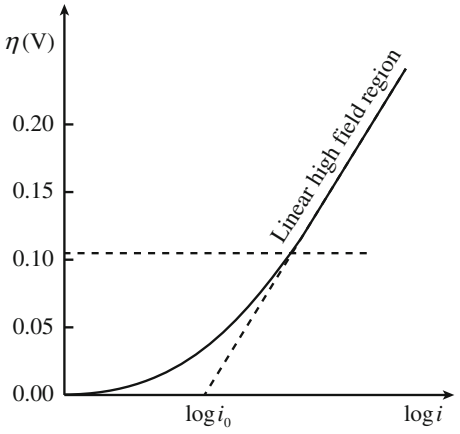

Fig. 15.15 Tafel line showing the exponential relationship at high overpotentials, yielding a linear relationship between η and log i linear (after [2])

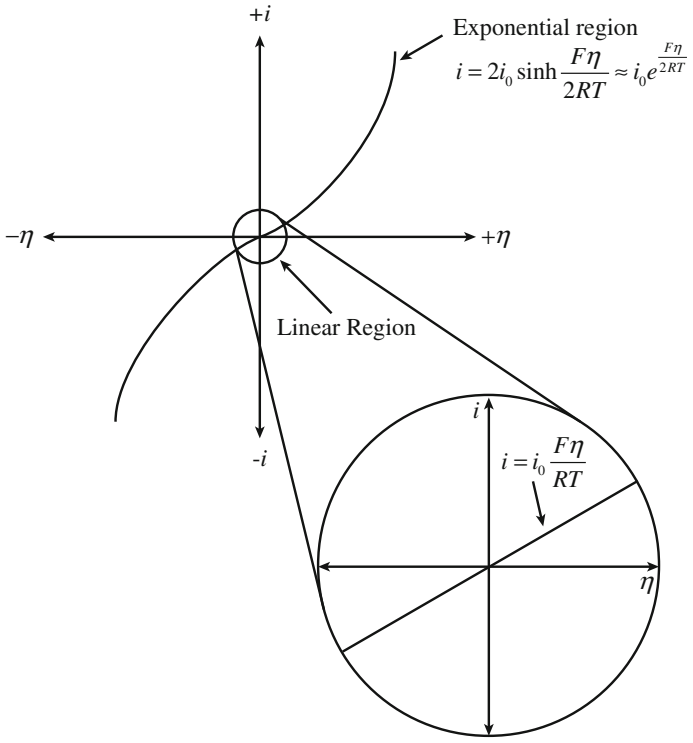

Fig. 15.16 At small overpotentials, the i versus η relationship is linear (after [2])

The second case is for very small η, in which the exponentials in Eq. (15.42) are small and expanding them and retaining only the first two terms of each exponential term yields:

$$\begin{aligned} i &\simeq i_0 \left[1 + \frac{(1-\beta)F\eta}{RT} - 1 + \frac{\beta F\eta}{RT} \right] \\ &\simeq i_0 \frac{F\eta}{RT}. \end{aligned} \tag{15.49}$$

This simplified expression is valid for $\eta \leq 0.01$ V. Note also that i is greater than zero for $\eta = \eta_A > 0$ and i is less than zero for $\eta = \eta_C < 0$. Note also that the current density is proportional to the overpotential as in Fig. 15.16; this is termed the linear region. Equation (15.49) can be written as follows:

$$i = \sigma_{m/s}\eta, \tag{15.50}$$

where $\sigma_{m/s}$ is the conductivity of the metal–solution interface.

15.4 Polarization

As described in Sect. 15.3, the potential of the electrode must be different from the equilibrium value for a net current to flow. The potential difference is the overpotential, η, and the relationship between the values of the net current density resulting from application of η constitutes a polarization curve. Activation polarization refers to the case in which the reaction at the electrode surface requires an activation energy in order to go. Activation polarization of any kind increases with current density, i, in accord with the Tafel equation. This is to be distinguished from other types of polarization such as concentration polarization and resistance polarization.

If we only consider a single electrode and large overpotentials, then the overpotential is related to the current by the Tafel equations (15.47). For anodic polarization using log rather than ln:

$$\begin{aligned} \eta_A &= A_A + B_A \log i_A \\ A_A &= -\frac{2.3RT}{(1-\beta)F} \log\, i_0; \quad B_A = \frac{2.3RT}{(1-\beta)F}, \end{aligned} \tag{15.51}$$

and for cathodic polarization:

$$\begin{aligned} \eta_C &= A_C + B_C \log i_C \\ A_C &= \frac{2.3RT}{\beta F} \log\, i_0; \quad B_C = -\frac{2.3RT}{\beta F}, \end{aligned} \tag{15.52}$$

as shown in Fig. 15.17. The situation describing single electrode kinetics is clear and uncomplicated. However, what happens when we consider anodic and cathodic processes occurring simultaneously. This is the subject of mixed potential theory.

15.4.1 Mixed Potential Theory

Mixed potential theory consists of two hypotheses:

1. Any electrochemical reaction can be divided into two or more partial oxidation and reduction reactions.
2. There can be no net accumulation of charge during an electrochemical reaction.

From this, it follows that the total rate of oxidation must equal the total rate of reduction. Consider the immersion of Zn in an HCl solution as in Fig. 15.18. Zinc corrodes rapidly with evolution of hydrogen gas. If a piece of zinc is immersed in HCl containing Zn ions, the electrode potential cannot simultaneously be at two reversible potentials (Zn and H_2). The only point in the entire system where the oxidation rate equals the reduction rate is at the intersection point, E_{corr}, as in

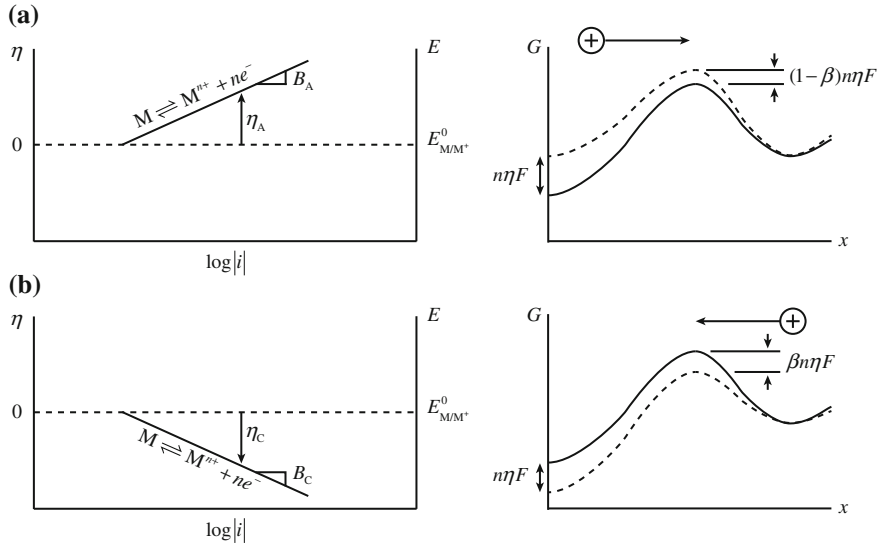

Fig. 15.17 Single electrode polarization curves and accompanying activation energy model for (**a**) anodic and (**b**) cathodic reactions

Fig. 15.18 Corrosion of zinc in HCl

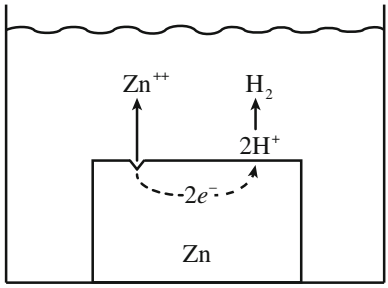

Fig. 15.19(a). Why must this be the potential of the cell? Because (1) charge must be conserved and (2) the entire Zn surface must be at a constant potential. Since it is an excellent conductor and since the H^+ reduction reaction occurs on the surface, it must be occurring at the same potential. The current density at this point corresponds to the rate of zinc dissolution as well as the rate of H_2 evolution. The reactions polarize each electrode in the direction of the other; zinc is polarized anodically and H is polarized cathodically.

If we put Fe into HCl, will it corrode faster or slower than Zn? Compare the polarization plot for Zn (Fig. 15.19(a)) to that for Fe (Fig. 15.19(b)). Note the exchange current densities for Fe/Fe^{++} and H/Fe compared to Zn/Zn^{++} and H/Zn. Although Zn has a higher tendency to corrode in acid due to its higher driving force (lower equilibrium potential compared to iron), Zn is a poor catalyst for H reduction. Thus, the corrosion rate of Fe is greater than Zn. This illustrates the fact

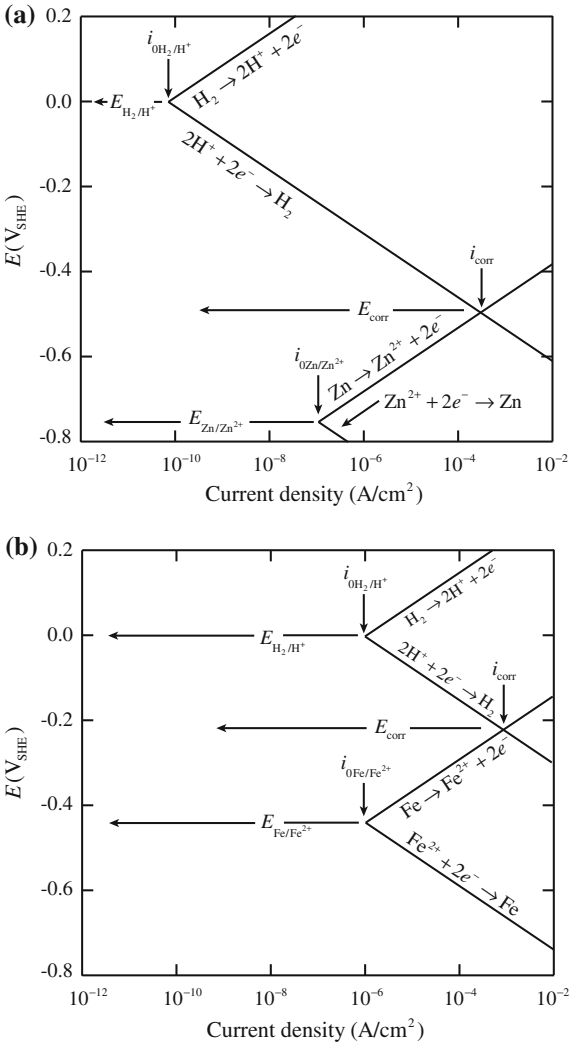

Fig. 15.19 Anodic and cathodic half-cell reactions present simultaneously on (**a**) a corroding zinc surface and (**b**) a corroding Fe surface (after [3])

that kinetics does not necessarily follow thermodynamics. That is, the corrosion rate of the system with a higher driving force is actually smaller. The variation in exchange current densities on various metal surfaces is illustrated in Fig. 15.20.

15.4.2 Galvanic Couples

Consider the coupling of an active metal to a noble metal, e.g., Zn and Pt as in Fig. 15.21. Pt cannot be oxidized, and there is no Pt^+ in solution to be reduced. With

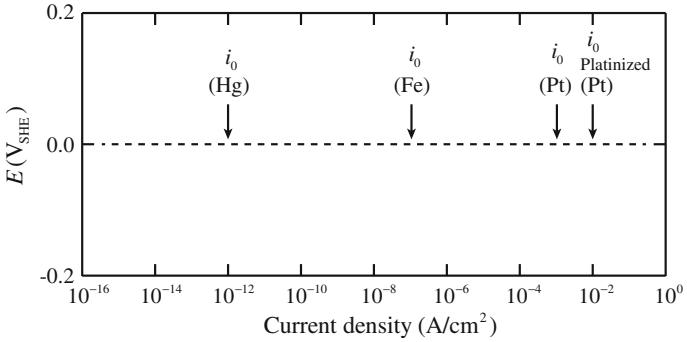

Fig. 15.20 Effect of the metal surface on the hydrogen–hydrogen ion exchange current density (after [3])

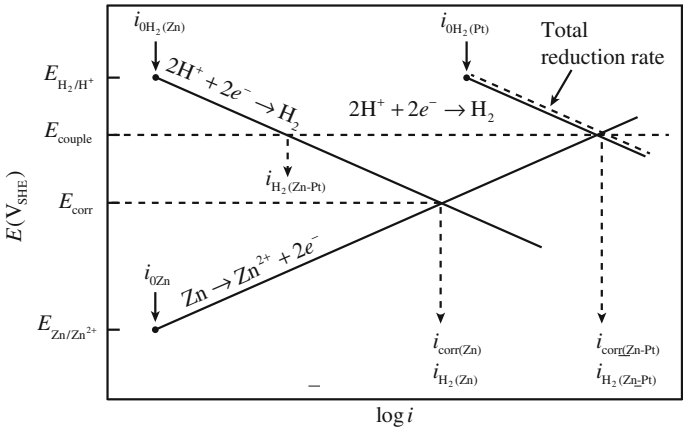

Fig. 15.21 Polarization diagram for a galvanic couple between an active and noble metal (after [3])

Zn and Pt uncoupled, $i_{0_{Zn/Zn^{++}}} = 10^{-6}$ A/cm^2 and $i_{0_{H/Zn}} = 10^{-6}$ A/cm^2. But coupling Zn to Pt results in a much larger value of $i_{cathodic}$ or hydrogen evolution. Why? Pt is a much better catalyst for H_2 evolution so electrons are delivered to the Pt surface where $i_{0_{H/Pt}} 10^{-3}$ A/cm^2. There is one oxidation reaction, $Zn \rightarrow Zn^{++} + 2e^-$, and one reduction reaction, $2H^+ + 2e^- \rightarrow H_2$, but at *two* locations. So there are two exchange current densities, $i_{0_{H/Zn}}$ and $i_{0_{H/Pt}}$ and $i_{0_{total}} = i_{0_{H/Zn}} + i_{0_{H/Pt}}$.

Note that the increase in the corrosion rate of Zn observed when this metal is coupled to Pt is the result of the higher exchange current density for hydrogen evolution on the Pt surface. It is not due to the more noble reversible potential of the Pt/Pt^+ electrode. To test this idea, compare a Zn/Au couple to a Zn/Pt couple. Figure 15.22 shows that since $i_{0_{H/Au}} \ll i_{0_{H/Pt}}$, the corrosion rate increase upon

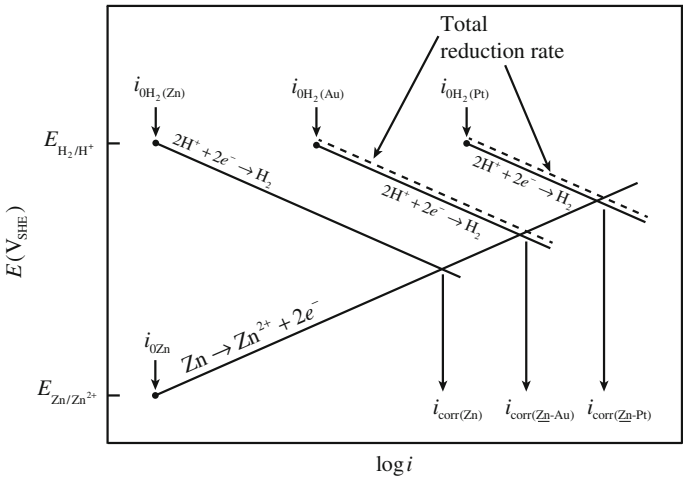

Fig. 15.22 Effects of platinum and gold galvanically coupled to zinc in dilute acid (after [3])

coupling to Au is less than that when coupling to Pt; $i_{corr(Zn)} < i_{corr(Zn-Au)} < i_{corr(Zn-Pt)}$. The reason why gold produces a less severe galvanic effect is not related to its reversible potential, but rather to the fact that it has a lower hydrogen exchange current density than does platinum.

Now, consider the coupling of two active metals: Zn and Fe as in Fig. 15.23(a). The polarization diagram is shown in Fig. 15.23(b). Upon coupling Zn to Fe, the following occurs as in Fig. 15.23(c):

(a) i_{Zn} increases (point a' → point a),
(b) i_{Fe} decreases (point b' → point b),
(c) $i_{H/Zn}$ decreases (point c' → point c), and
(d) $i_{H/Fe}$ increases (point d' → point d).

The Zn electrode is no longer at equilibrium since $i_{anodic} > i_{cathodic}$ (point a > point c) as in Fig. 15.24(a). For the Fe electrode, the reverse is true since $i_{anodic} < i_{cathodic}$ (point b < point d) as in Fig. 15.24(b). Fe is cathodically protected by making it act as the cathode. Since H^+ reduction on the surface of Fe is the main reaction, the corrosion of Fe is reduced. In this case, Zn is acting as a sacrificial anode. In general, in a couple of two active metals, the more active metal becomes the anode and cathodically protects the less active metal.

Finally, consider the corrosion reaction described in Fig. 15.23 when an oxidizer such as Fe^{3+} is added to the solution, as shown in Fig. 15.25. Note that there are now three redox systems: metal–metal ion, hydrogen ion–hydrogen gas, and ferric–ferrous ions. The basic principles of mixed potential theory still apply. At steady state, the total rate of oxidation must equal the total rate of reduction to satisfy the charge conservation principle, and E_{corr} is determined where the two are equal. Starting at the most noble half-cell electrode potential, $E_{Fe^{3+}/Fe^{2+}}$, and proceeding in the

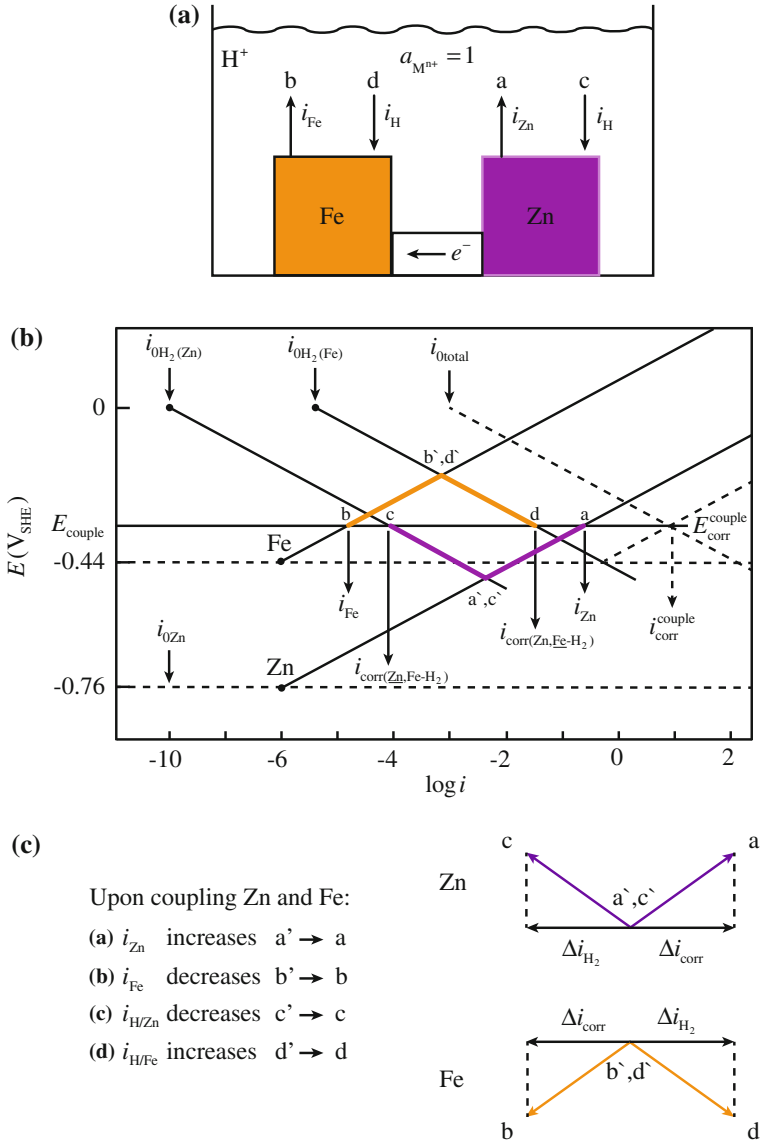

Fig. 15.23 Galvanic coupling of two active metals: (**a**) Fe and Zn in acid, (**b**) polarization diagram, (**c**) exchange current densities (after [2])

negative (active) direction, the total reduction current density for hydrogen reduction E_{H_2/H^+} is reached, at which point the reduction current density for hydrogen must be added. The total reduction current density then follows the parallel dashed line marked "total reduction" until the half-cell electrode potential for metal oxidation is reached, when another increase occurs due to reduction of M^+ to M.

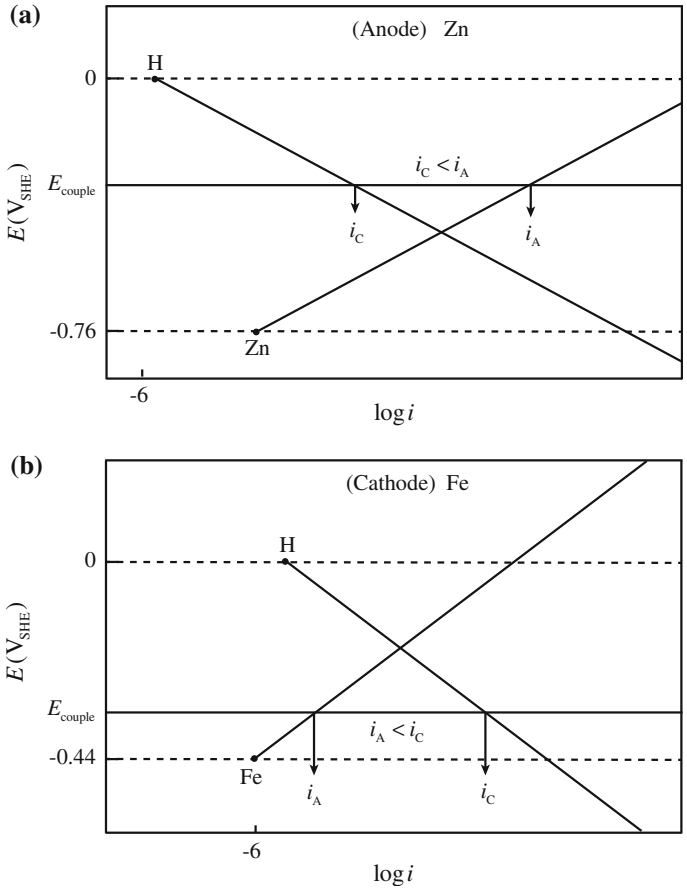

Fig. 15.24 Single electrode polarization diagrams for (**a**) Zn and (**b**) Fe in Fig. 15.23

The total oxidation current is determined in a similar manner, starting with the most active half-cell electrode potential in the system, E_{M/M^+}. The total oxidation current density follows the line to more positive potentials for oxidation of M to M^+ until E_{H_2/H^+} is reached, at which point a current density for oxidation of H_2 to H^+ must be included. The total current density for oxidation follows the parallel line marked "total oxidation" until $E_{Fe^{3+}/Fe^{2+}}$ is reached and another addition is included for oxidation of Fe^{2+} to Fe^{3+}.

The corrosion potential, E_{corr}, is defined in Fig. 15.25 by the intersection of the total oxidation and total reduction lines where the two are equal, fulfilling the charge conservation principle. Because $M \rightarrow M^+ + e^-$ is the only oxidation reaction present, the total oxidation current density is also the corrosion rate, i_{corr}. However,

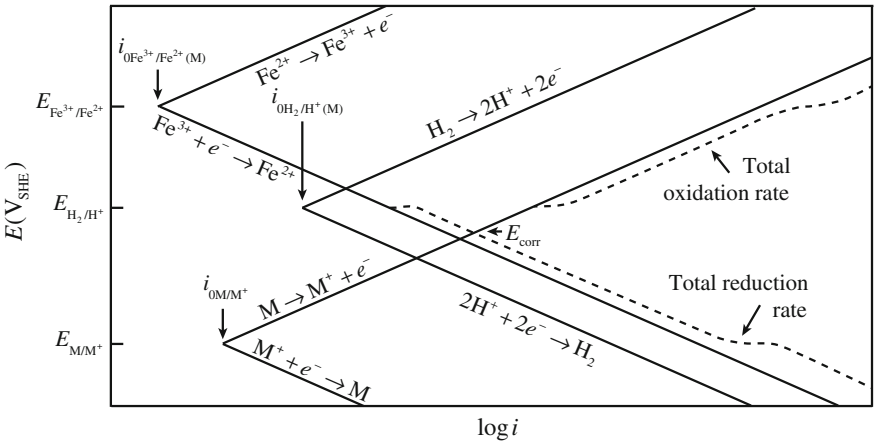

Fig. 15.25 Determination of the corrosion potential for a corroding metal M exposed to an acid solution with a second oxidizer, Fe^{3+}/Fe^{2+} (after [2])

both Fe^{3+} and H^+ are being reduced in this system, and the sum of their rates, $i_{Fe^{3+}\rightarrow Fe^{2+}} + i_{H^+\rightarrow H_2}$, is equal to total reduction, which is in turn equal to total oxidation, or i_{corr}:

$$i_{corr} = i_{Fe^{3+}\rightarrow Fe^{2+}} + i_{H^+\rightarrow H_2}.$$

The two reduction rates are defined in Fig. 15.25 by the intersection of the horizontal equipotential line at E_{corr} with the polarization curves for the reduction rates of each half-cell reaction.

15.4.3 Anode/Cathode Area Ratio

Until now, it has been assumed that anodic and cathodic areas were equal. But what if the areas are unequal? The issue of anode and cathode areas for three different cases is shown in Fig. 15.26. In the polarization diagram, E is plotted versus the logarithm of the current, log I, not the current density, log i. Although the exchange current density may remain the same, the exchange current changes. As the cathode area increases relative to the anode, the cathodic current will drive the anodic current higher so more oxidation must occur at the anode. Increasing the area, A, of the cathode displaces the H_2/Pt curve to the right, increasing the corrosion of Zn. Since:

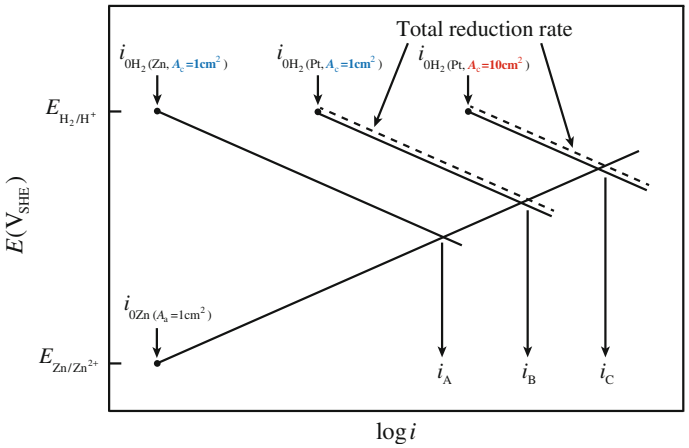

Fig. 15.26 Effect of cathode surface area on the galvanic interaction between zinc and platinum in dilute acid solution (after [2])

$$i_A A_A = i_C A_C, \tag{15.53}$$

then

$$i_A = i_C \frac{A_C}{A_A}. \tag{15.54}$$

Also, since $I_A = I_C$ always, then $|I_A| = |I_C|$ is greater when $A_C/A_A > 1$. So if we increase A_C/A_A, we increase i_A. An extreme case of this process is pitting corrosion.

15.4.4 Multiple Cathodic Reactions

Consider the association between the Pourbaix and polarization diagrams as shown for Fe in Fig. 15.27. This picture is correct for a deaerated electrolyte because in this case, the only reduction reaction possible is that of H^+. But suppose the solution is aerated. Depending upon the potential, oxygen gas may need to be considered. In addition to the reduction reaction $2H^+ + 2e^- = H_2$, we may have $1/2O_2 + 2H^+ + 2e^- = H_2O$. Figure 15.28 shows the effect of addition of oxygen to the solution containing Fe on E_{corr} and i_{corr}. Note that both E_{corr} and i_{corr} increase as a result of aeration.

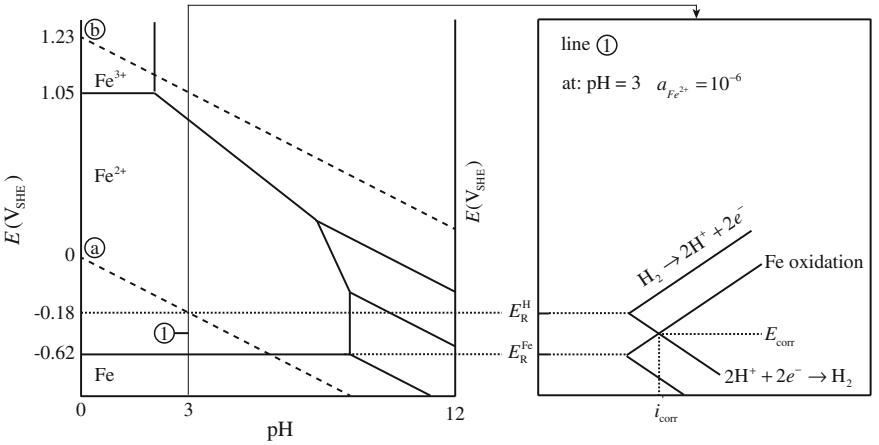

Fig. 15.27 Association between Pourbaix and polarization diagrams in the active region for iron

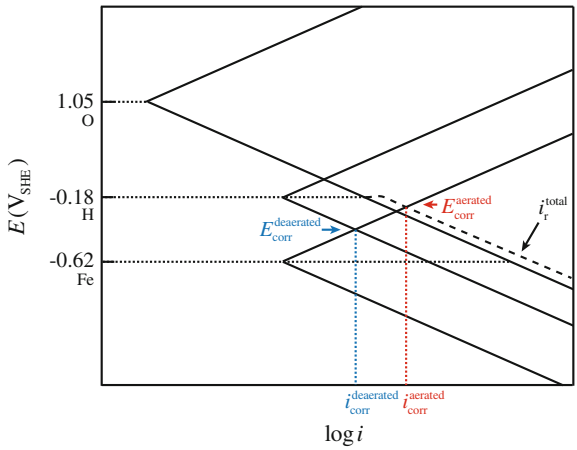

Fig. 15.28 Effect of multiple reduction reactions on the corrosion of iron in acid

15.4.5 Other Types of Polarization

Two other types of polarization of importance in alloys used in reactor systems are concentration polarization and resistance polarization. Consider the evolution of hydrogen at an electrode. At low reduction rates, the distribution of hydrogen ions in the solution adjacent to the electrode surface is relatively uniform. But at very high reduction rates, the region adjacent to the electrode surface will become depleted of H^+ ions. Further increases in the reduction rate will be limited by the diffusion rate of hydrogen ions to the electrode surface. The limiting rate is the limiting diffusion current density, i_L. The same can be true for anodic dissolution where the rate of removal of anodic products (dissolved cations) does not increase

proportionally with the dissolution current and a disproportionate anodic overpotential is required to further increase the rate of dissolution.

The situation is one where the charge transfer reaction is in virtual equilibrium, but the interfacial concentration, C, of the electron acceptor M^{n+} is not the bulk value, C_0, but $C < C_0$. If a current is passing through the interfaces, what is the potential difference across the interface? For solutions near equilibrium (no activation polarization), the current is zero and the potential difference across the interface is given by the Nernst equation:

$$E_e = E^0 + \frac{RT}{nF} \ln\, C_0. \tag{15.55}$$

What concentration should be used in Eq. (15.55) for the potential corresponding to a current density of i? It cannot be C_0 because we know that $C < C_0$, so:

$$E = E^0 + \frac{RT}{nF} \ln\, C. \tag{15.56}$$

This says that the passage of current has made the potential depart from the zero current value, E_e. Thus, $E - E_e$ is a potential difference produced by a *concentration change* at the interface and is known as the concentration overpotential, η_{conc}. The rate of dissolution is i/nF and, from Fick's second law, is equal to $(D[C - C_0])/\delta$, where D is the diffusion coefficient, C and C_0 are the ionic concentrations in the electrode surface and in the bulk, respectively, and δ is the thickness of the diffusion layer. From the Nernst equation, the overpotential, or polarization arising from concentration effects, η_{conc}, is as follows:

$$\eta_{conc} = E - E_e = \frac{RT}{nF} \ln \frac{C}{C_0}, \tag{15.57}$$

and since:

$$C = C_0 - \frac{i\delta}{DnF}, \tag{15.58}$$

then:

$$\eta_{conc} = \frac{RT}{nF} \ln \left(1 - i \frac{\delta}{DC_0 nF}\right). \tag{15.59}$$

As $\eta \rightarrow \infty$, the critical limiting or diffusion current density is given by:

$$i_L = \frac{DC_0 nF}{\delta}. \tag{15.60}$$

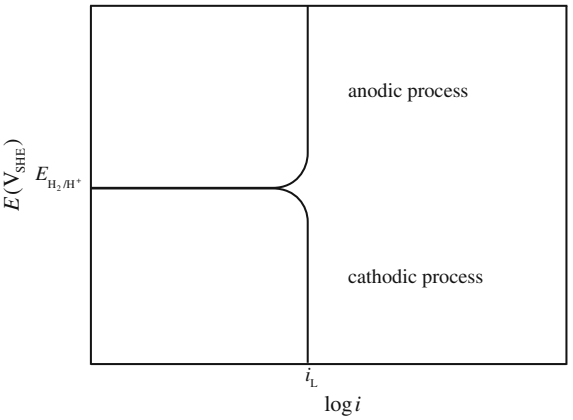

Fig. 15.29 Concentration polarization diagram in the absence of activation polarization

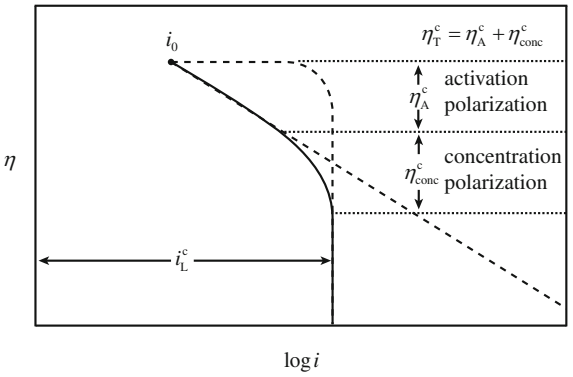

Fig. 15.30 Polarization diagram with combined activation and concentration polarization (after [3])

The potential change resulting from concentration polarization can be expressed as follows:

$$\eta_{\mathrm{conc}} = \frac{2.3\,RT}{nF}\log\frac{i_{\mathrm{L}} - i_{\mathrm{A}}}{i_{\mathrm{L}}}, \tag{15.61}$$

where i_A is the externally applied current density. The limiting current density is shown in Fig. 15.29 in the absence of activation polarization. Note that when $i_A = i_L$, $\eta \to \infty$, and when $i_C = i_L$, $\eta \to -\infty$. Usually, activation and concentration polarization both occur at an electrode. At low reaction rates, activation polarization controls, while at high reaction rates, concentration polarization becomes controlling. The total polarization of the electrolyte is the sum of the contributions of activation and concentration polarization, as shown in Fig. 15.30. The total anodic and cathodic polarization is then the sum of Eq. (15.61) and either Eq. (15.51) or Eq. (15.52):

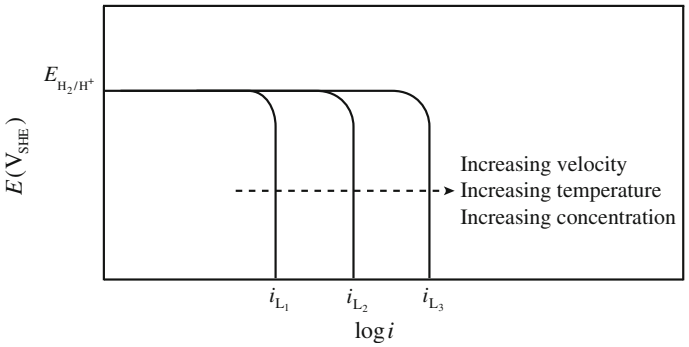

Fig. 15.31 Effect of different solution conditions on the limiting current density in concentration polarization (after [3])

$$\eta_A^T = \frac{2.3\,RT}{(1-\beta)nF}\log\frac{i}{i_0} + \frac{2.3\,RT}{nF}\log\frac{i_L^A - i}{i_L^A}$$
$$\eta_C^T = -\frac{2.3\,RT}{\beta nF}\log\frac{i}{i_0} - \frac{2.3\,RT}{nF}\log\frac{i_L^C - i}{i_L^C}. \tag{15.62}$$

The limiting current density is a function of agitation, temperature, concentration, and position of the anode, as shown in Fig. 15.31. Consider a metal immersed in a corrosive system in which the reduction process is under diffusion control as illustrated in Fig. 15.32(a). Note that with increasing solution velocity (agitation), the corrosion rate increases up to point D. However, as velocity is increased further, the reduction reaction becomes activation-controlled. As a consequence, the corrosion rate becomes independent of velocity at very high velocities as in Fig. 15.32(b).

Resistance polarization is the third type of polarization that can occur on electrodes in aqueous solution. An electrolyte through which a current is passing will contribute to the overpotential by a factor:

$$\eta_R = i_A \times R, \tag{15.63}$$

where i_A is the current density, R is the resistance of the path travelled by the current ($\rho L/A$), ρ is the solution resistivity, L the path length, A the area, and η_R is the resistance polarization, otherwise known as the *IR* drop as in Fig. 15.33. The IR drop may be high in poorly conducting electrolytes or in cases where a film forms. Bubbles and cavities also add to resistance. The total overpotential is then as follows:

$$\eta_T = \eta_A + \eta_{conc} + \eta_{R.} \tag{15.64}$$

The shape of the polarization curve is then more complicated as it is composed of three separate effects: activation energy requirements, concentration effects, and

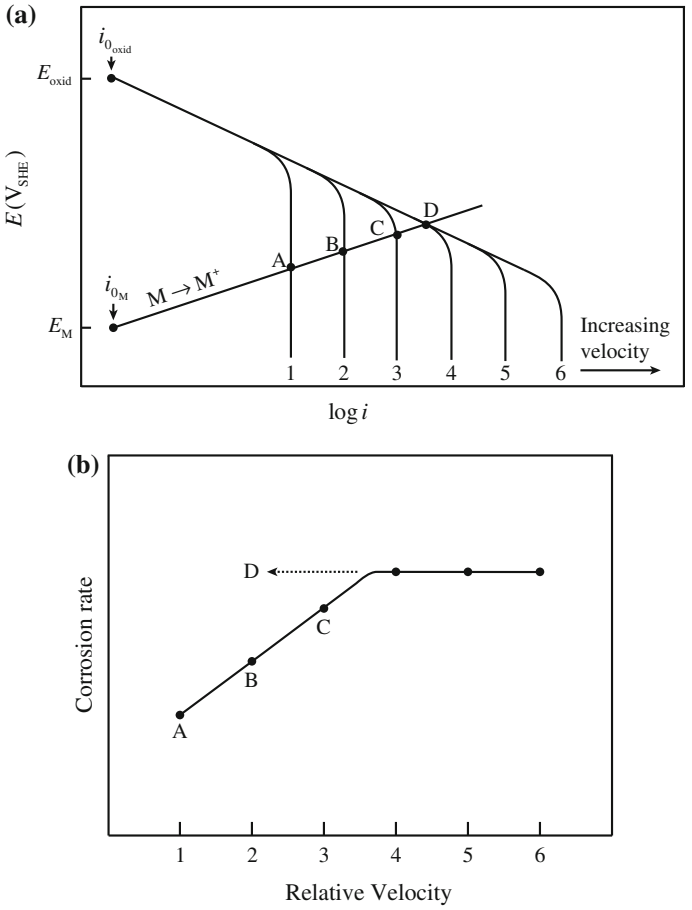

Fig. 15.32 Effect of solution velocity on (**a**) electrochemical behavior and (**b**) corrosion rate of an *active* metal corroding with a diffusion-controlled cathodic process (after [3])

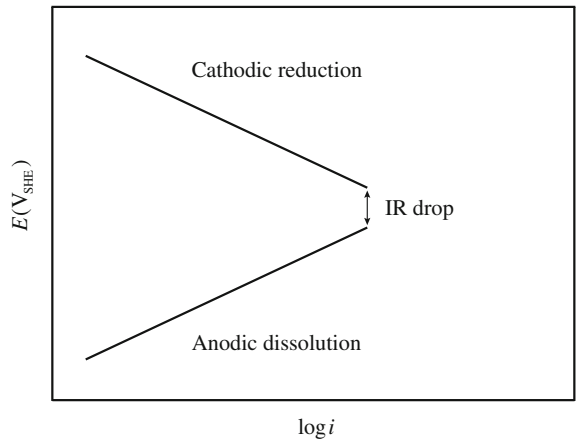

Fig. 15.33 IR drop between sites of cathodic and anodic reactions

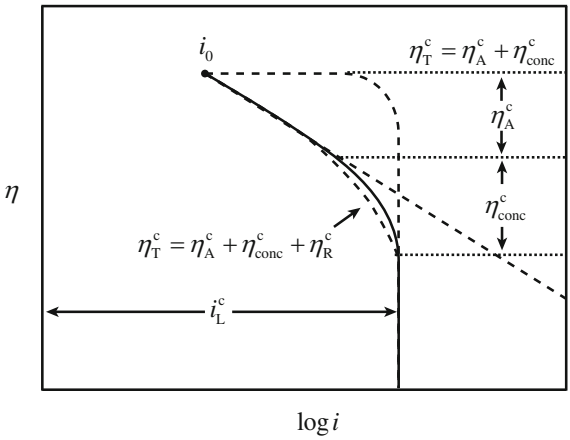

Fig. 15.34 Polarization diagram with combined activation, concentration, and resistance polarization

resistance effects. Figure 15.34 shows the makeup of the total overpotential by the three contributions.

Both resistance of the electrolyte and polarization of the electrodes limit the magnitude of current produced by a galvanic cell. When polarization occurs mostly at the anode, the corrosion reaction is anodically polarized as in Fig. 15.35(a). When polarization occurs mostly at the cathode, the corrosion rate is cathodically controlled as in Fig. 15.35(b). Resistance polarization controls the total polarization when the electrolyte resistance is so high that the resultant current is not sufficient to polarize either the anode or cathode. Figure 15.35(c) shows the case in which the corrosion current is controlled by the IR drop through the electrolyte. However, mixed control occurs when polarization occurs to some degree at both the anode and cathode as in Fig. 15.35(d). If the anodic area of the corroding metal is small (say due to a porous film), there may be considerable anodic polarization accompanying corrosion even though measurement shows that the unit area of bare anode polarizes only slightly at a given current density. Figure 15.36 shows the case where the area of the anode is half that of the cathode.

In corrosion of zinc amalgam (Zn + Hg) in acid chloride, Hg is polarized to nearly the corrosion potential of Zn. Mercury atoms act as cathodes, and Zn atoms act as anodes. The corrosion reaction is controlled almost entirely by the rate of hydrogen evolution at the cathodic areas resulting in a polarization diagram shown in Fig. 15.37. So the high hydrogen overvoltage of Hg limits the corrosion rate of amalgams in non-oxidizing acids.

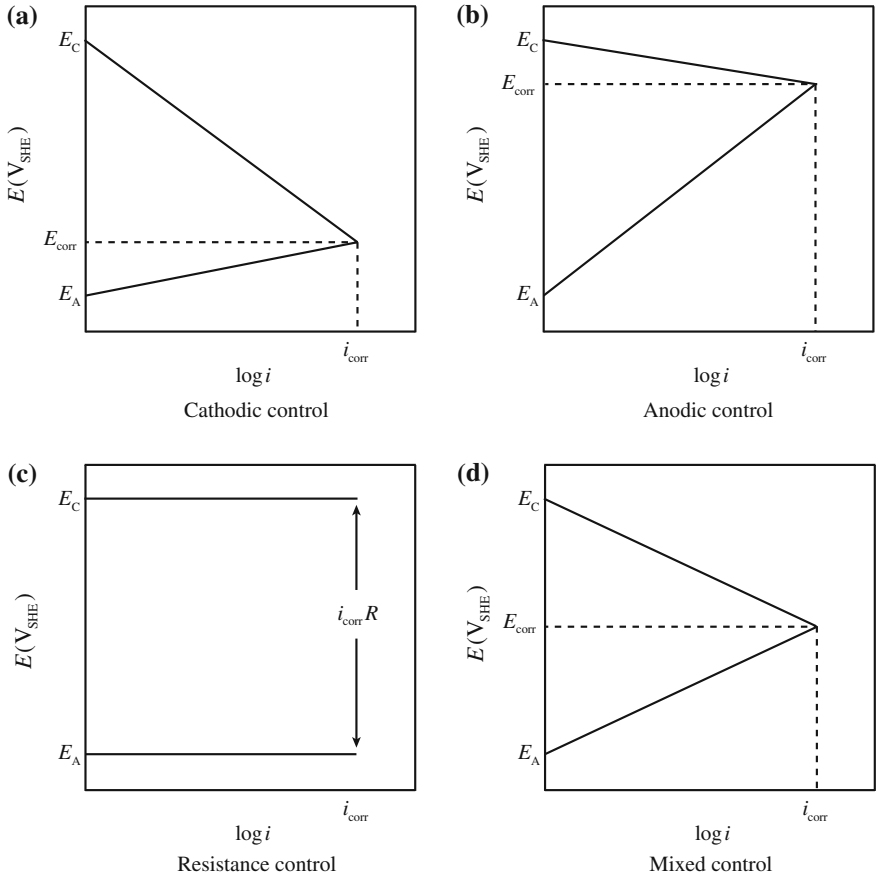

Fig. 15.35 Polarization of Zn in dilute acid occurring (**a**) predominantly at the anode, (**b**) predominantly at the cathode, (**c**) by resistance control, and (**d**) by mixed control (after [4])

15.5 Passivity

A strict definition of passivity does not exist. In an engineering sense, passivity is a state in which the metal is covered with a surface film and the corrosion rate is very low. A metal is considered to be passive if it substantially resists corrosion in a given environment resulting from marked anodic dissolution. A metal is also considered to be passive if it substantially resists corrosion in a given environment despite a marked thermodynamic tendency to react. The polarization diagram for a passivating metal is much different than that for an active metal. Figure 15.38 shows the polarization diagram for a passive metal. As the potential increases above E_{corr}, the rate of metal dissolution increases. The highest rate of corrosion is denoted the critical current density, i_{crit}. The lower portion of the anodic curve exhibits a Tafel relationship up to i_{crit}, which is the current required to generate a sufficiently high

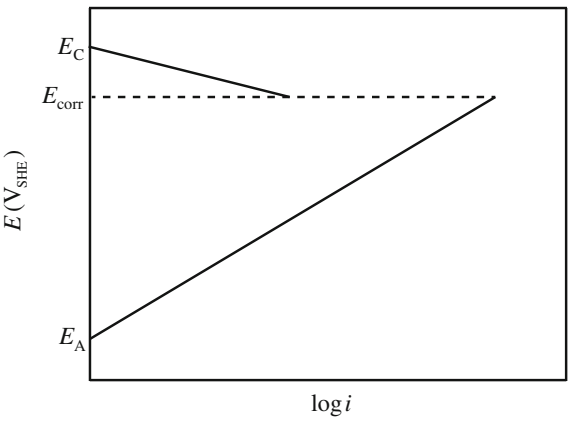

Fig. 15.36 Polarization diagram for the case where the anode area equals one-half of the cathode area (after [4])

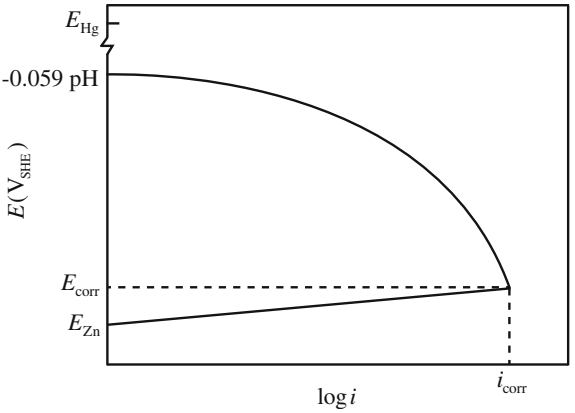

Fig. 15.37 Polarization diagram for zinc amalgam in deaerated HCl (after [4])

concentration of metal ions such that the nucleation and growth of a surface film can proceed. The potential corresponding to i_{crit} is called the primary passive potential (E_{pp}), and it represents the transition of a metal from an active state to a passive state.

Due to the onset of passivity, log i starts to decrease sharply beyond E_{pp} due to the film formation on the metal surface. Log i can drop several orders of magnitude below log i_{crit}. The potential at which the current becomes virtually independent of potential and remains virtually stationary is called the Flade potential (E_F). It represents the onset of full passivity on the metal surface. Actually, it is defined as the potential at which the metal changes from a passive to an active state and is normally not much different from E_{pp} in value.

Flade potential

If a metal is anodically passivated and the applied potential is removed, the potential of the specimen becomes active again. The potential corresponding

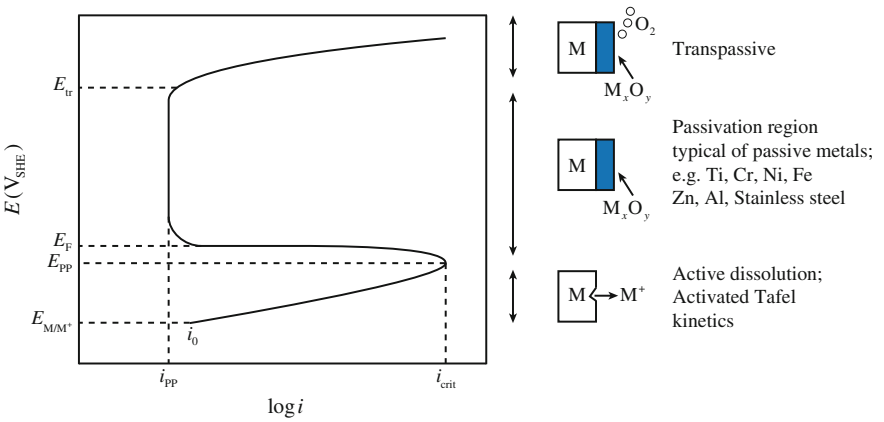

Fig. 15.38 Schematic of active–passive polarization behavior

to the re-establishment of active conditions is called the Flade potential. It is pH dependent:

$$E_F = E_F^0 - 0.059\text{pH},$$

where E_F^0 is the Flade potential at pH = 0. The potential is associated with the dissolution of the protective passive film. The stability of passivity is related to the Flade potential assuming the following anodic reaction:

$$M + H_2O \rightarrow OM + 2H^+ + 2e^-,$$

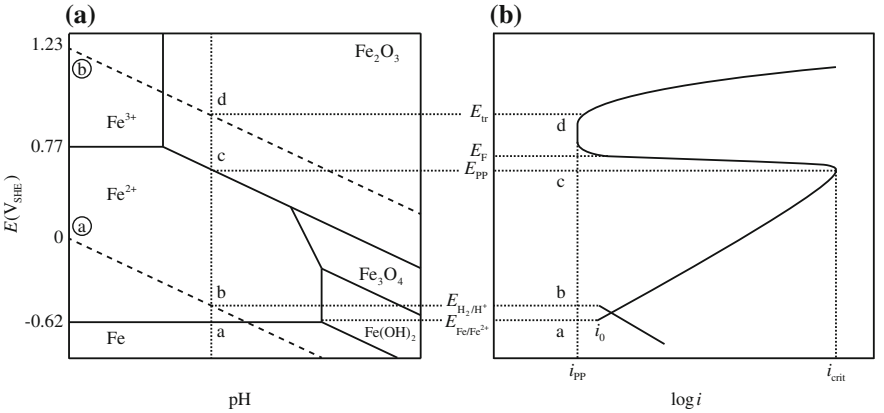

Fig. 15.39 Relationship between (**a**) E-pH diagram and (**b**) polarization diagram for Fe in the passive region

where E_F is the potential for the reaction. Note that for Fe, E_F^0 corresponds closely to the line separating Fe^{++} and Fe_2O_3 in Fig. 15.39. $E_F^0 = 0.63$ V for iron versus −0.20 V for Cr indicating a greater stability of the passive film on Cr.

The minimum current density required to maintain the metal in a passive state is called the passive current density (i_{pp}). At i_{pp}, the metal dissolution occurs at a constant rate. As the potential is increased in the noble direction, the film begins to thicken. According to electric field theory, dissolution proceeds by transport of ionic species through the film under the influence of an electric field. As the potential increases in the noble direction, the film thickens in order to maintain a constant electric field ($\Delta E/x$). Film thickening proceeds by transport of cations, M^{++} outward, and the combination of ions with $O^{=}$ or OH^{-} inward.

According to chemical attack and film reformation theory, the dissolution process is a chemical process and does not depend on potential. The film that is dissolved is immediately replaced by a new film, and a balance is struck between dissolution and reformation. The passive region ends at the point where oxygen is anodically evolved:

$$2H_2O \rightarrow O_2 + 4H^+ + 4e^- \quad \text{(acid)}$$

or

$$4OH^- \rightarrow O_2 + 2H_2O + 4e^- \quad \text{(neutral)}$$

The evolution of oxygen causes a sharp increase in the current. This is the transpassive region, and the potential at which it begins is the transpassive potential (E_{trans}). In some cases, transpassivity may be observed due to the breakdown of the protective film. Perhaps at more noble potentials, the film is not sufficiently protective to keep the metal in the passive state. It may become thicker, unstable, and non-adherent and eventually breakdown. It dissolves as a hydrolyzed cation in a higher oxidation state, for example, when chromium is oxidized from the +3 to the +6 state:

$$Cr^{3+} + H_2O = HCrO_4^-(aq) + 7H^+ + 3e^-.$$

The passivation of a metal can be understood by considering the relationship between the potential–pH diagram and the polarization curve as in Fig. 15.39. Figure 15.39(a) shows the Pourbaix diagram, and Fig. 15.39(b) shows the accompanying polarization plot for iron. As the potential is raised at the pH noted by the dashed vertical line, the dissolution of Fe to Fe^{++} will occur at a potential corresponding to point "a." As the potential is increased, the corrosion current rises as shown in Fig. 15.3(b). At point "c" in the Pourbaix diagram, a stable film, Fe_2O_3, will form, causing the corrosion current to drop significantly. At point "d," water begins to electrolyze. The stable form of oxygen changes from H_2O to O_2:

$$2H_2O \rightarrow O_2 + 4H^+ + 4e^-.$$

This is the anodic reaction above the oxygen line ⓑ. The dissolution is not necessarily increasing in the transpassive region just because the current increases. The current we are measuring occurs as a result of the evolution on O_2 and not the dissolution of Fe metal.

15.5.1 Theories of Passivation

There exist two basic theories of passivation. The dissolution–precipitation mechanism holds that if a metal (e.g., Ni) is immersed in acid (e.g., H_2SO_4) and the potential of the Ni electrode is increased in the positive direction, there occurs a critical potential at which a film of $Ni(OH)_2$ suddenly forms on the surface. However, the film forms negative to the passivation potential and is therefore a precursor or prepassive film. Evidence exists to suggest that the precursor film is an electrical insulator, while the passive film formed above E_{pp} is an electronic conductor. The high conductivity causes a collapse of the potential drop across the film, and without a potential gradient to drive the ions, they do not drift through the film from metal surface to the solution, so dissolution (corrosion) ceases. The evidence to support this mechanism lies in the observation of high rates of O_2 evolution in the transpassive region which requires efficient transfer of electrons from the film to the metal to occur.

The question then arises as to how the film forms? As the dissolution current rises rapidly, the interfacial concentration of dissolved ions reaches the solubility limit and a precipitate forms ($Ni(OH)_2$) in the case of nickel. This is the dissolution–precipitation process for spontaneous passivation. It must be realized that if the current density is low enough, diffusion transports the ions away as they are formed and does not allow their concentration to build up sufficiently for precipitation.

The adsorption theory says that passivation arises from the formation of a monolayer of adsorbed oxygen. The presence of oxygen may, for example, block a kink site in the dissolving metal, lowering the free energy of the initial state of the atom in its dissolution reaction so that it no longer dissolves with the former rate. That is, the exchange current density for dissolution has been reduced several orders of magnitude. In this case, the adsorbed films act as a kinetic limitation reducing the exchange current density i_0, for the dissolution reaction. Uhlig [4] postulated that chemisorbed oxygen is responsible for establishing passivity. Chemisorption of oxygen is favored by the presence of uncoupled d-electrons in the transition metals. In Fe–Cr alloys, Cr acts as an acceptor for uncoupled d-electrons from iron. When alloyed with Cr at concentrations less than 12 %, uncoupled d-electron vacancies in Cr are filled from the excess Fe and the alloy acts like unalloyed iron, which is non-passive in deaerated dilute acid solutions. Above 12 % Cr, the alloys are passive in such solutions because uncoupled d-electrons are available to foster adsorption. During film thickening, metal cations are assumed to migrate into the film from the underlying metal, as well as protons from solution.

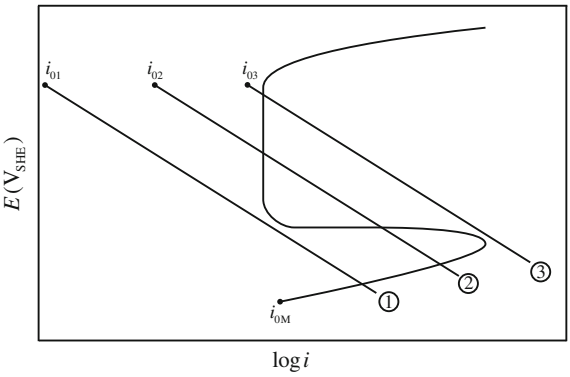

Fig. 15.40 Polarization diagram for an active–passive metal in a corrosive solution

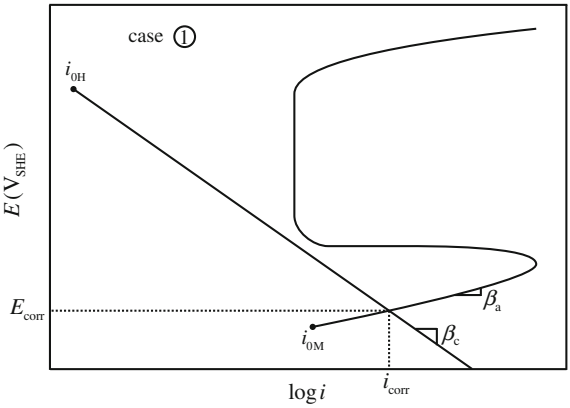

Fig. 15.41 Polarization diagram for case ① in Fig. 15.40 illustrating the condition for corrosion (e.g., stainless steel or Ti in aerated H_2SO_4)

15.5.2 Behavior of an Active–Passive Metal in Acid

Three cases may occur when an active–passive metal is exposed to a corrosive environment, shown in the polarization diagram of Fig. 15.40, and individually in Figs. 15.41, 15.42, and 15.43. In case ① in Fig. 15.40, the cathodic curve intersects the anodic curve in the active region. Figure 15.41 illustrates this case, which would occur for Ti or stainless steel immersed in deaerated H_2SO_4. Note that E_{corr} and i_{corr} occur in the active region and the metal or alloy will corrode rapidly. Case ③ (Fig. 15.42) is one of self-passivation in which SS or Ti is immersed in oxygenated acid. Note that spontaneous passivation will occur, resulting in a higher E_{corr} and a low i_{corr}. From an engineering standpoint, this is a desirable situation. However, note that spontaneous passivation only occurs if the cathodic reaction clears the tip of the anodic nose. The last case, case ② (Fig. 15.43) is one of unstable passivity as there exists three possible intersection points where $i_{ox} = i_{red}$, and three corresponding values of E_{corr}. Point "b" is unstable, and the system may exist in either the "a" (active) or "c" (passive) states.

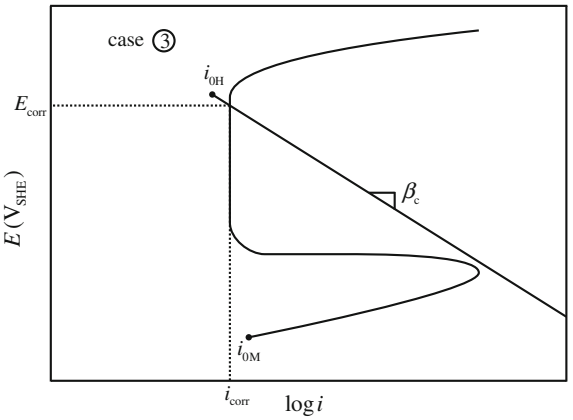

Fig. 15.42 Polarization diagram for case ③ in Fig. 15.40 illustrating spontaneous passivation (e.g., stainless steel or Ti in deaerated H_2SO_4)

15.5.3 Factors Affecting Active–Passive Corrosion Behavior

Several factors can affect the corrosion behavior of an active–passive metal. An increase in the acid concentration or the temperature of the solution results in a decrease in the passive potential range, an increase in the current density, and an increase in the corrosion rate at all potentials as in Fig. 15.44. Increasing the oxidizer concentration increases the potential of the redox half-cell according to the Nernst equation. Figure 15.45(a) shows the effect of increasing the concentration of an oxidizer on the corrosion behavior of an active–passive metal. An increase in concentration from "1" to "2" results in an increase in potential from "A" to "B." At "3," the alloy may exist in either the active "C" or passive "D" states. For concentrations "4–6," the passive state is stable and at "7" and "8," there is a transition to the transpassive state.

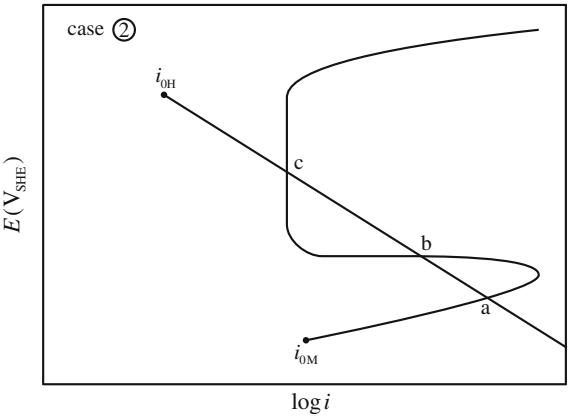

Fig. 15.43 Polarization diagram for case ② in Fig. 15.40 illustrating unstable passivity

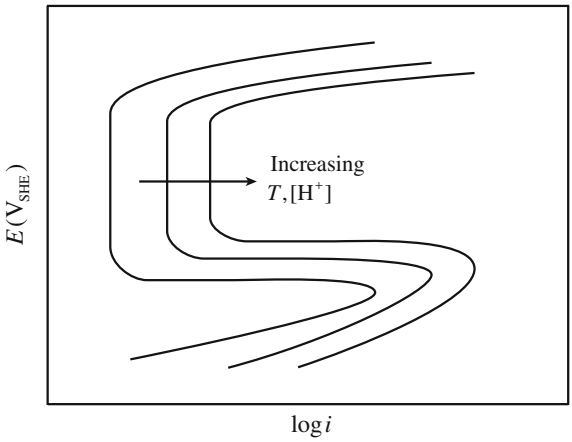

Fig. 15.44 Effect of increasing acid concentration and temperature on passivity (after [2])

Corrosion rate is plotted as a function of concentration in Fig. 15.45(b). In region BCD, either active or passive states may exist, but the film will not form until concentration D is reached. The corrosion rate stays low until the transpassive range is reached. When the process is reversed, the corrosion rate retraces its steps from transpassive to passive. But once the passive film is formed, it is retained at concentrations lower than that needed for its formation. So in region DC'B, we have borderline passivity in which any surface disturbance (scratching) will destabilize the film and corrosion can increase to the active state. This explains the behavior of iron in nitric acid. Immersion of iron into concentrated nitric acid results in the formation of a protective film as in Fig. 15.46(a). If the solution is then changed to dilute nitric acid (Fig. 15.46(b)), nothing happens unless the surface film is disturbed by, say, scratching, which will cause rapid dissolution of the iron sample Fig. (15.46(c)) Note that rapid dissolution in dilute nitric acid will occur if the bare metal sample is immersed directly into the solution since no protective film exists.

An example of the effect of solution agitation is shown in Fig. 15.47 for an active–passive metal corroding in an electrolyte under diffusion control [3]. Curves 1–5 correspond to increases in the limiting diffusion current density with increasing velocity as in Fig. 15.47(a). As the velocity is increased, the corrosion rate increases along the path ABC. When velocity is increased beyond 3, there is a rapid transition from point C in the active region to point D in the passive state. These results are shown in terms of velocity versus corrosion rate in Fig. 15.47(b). The difference in velocity dependence between an active metal (Fig. 15.32) and one demonstrating active–passive behavior (Fig. 15.47) is the result of the unusual dissolution behavior of active–passive metals. This behavior is typical of all active–passive metals that are corroding under diffusion control.

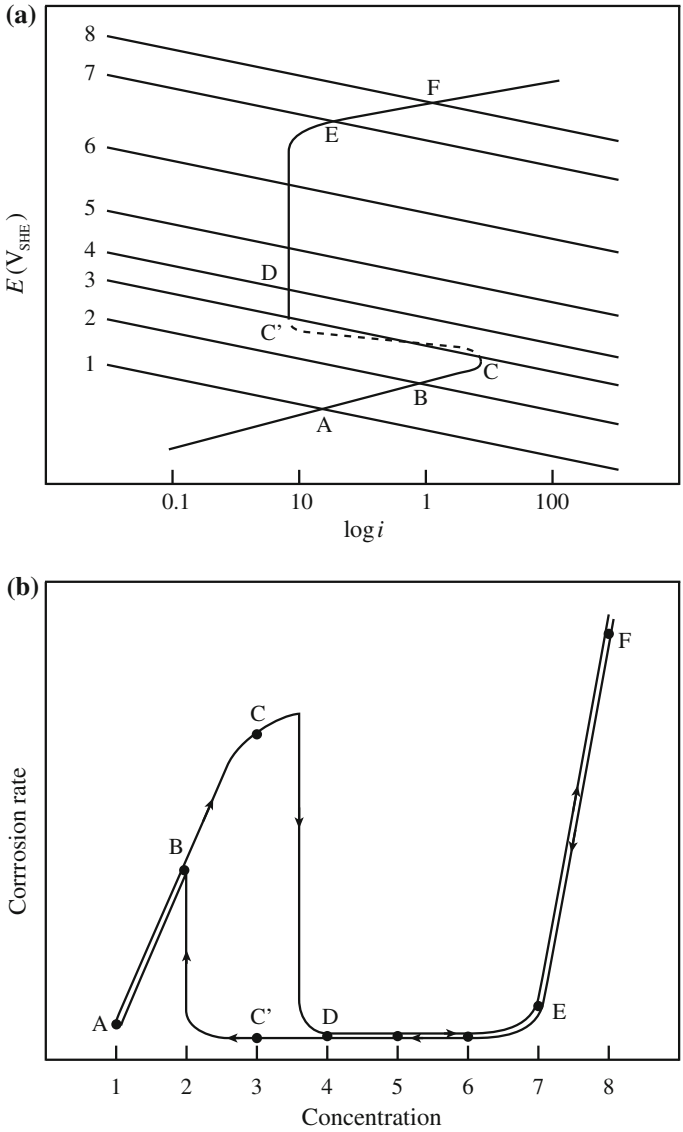

Fig. 15.45 Effect of oxidizer concentration on (**a**) corrosion, and (**b**) corrosion rate of an active–passive metal (after [2])

15.5.4 Control of Passivity

Two general rules can be applied to control passivity. If corrosion is driven by an activation-controlled reduction process, an alloy that exhibits a very active primary passive potential should be selected for use in the environment. This case is

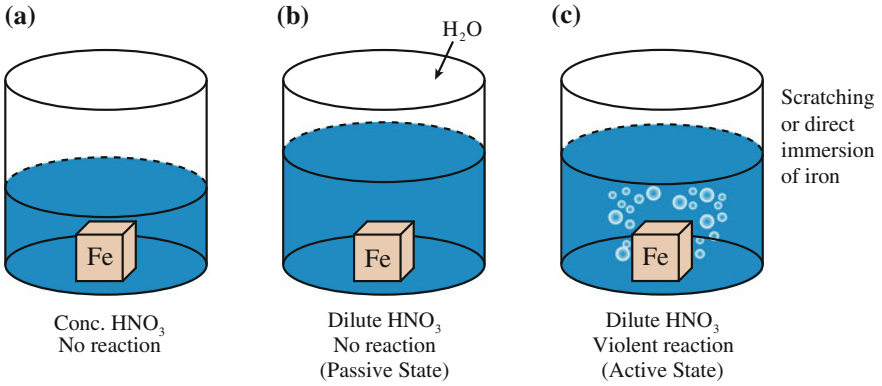

Fig. 15.46 Schematic illustration of Faraday's passivity experiment with iron (after [3])

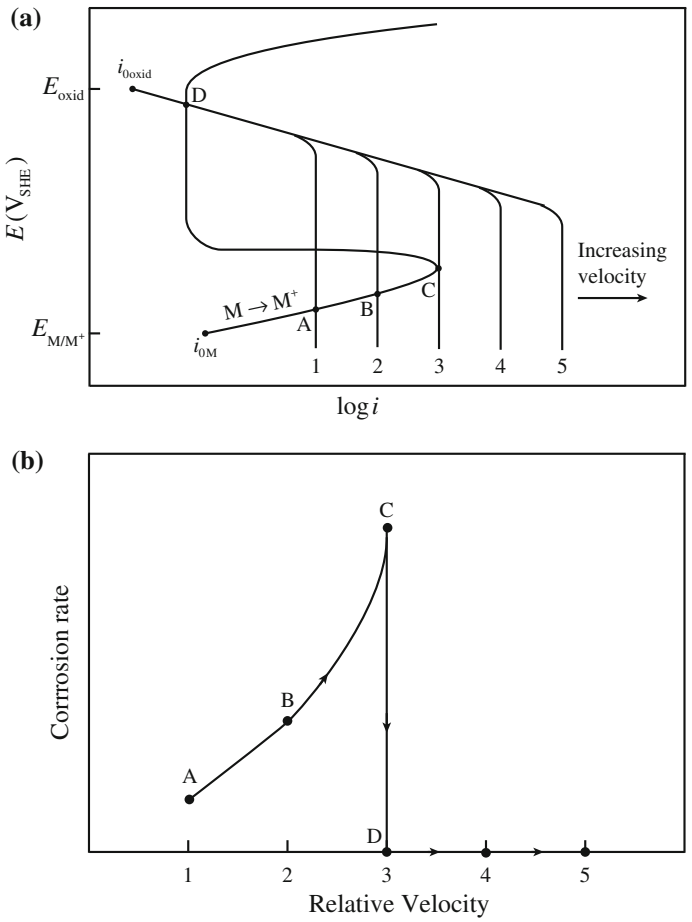

Fig. 15.47 Effect of solution velocity on (**a**) electrochemical behavior and (**b**) corrosion rate of an *active–passive* metal corroding under diffusion control (after [3]) Fontana 10.5 and 10.6

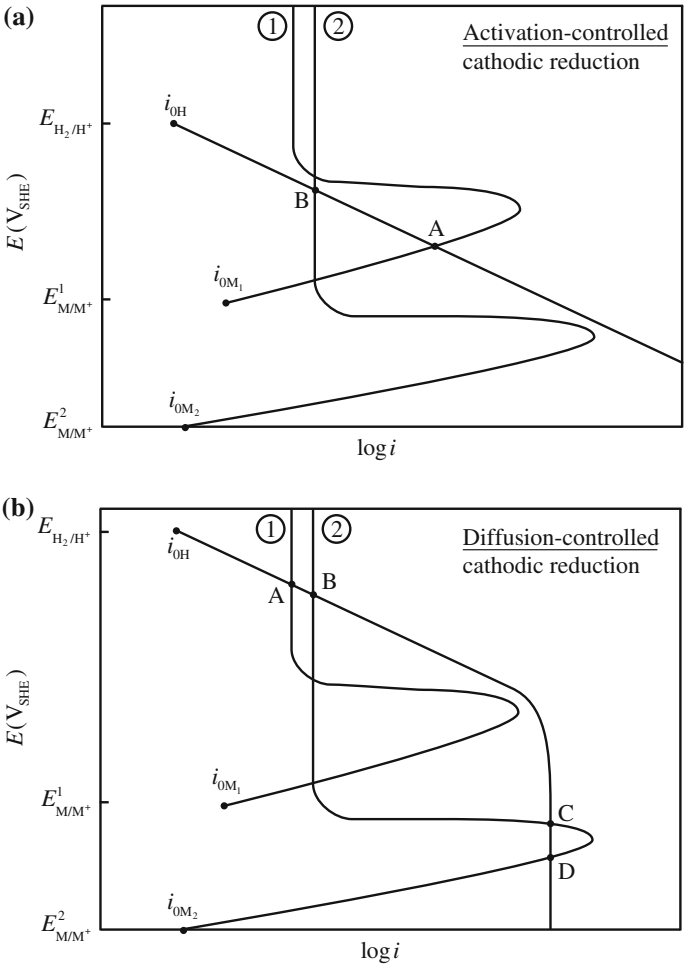

Fig. 15.48 Polarization diagram for (**a**) activation-controlled and (**b**) diffusion-controlled cathodic reduction reaction

illustrated in Fig. 15.48(a) in which alloy ② is the better selection as the corrosion current corresponding to the corrosion potential will be the passivation current which will be low (point "B") compared to that where the corrosion potential is in the active region (point "A"). If the reduction process is under diffusion control, then an alloy with a smaller critical current density is preferable. As shown in Fig. 15.48(b), alloy ① is the better choice.

The tendency for passivation can be increased by alloying additions that decrease i_{crit}. This would include additions such as Mo, Ni, Ta, and Nb to Ti and Cr. The potential of these elements is active, and their corrosion rate is low. Alloying elements that passivate more readily than the base metal will reduce i_{crit} and induce

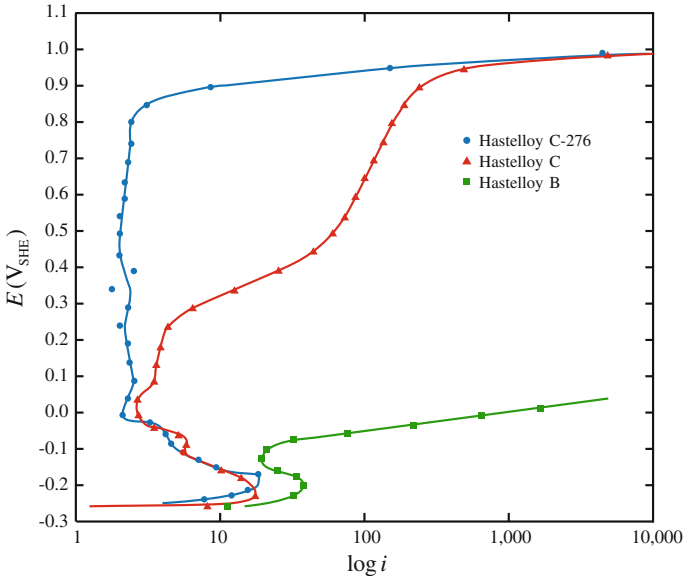

Fig. 15.49 Comparison of potentiostatic anodic polarization of nickel alloys in 1 N H_2SO_4 at ambient temperature (after [2])

passivity. Examples are Cr and Ni additions to Fe, which reduce i_{crit} and increase passivity. Ni additions to Cu (e.g., Cu–10Ni or Cu–30Ni) also promote passivity. An example of the influence of alloying elements is shown in Fig. 15.49 for nickel-base alloys. Hastelloy B is a Ni–25Mo alloy and shows only a hint of passivity. Addition of Cr and Fe at the expense of Mo to form Hastelloy C (Ni–15Cr–15Mo–5Fe) gives a low i_{crit} and an active E_{pp}, but i_{pass} increases steadily in the passive regime. Hastelloy C-276 is essentially the same as Hastelloy C but with very low Si and C levels. The restriction on Si and C reduces precipitation, which adversely affects corrosion at localized sites. Either alloy is acceptable for use in reducing conditions, Hastelloy C is acceptable in moderately oxidizing conditions, and Hastelloy C-276 is required in highly oxidizing conditions.

Consider four alloys (A–D) under three conditions: 1 = reducing, 2 = moderately oxidizing, and 3 = highly oxidizing, as shown in Fig. 15.50. Under reducing conditions (1), alloys A and B have superior corrosion resistance due to lower corrosion rates in the active state without oxidizers. Alloys C and D are passive, but this is unnecessary under reducing conditions and elements that promote passivity, such as Cr, are very expensive. In moderately oxidizing environments (2), alloy C is the obvious choice. Alloy D is borderline passive, and an active state is also possible. Alloy B is passive, but the passive current density is large compared to that for alloy C. In highly oxidizing environments (3), alloy D is best since the reduction curve exceeds the critical current density for passivation and the corrosion

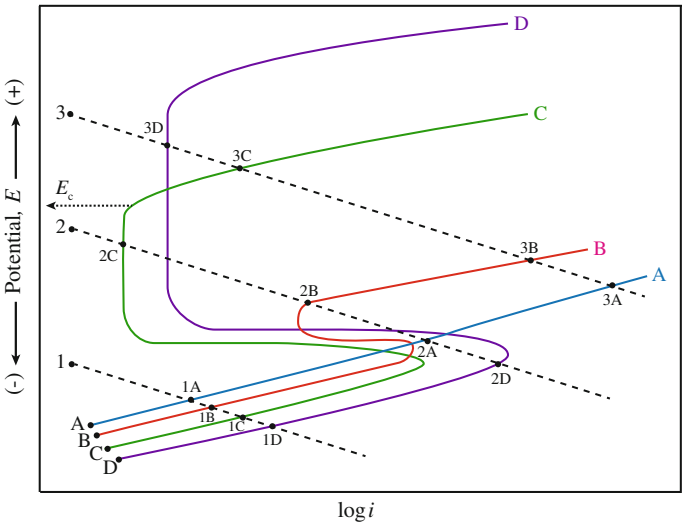

Fig. 15.50 Schematic anodic polarization curves for hypothetical alloys A, B, C, and D, illustrating behaviors in various chemical conditions: *1*—reducing, *2*—moderately oxidizing, and *3*—highly oxidizing (after [2])

rate is low. Passivity breaks down for alloy C at E_c and i_{corr} increases. Neither alloys A nor B have any resistance to corrosion in this environment.

The following rules may be adopted for the behavior of metals and alloys in aqueous media:

1. In the active state, the corrosion rate is proportional to the anodic current density whether or not the alloy is of the active–passive type.
2. The current density for the reduction reaction must exceed the critical current density for passivation, i_{crit}, to ensure a low corrosion rate in the passive state.
3. Borderline passivity in which either the active or the passive state may be stable should be avoided.
4. Breakdown of the passive film in oxidizing conditions due to transpassivity or initiation of localized corrosion should be avoided.
5. The passive state in oxidizing conditions is essential for corrosion resistance, but reasonably small variations in the passive current density may not be significant.

15.5.5 Galvanic Couples of Active–Passive Metals

Consider the coupling of Ti to Pt as shown in the polarization diagram in Fig. 15.51. Upon coupling, Ti spontaneously passivates and its corrosion rate drops to i_{corr}^{Ti-Pt}. Note that this is an exception to the rule that when coupling two metals, the

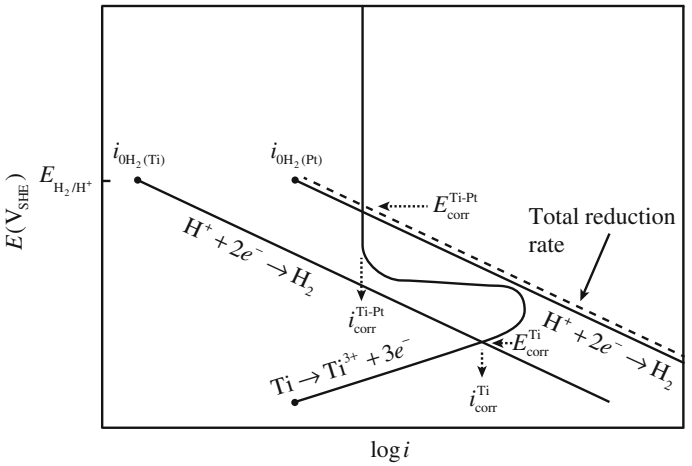

Fig. 15.51 Spontaneous passivation of titanium by galvanically coupling to platinum (after [3])

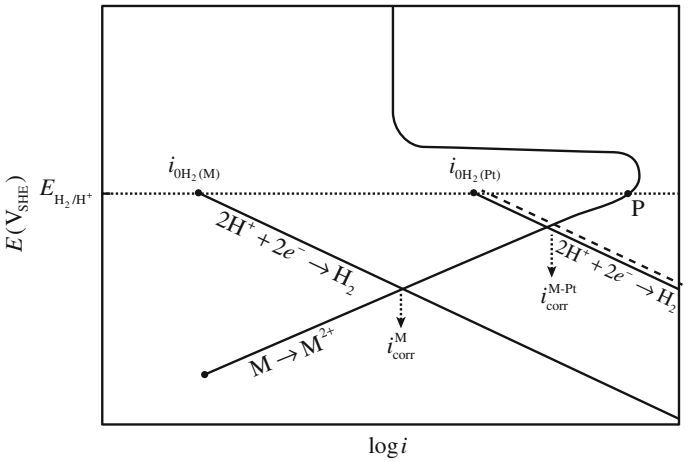

Fig. 15.52 Galvanic couple between an active–passive metal and platinum in deaerated acid (after [3])

corrosion rate of the metal with the most active corrosion potential is accelerated. The behavior in Fig. 15.51 can only occur if the passive region of the metal begins at a potential more active than the reversible potential of the redox system. In fact, only Cr and Ti exhibit this behavior. If the passive range of a metal begins at potentials more noble than the reversible hydrogen potential, coupling to Pt in the absence of oxidizers increases the corrosion rate. An example is the coupling of Fe to Pt in an acid solution as in Fig. 15.52.

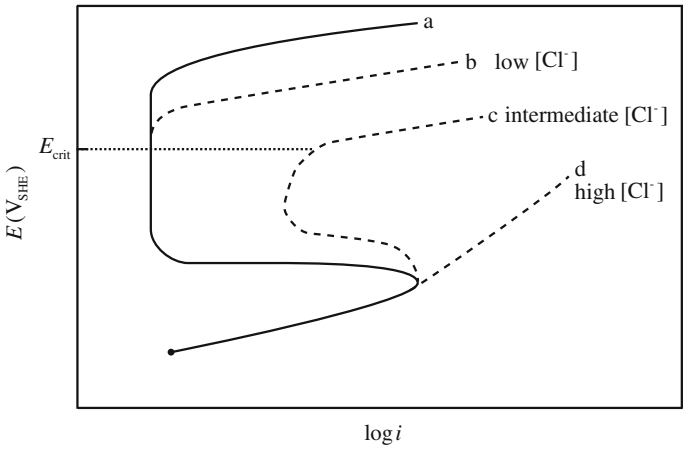

Fig. 15.53 Effect of Cl^- concentration on the polarization behavior of an active–passive metal (after [2])

15.5.6 Pitting of Passive Metals

Chloride ions and, to a lesser extent, other halogens can break down passivity or prevent its formation in Fe, Cr, Ni, Co, and stainless steels. According to the oxide film theory of passivity, Cl^- penetrates the oxide film through pores or defects easier than, e.g., $SO_4^=$. According to the adsorption theory, Cl^- adsorbs on the metal surface in competition with O_2 or OH^- and once in contact, favors hydration of metal ions, thus increasing the ease with which they enter solution. That is, they increase the exchange current for metal dissolution over that with O_2 present. The breakdown occurs locally at preferred sites. These sites become minute anodes surrounded by large cathodes (passive region). The potential difference between the two may reach ~ 0.5 V or more setting up active–passive cells. High current densities at the anode cause high rates of penetration. Note that in the presence of Cl^-, the apparent transpassive region shifts to more active potentials. Actually, this is not transpassive behavior; oxygen is not being evolved, rather there is intense local dissolution. The critical potential decreases with increasing Cl^- concentration until the surface can no longer form a passive film. Figure 15.53 shows the effect of increasing Cl^- concentration on the pitting potential. Note that in this case, the current increase above E_{pit} is *not* due to oxygen, but rather to localized corrosion at the pit.

This raises the question of the significance of a critical potential for pitting (pitting potential, E_{pit}). According to one view, this is the value needed to build up an electrostatic field within the passive or oxide film sufficient to induce Cl^- penetration to the metal surface. The incubation time for pitting is related to the time required for penetration of Cl^- through the oxide film. In terms of the adsorption theory, the metal typically has greater affinity for oxygen than for Cl^-,

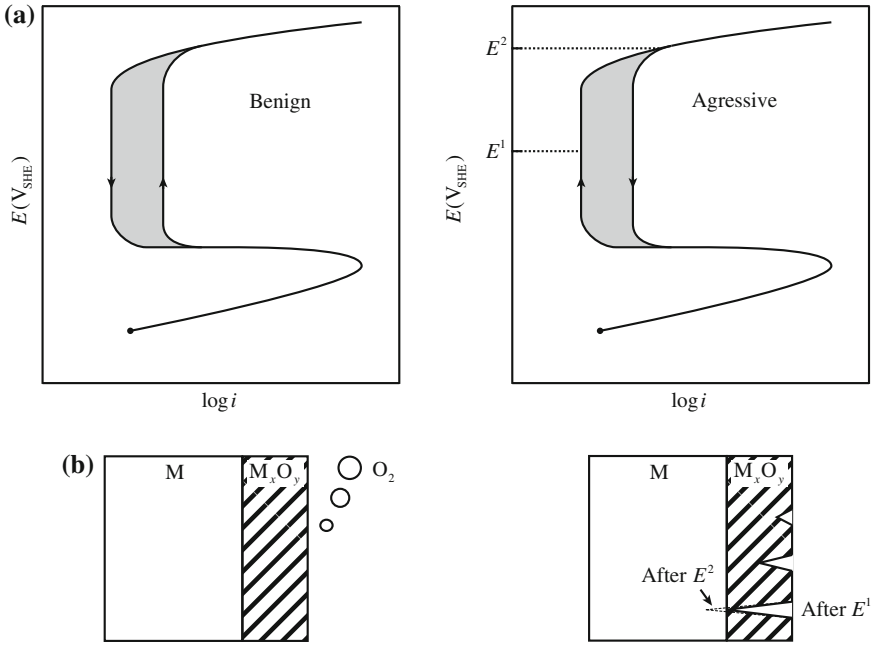

Fig. 15.54 Hysteresis effects in cyclic polarization (**a**) in an acid solution under a spontaneous passivation condition and (**b**) in the presence of Cl^- ions or other halogens

but as the potential is made more noble, the concentration of Cl^- at the surface increases to a value that allows Cl^- to displace oxygen.

The difference between aggressive and benign environments in the polarization behavior of an active–passive metal is illustrated in Fig. 15.54. In an aggressive environment containing Cl^- as in Fig. 15.54(a), pitting occurs at high potential. Upon decreasing the potential, the defective passive film is not as protective, resulting in a higher corrosion current than on voltage ascension. In a benign environment as in Fig. 15.54(b), only oxygen gas is generated at high potential and the stable oxide formed on the way up in potential provides for a lower corrosion current during descending voltage.

Inhibitors can be used to counter the effects of an aggressive environment. As shown in Fig. 15.55, in deaerated acid (non-aggressive condition), the metal is in the active state at E^a_{corr}. In an aerated acid (non-aggressive condition), the more noble corrosion potential, E^b_{corr}, results in a low corrosion current. In an aerated acid with an aggressive (Cl^-) environment, E^c_{corr} is more noble than E_{crit} and pitting occurs. The use of an inhibitor such as $NaNO_3$ for stainless steel in acetic acid (aggressive) displaces the critical pitting potential to more noble potentials such that E_{corr} is in the passive region.

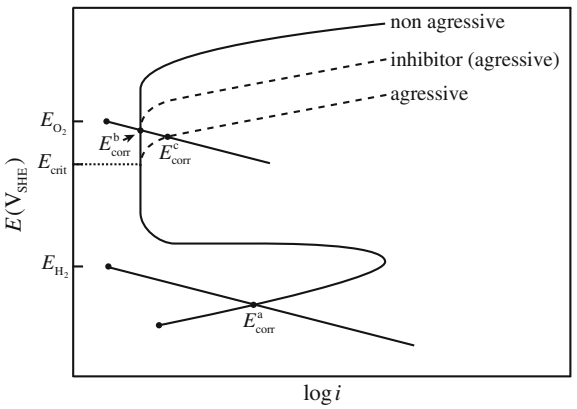

Fig. 15.55 Role of inhibitors on the polarization diagram of an active–passive alloy

15.6 Crevice Corrosion

Crevice corrosion is a form of corrosion that occurs in occluded locations where the solution in the crevice has limited exchange with that outside the crevice. It may be a region in which two metal surfaces are in close proximity but open enough to allow some solution to enter. It can also be in the form of a crack in a metal in which the crack tip is well away from the sample surface and the crack width is small. Crevice corrosion is characterized by intense localized corrosion rates and is usually associated with small volumes of stagnant solutions. In a crevice, the corrosion process consumes the dissolved oxygen, impairing passivity and increasing the concentration of metal ions, which attract negatively charged cations such as Cl^- from the bulk solution. The potential for initiation of crevice corrosion is more active than E_{pit} due to favorable geometric conditions for deaeration and chlorination. This is why any alloy that pits will exhibit crevice corrosion, but not the reverse. Although crevice corrosion can result from a difference in metal ion and oxygen concentrations, more processes are involved.

Consider a riveted metal plate immersed in aerated seawater (pH = 7), Fig. 15.56. The overall reaction is as follows:

$$\text{Oxidation:} \quad M \rightarrow M^{2+} + 2e^-$$
$$\text{Reduction:} \quad O_2 + 4H^+ + 4e^- \rightarrow 2H_2O.$$

Initially, these reactions occur uniformly over the entire metal surface and charge is conserved (Fig. 15.56(a)). After a short time, the oxygen in the crevice is depleted because of restricted access. The consumption of H^+ causes an increase in the pH. In basic environments, the anodic and cathodic reactions are as follows:

$$\text{Oxidation:} \quad M \rightarrow M^{2+} + 2e^-$$
$$\text{Reduction:} \quad O_2 + 2H_2O + 4e^- \rightarrow 4OH^-.$$

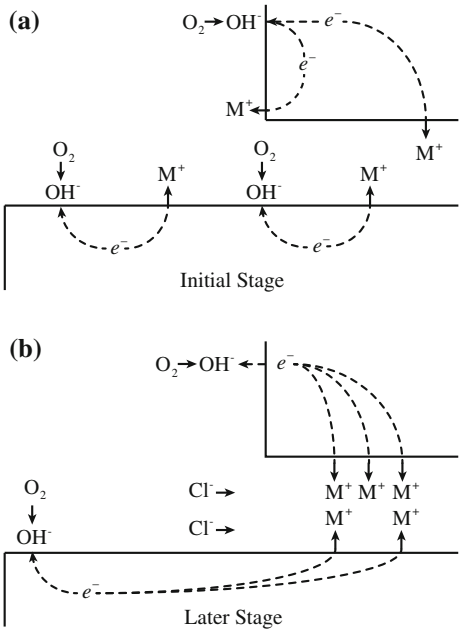

Fig. 15.56 Crevice corrosion (**a**) the initial stage and (**b**) later stage

Due to metal hydrolysis in a basic electrolyte, we have $M^{2+} + 2H_2O \rightarrow M(OH)_2 + 2H^+$ and the pH decreases (Fig. 15.56(b)). In both cases, increased resistance in the crack or crevice due to gas bubbles, for example, leads to an Ohmic drop causing a decrease in potential at the tip of the crack relative to the sample surface by up to several hundred millivolts. The result of these processes is shown in Fig. 15.57 for aerated water in which the crack tip condition is driven to a lower potential and an intermediate pH, both of which are considerably different than those at the sample surface.

As deaeration occurs in the crevice, the reduction reaction can continue, but it will be shifted to the external surface. After a while, the excess positive charge in the crevice due to continued metal dissolution will drive Cl^- migration into the crevice or crack to balance the overall charge. The increased metal chloride concentration hydrolyzes water:

$$M^+Cl^- + H_2O = MOH \downarrow + H^+Cl^-,$$

producing an insoluble hydroxide and a free acid. The pH drops and metal dissolution are accelerated, thus increasing Cl^- migration into the crevice. The process, shown in Fig. 15.57, is autocatalytic and rapidly accelerating.

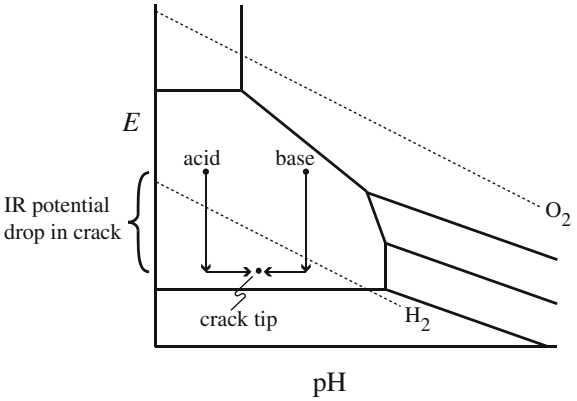

Fig. 15.57 Schematic Pourbaix diagram showing the change in potential and pH of basic and acidic bulk solutions versus the crack tip

15.7 Stress Corrosion Cracking

Stress corrosion cracking is the premature cracking of an alloy in the presence of a tensile stress and a corrosive environment. Historically, SCC was believed to occur only when three conditions were fulfilled: a susceptible alloy, a specific environment, and a tensile stress. In practice, most alloys are susceptible to SCC over a range of environments. The term *alloy* should be interpreted broadly so as to incorporate commercially pure metals since SCC is known to be a strong function of impurity content of pure metals. Similarly, the environment needs to be broadly interpreted to potentially all environments other than noble gases, since many gases, aqueous solutions, and liquid metals can promote SCC. The distinguishing characteristic of SCC is the requirement of a stress. While localized corrosion can occur in a stress-free environment, SCC can only occur with the imposition of a tensile stress. Figure 15.58 shows a stress–strain curve for an alloy in an inert environment compared to one in which the alloy is susceptible to stress corrosion cracking. SCC reduces the strain to failure as well as the maximum stress. Cracking may be either transgranular (TG) (e.g., 304 stainless steel in boiling $MgCl_2$ at 154 °C) or intergranular, IG (e.g., 304 stainless steel in 288 °C water as in Fig. 15.59). Typically, when the general corrosion rate is high, SCC susceptibility is low, and when the general corrosion rate is low, the SCC susceptibility is high.

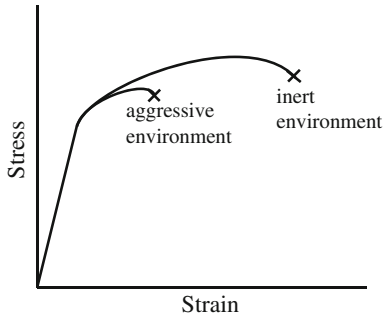

Fig. 15.58 Effect of the environment on stress–strain behavior of metals undergoing stress corrosion cracking

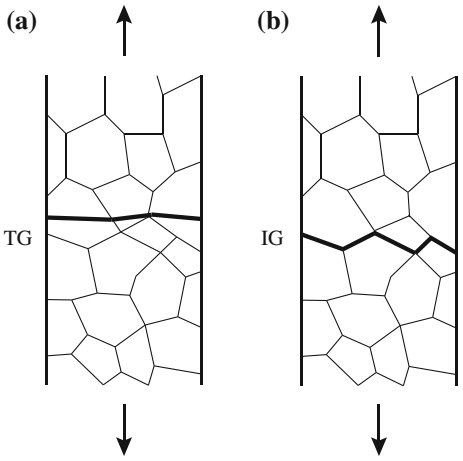

Fig. 15.59 Schematic illustrations of (**a**) transgranular stress corrosion cracking and (**b**) intergranular stress corrosion cracking

A distinction is often made between stress corrosion cracking, hydrogen embrittlement, and corrosion fatigue. Stress corrosion cracking is used here to refer to the broad category of cracking in a metal or alloy due to chemical or electrochemical processes involving the combination of environment and stress. In this context, hydrogen produced by the corrosion reaction is a form of stress corrosion cracking, yet hydrogen absorption from the gaseous state is not. SCC is often distinguished from corrosion fatigue by constant or monotonically increasing loading versus cyclic loading. Corrosion fatigue and hydrogen embrittlement will be discussed later in the chapter.

Stress corrosion cracking often exhibits some of the following characteristics [5]:

- Localization of damage is in the form of TG or IG cracks;
- Some of the most susceptible alloys are often very corrosion resistant (e.g., the corrosion rate of stainless steel in boiling $MgCl_2$ is essentially zero, but it is highly susceptible to TGSCC);
- Resistance to SCC depends on alloy composition;
- SCC exhibits a strong dependence on microstructure;
- Alloys that are ductile in an inert environment fail in a brittle manner; and
- Cathodic polarization mitigates the initiation of SCC.

Stress corrosion cracking often takes some time to occur, requiring an incubation period. Following initiation, cracks propagate at a slow rate until the stresses in the remaining ligament exceed the fracture stress and failure occurs due to overload. The SCC process is often characterized by the following stages:

- Crack initiation followed by stage 1 propagation;
- Stage 2 or steady-state crack propagation; and
- Stage 3 crack propagation or final failure.

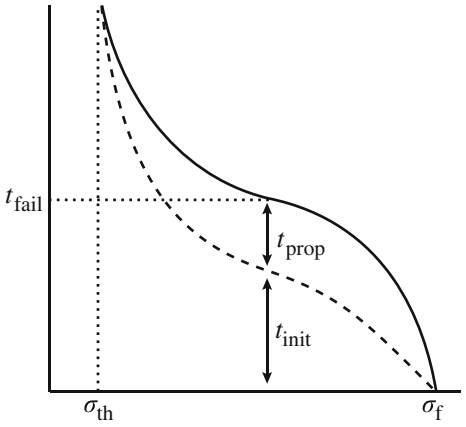

Fig. 15.60 Failure time as a function of stress for an alloy undergoing stress corrosion cracking. Failure time is the sum of the crack initiation time and the crack propagation time

However, not all alloys exhibit these stages or the stages may not be distinct or easily identifiable. To distinguish and quantify these stages of fracture, various SCC tests have been developed and are briefly summarized here.

15.7.1 SCC Tests

Stress corrosion cracking tests fall into three basic categories: static loading of smooth samples, static loading of precracked samples, and slow strain rate testing. Static loading of smooth samples provides the time to failure as a function of applied stress as the measure of the degree of stress corrosion cracking susceptibility. Figure 15.60 shows a plot of the time to failure versus stress for an alloy undergoing stress corrosion cracking. The minimum stress at which failure occurs is known as the threshold stress, σ_{th}, for SCC. The failure time includes both the initiation time, t_{init}, and the propagation time, t_{prop}, so that $t_{fail} = t_{init} + t_{prop}$. This test is useful for determining the maximum stress that can be applied without SCC failure in a specific environment. Examples of this test are the C-ring, U-bend, and the O-ring tests as shown in Fig. 15.61. In these tests, the sample is stressed to a fixed deflection and then held at that displacement for the duration of the test. In this mode, stress relaxation can occur so that the stress will decrease as the test progresses. As such, fixed load tests have been developed in which the load remains constant for the duration of the test.

In static loading of precracked samples, a constant load or fixed crack opening displacement is applied to a sample with a precrack such as a compact tension (CT) or a double cantilever beam (DCB) specimen. The crack length is measured as a function of time, yielding a crack propagation rate (or crack velocity) that can be described as a function of the stress intensity, K. Figure 15.62 shows a plot of a da/dt versus K curve in which the three stages of cracking are shown. As discussed in Chap. 14, K is a

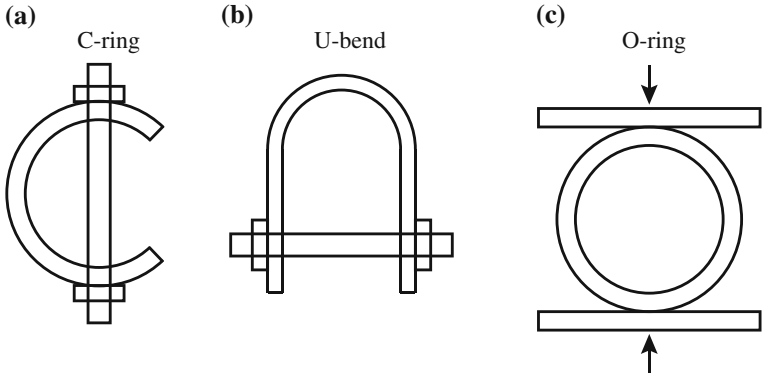

Fig. 15.61 Common constant deflection tests used to assess the relative susceptibility of an alloy to stress corrosion cracking; (**a**) C-ring, (**b**) reverse U-bend, and (**c**) O-ring

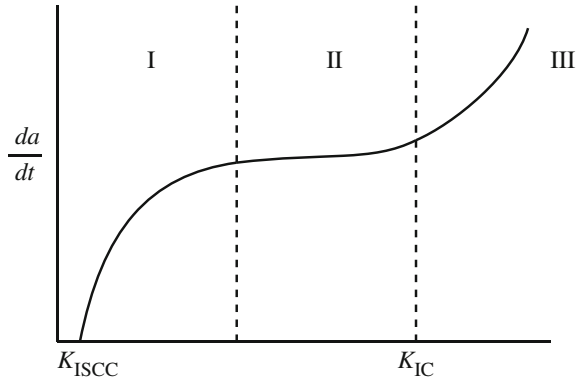

Fig. 15.62 Crack growth rate as a function of the crack tip stress intensity. Note that region II is independent of stress intensity, indicating the effect of the aggressive environment

function of applied stress, specimen geometry, and the square root of crack length. In the absence of a corrosive environment, fracture occurs when $K \geq K_{Ic}$, the plane strain fracture toughness. The effect of the corrosion environment is to lower the value of K at which cracking occurs. The existence of the plateau characteristic of stage II cracks is due to the environment. That is, in the regime where the environment has a strong impact, crack velocity is independent of the stress intensity factor.

The slow strain rate test involves the application of a slowly increasing strain, usually by applying a constant displacement rate, on a smooth bar or precracked sample. The ductility in the corrosive environment is a measure of SCC susceptibility and is plotted against the strain rate and can be compared with that in an inert environment (Fig. 15.63). As shown, various measures can be used to indicate susceptibility, such as strain to failure, reduction in area, fracture energy, or percent of the fracture surface that is due to SCC (TG or IG). Stress corrosion cracking susceptibility is manifest in a reduction in ductility at lower strain rates since there

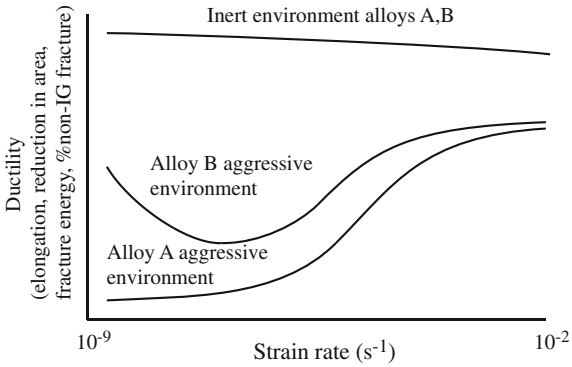

Fig. 15.63 Strain rate dependence of various measures of ductility. Alloys with no environmental effect have minimal strain rate dependence. In an aggressive environment, low strain rates are the most aggressive and cause the greatest reduction in ductility (after [5])

is sufficient time for the environment to induce SCC. As the strain rate rises, the time available for corrosion is reduced and the ductility approaches that in an inert environment. At very low rates, ductility can also increase as the strain rate is too slow to keep up with the effect of the environment. Known as constant extension rate tensile (CERT) or slow strain rate tensile (SSRT) tests, these tests are excellent indicators of the relative susceptibility of alloys to cracking in an environment, or for studying the influence of metallurgical variables. However, since they combine both the initiation and propagation stages, they are not as effective in determining the initiation stage, which is how they have traditionally been used. In most cases, they are effective in evaluating moderate to severe SCC.

15.7.2 SCC Processes

Specific mechanisms of SCC will be discussed later, but it is instructive here to consider the basic processes behind these mechanisms. Many proposed mechanisms are based on either anodic or cathodic processes, but some are purely chemical oxidation. Figure 15.64 illustrates some of the mechanisms proposed for stress corrosion crack growth. A mechanism must explain the actual crack propagation rates, fractographic features, and the formation of cracks. Atomistically, this amounts to explaining how atomic bonds are broken, which is believed to occur by either chemical oxidation or chemical solvation and dissolution or mechanical fracture (ductile or brittle). Ultimately, mechanical fracture is assumed to be stimulated or induced by interactions between the material and the environment. Certain processes or events must occur for sustained crack propagation to be possible. The potential rate-determining steps include [5]:

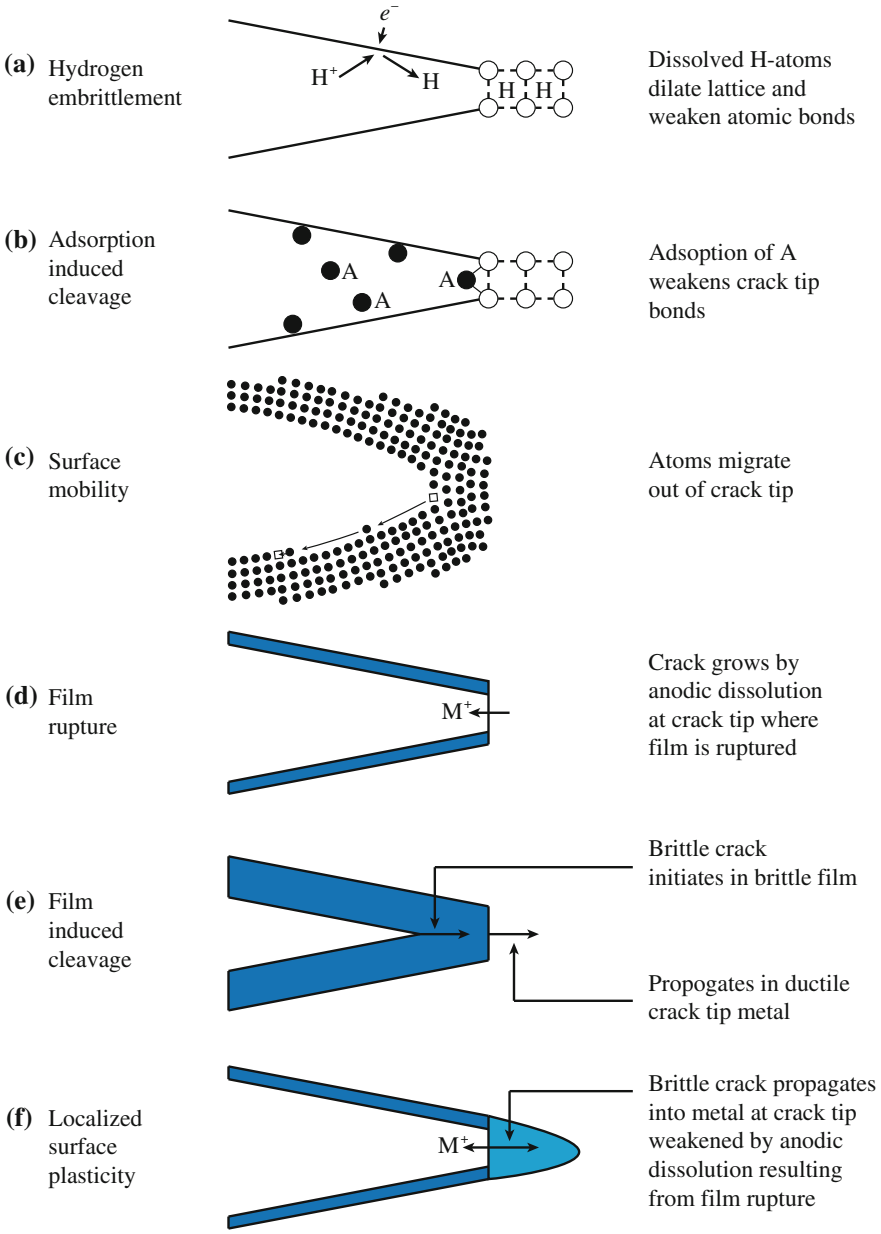

Fig. 15.64 Schematic illustration of crack tip processes that may be occur during environmentally assisted crack propagation (after [2])

- Mass transport along the crack to the crack tip;
- Reactions in the solution near the crack;
- Surface adsorption at or near the crack tip;
- Surface diffusion;
- Surface reactions;
- Adsorption into the bulk;
- Bulk diffusion to the plastic zone ahead of the crack tip;
- Chemical reactions in the bulk; and
- Rate of interatomic bond rupture.

In addition to these processes, the passivation of the surface layer by a protective oxide is an important process that can strongly affect stress corrosion cracking. Environmental parameters that affect crack propagation in aqueous solutions include:

- Temperature;
- Pressure;
- Solute species;
- Solute concentration and activity;
- pH;
- Electrochemical potential;
- Solution viscosity; and
- Agitation/flow rate.

An important factor in the cracking process is that the environment in occluded sites such as a crack tip can differ significantly from that in the bulk solution. If an alteration to the bulk environment allows the formation of a critical SCC environment at the crack nuclei, then crack propagation will result. If the bulk cannot maintain this local crack tip environment, then crack propagation will be retarded. SCC propagation rates are also influenced by a variety of mechanical and metallurgical factors, such as:

- The magnitude of the applied stress or the stress intensity factor, *K;*
- Stress state: plane stress versus plane strain;
- Loading mode at the crack tip;
- Alloy composition (nominal and local);
- Metallurgical condition (second phases in the grain boundary and matrix, phase composition and shape, grain size, grain boundary segregation, strength level, residual stress); and
- Crack geometry (length, aspect ratio, crack opening).

15.7.3 Metallurgical Condition

As stated earlier, pure metals are much less susceptible to SCC than alloys or commercial purity metals [2]. However, “pure” may mean 99.9999 % or better, so it

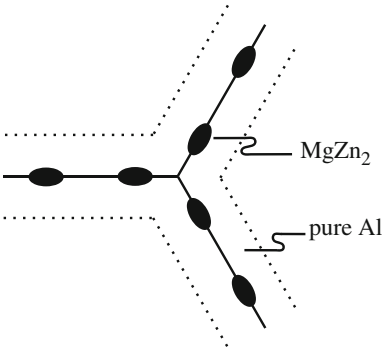

Fig. 15.65 Formation of $MgZn_2$ and depletion of Mg and Zn from the grain boundary, leading to a weak grain boundary and intergranular stress corrosion cracking in an aluminum alloy

is a very subjective term. Conversely, grain boundary chemistry and structure often play significant roles in SCC. Intergranular cracking of high purity iron is due to grain boundary impurities. Aluminum alloy 7075 (Al–Zn–Mg) fails intergranularly in chlorides and halides due to grain boundary depletion of magnesium and zinc caused by precipitation of $MgZn_2$ at the boundary (Fig. 15.65). The $MgZn_2$ phase dissolves preferentially, leaving holes in the grain boundary, and the weak aluminum bridges rupture mechanically.

The strong dependence of cracking in Fe–18Cr–xNi alloys on the nickel content in pure water or 0.1 % NaCl at high temperature is an example of the effect of bulk alloy content on SCC. The greatest susceptibility to IGSCC in pure water occurs at high concentrations of Ni (>70 wt%) and in 0.1 % NaCl at both high (IGSCC) and low (TGSCC) concentrations of Ni as in Fig. 15.66. Grain size can influence SCC, with susceptibility increasing with grain size. As grains become larger, dislocation pileups at grain boundaries become longer, producing higher local stresses and strains (according to the Hall–Petch relation), and higher susceptibility to SCC (Fig. 15.67).

15.7.4 Crack Initiation and Crack Propagation

The stress corrosion cracking process is often subdivided into initiation and propagation stages. Common sites for SCC crack initiation are as follows:

- Preexisting or corrosion-induced surface features such as grooves and burrs;
- Corrosion-induced pits;
- Intergranular corrosion or slip-dissolution processes. Intergranular corrosion-initiated SCC requires differing local grain boundary chemistry (e.g., sensitized stainless steels for grain boundary segregation). Slip dissolution-initiated SCC requires local corrosion at emerging slip planes in primarily, low stacking fault materials.

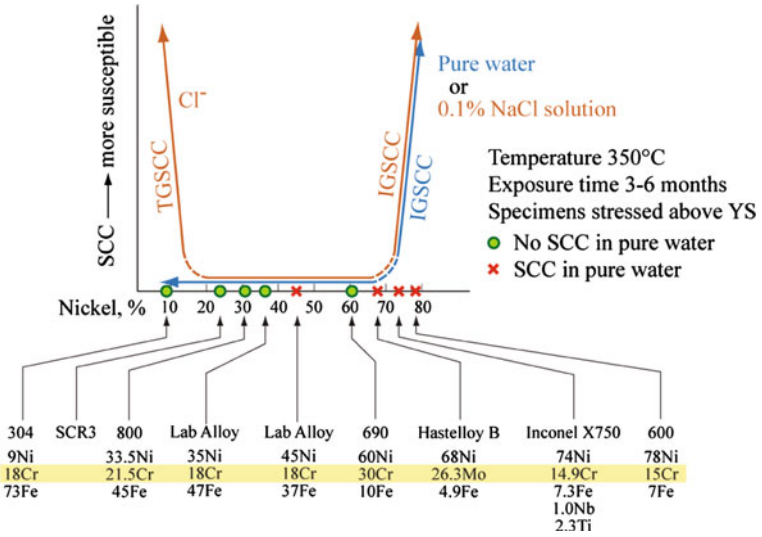

Fig. 15.66 SCC severity of austenitic alloys as a function of nickel content in pure water or 0.1 % sodium chloride solution at high temperature (courtesy of R.W. Staehle [6])

While crack initiation is of great concern, there is a distinct lack of understanding of the mechanism of stress corrosion crack initiation due to the complexity of the process and the difficulty in defining the initiation phase. Further, the distinction between crack initiation and propagation phases is not sharp. Nevertheless, the importance of the crack initiation phase cannot be overstated. Figure 15.68 shows a plot of the cumulative failure fraction of Inconel alloy 600 (Ni–16Cr–9Fe) steam generator tubes in a typical once-through steam generator as a function of effective full power years (EFPY). Note that cracking on the secondary side (freespan IGSCC) in the hot leg does not appear until about 10 years after startup. Yet, by the 13-year mark, this degradation mode grew to dominate all other failure modes in the

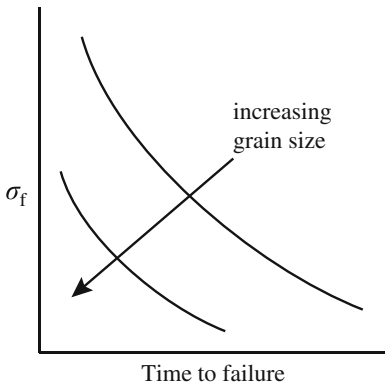

Fig. 15.67 Effect of grain size on the relation between failure stress and time to failure by SCC

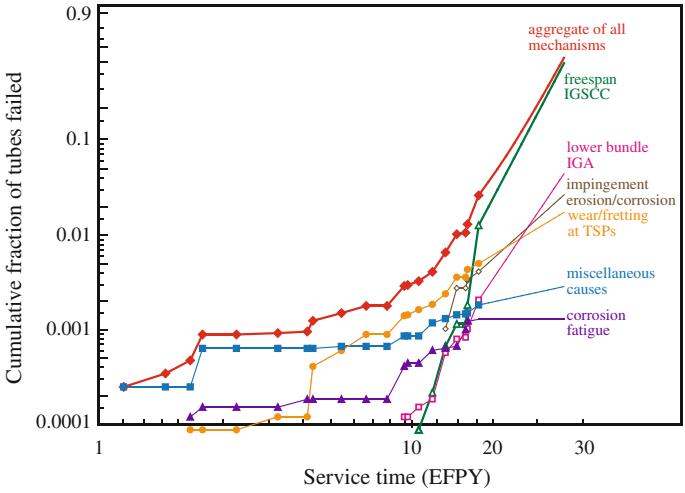

Fig. 15.68 Cumulative fraction of failed steam generator tubes for various modes of degradation of a typical once-through steam generator. Note that freespan IGSCC did not become measurable until about 10 years, and after 13 years, it accounted for more failures than all other modes combined

steam generator combined. In fact, the growth rate was so fast that the decision was made to replace the steam generator within two years after these data were accumulated. Clearly, in this case, initiation required considerable time, but once it occurred, propagation of the crack proceeded rapidly.

Cracks may initiate at preexisting surface flaws, or corrosion processes may create a surface flaw by pitting or localized corrosion, e.g., grain boundary attack or crevice corrosion. However, the conditions under which a crack will propagate are not necessarily the same. Both thermodynamic requirements and kinetic conditions must be met for a crack to initiate or to grow.

15.7.5 Thermodynamics of SCC

Without oxidation or anodic dissolution, cracks would not advance. The occurrence of simultaneous film formation and oxidation during stress corrosion crack growth can be understood from Fig. 15.69, which shows a crack in which dissolution is

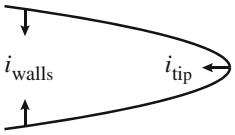

Fig. 15.69 Schematic illustration showing corrosion current from the walls and the tip of a crack

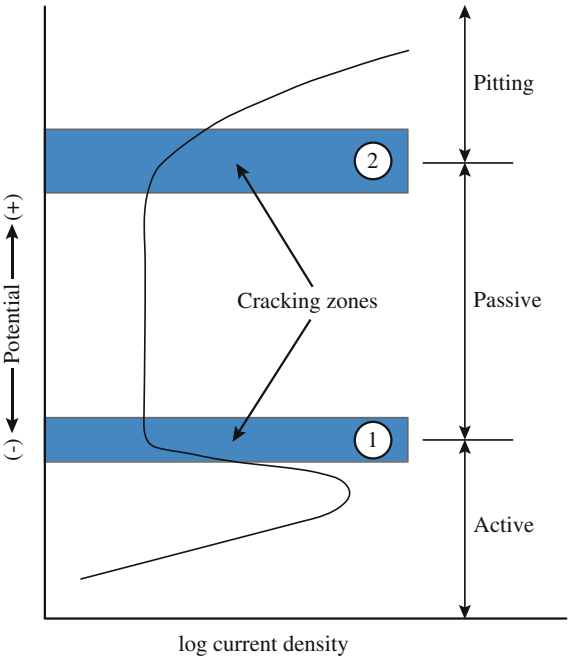

Fig. 15.70 Schematic anodic polarization curve showing the potential ranges over which susceptibility to stress corrosion cracking occurs (after [7])

occurring at both the crack tip and crack walls. The ratio of anodic currents from the walls relative to the crack tip is the critical parameter. The ratio i_{walls}/i_{tip} must be $\ll 1$ for a crack to propagate, otherwise the crack will blunt.

Figure 15.70 shows a polarization curve for an active–passive alloy. Note that there are two zones where SCC is most likely to occur. In zone ①, the alloy is in the active-to-passive film transition so that the simultaneous condition for film formation on crack walls and corrosion at the crack tip are met. In zone ②, similar conditions are met with the added factor that these potentials are above the pitting potential and cracks can initiate from pits. Practically, IGSCC can occur over the entire range between and including zones ① and ② because chemical inhomogeneities at the grain boundary produce a different electrochemical response relative to the bulk material.

An overlay of the regimes in which SCC occurs on the Pourbaix diagram will identify the phases that correlate with cracking. Figure 15.71 shows a Pourbaix diagram for nickel and iron in 300 °C water in which SCC is associated with potentials and pHs that follow the Ni/NiO stability line. The effect of many environmental parameters such as pH, oxygen concentration, and temperature on the thermodynamic conditions for SCC can be related to their effect on the potential–pH diagram. For materials in which SCC occurs by a hydrogen-induced subcritical crack growth mechanism, the thermodynamic requirement for crack growth is governed by the hydrogen reduction line ⓐ. The range of potentials at which H is available to cause crack growth increases and becomes more oxidizing with

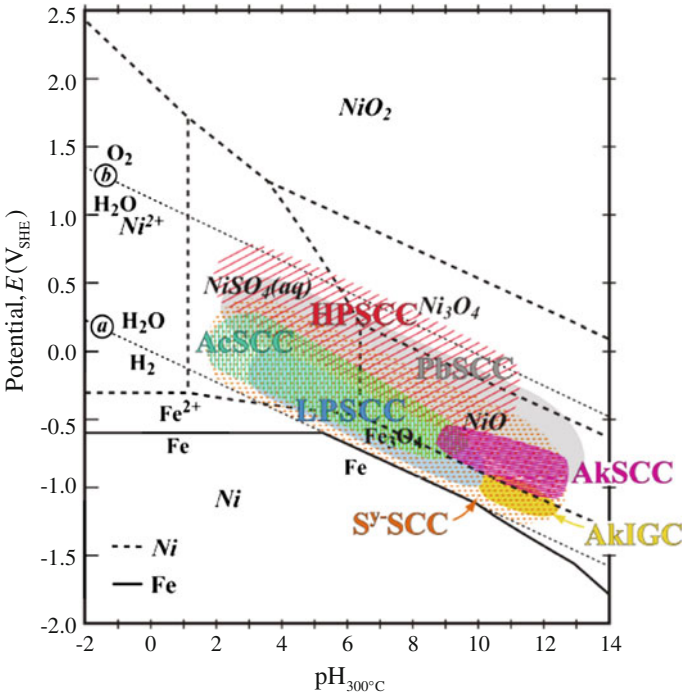

Fig. 15.71 Various SCC submodes as a function of potential and pH plotted over the Ni and Fe stability diagrams at 300 °C. Modes of SCC in Alloy 600 affected by environmental chemistry. Regimes in the figure are as follows: *AcSCC* acidic-induced SCC, *AkSCC* alkaline-induced SCC, *HPSCC* high-potential-induced SCC, *LPSCC* low-potential-induced SCC, *AkIGC* alkaline-induced intergranular corrosion, *PbSCC* lead-induced SCC, and *Sy-SCC* sulfide-induced SCC (from [8])

decreasing pH. However, the potential and pH at the tip of a crack can differ substantially from that at the free surface due to production, reaction, and diffusion of oxygen or metal ions within the crack, as described in Sect. 15.6.

15.7.6 Kinetics of SCC

As with the thermodynamic conditions for SCC, environmental parameters such as potential, pH, oxygen concentration, and temperature along with crack geometry and crack tip chemistry strongly affect crack growth kinetics. For the case of a crack growing by anodic dissolution alone, the total crack advance is a function of the total anodic charge transfer (integral of current over time) at the crack tip, and therefore, the crack velocity is a function of the average crack tip current density. A limiting velocity can be described for a crack advancing under pure anodic dissolution by the following Faradaic relationship:

$$\dot{a} = \frac{\mathrm{da}}{\mathrm{d}t} = \frac{i_{\mathrm{a}} M}{nF\rho}, \tag{15.65}$$

where i_{a} is the anodic current density of a bare surface, M is the atomic weight, n is the valence, F is Faraday's constant, and ρ is the density. Equation (15.65) assumes that the crack tip is maintained in a bare condition, while the crack walls are relatively inactive (to prevent blunting). A number of factors can reduce crack velocity, principle among them is the formation of a film which covers the crack tip. Other factors that can limit crack velocity are as follows:

- Limits on diffusion of species into or out of the crack;
- Crack growth away from the principal stress;
- Changes in local alloy chemistry; and
- Corrosion of the crack walls.

A model for crack propagation based on crack tip dissolution will be presented in Sect. 15.7.8.

15.7.7 Mechanisms of Stress Corrosion Cracking

By virtue of its nature, stress corrosion cracking refers to a chemical or electrochemical process involving oxidation and reduction reactions where the thermodynamic tendency is described by the Nernst equation. Under certain conditions, these reactions can manifest themselves in the form of a stress corrosion crack. The mechanisms by which these cracks form and propagate are not completely agreed upon. The leading theories are active path SCC and the film rupture model.

Active Path SCC

Active path SCC was first proposed in the 1940s to explain rapid grain boundary attack and is based on the establishment of galvanic cells between the base metal and anodic paths set up by heterogeneous phases (or segregated elements) along grain boundaries or slip planes. Active path SCC also refers to preferential dissolution of a phase in the alloy. The applied stress ruptures oxide films and exposes fresh metal to dissolution. The idea behind this theory is that preferred dissolution occurs at slip planes due to the increased number of preferred sites. Plastic deformation is essentially "feeding" bare material to the electrolyte for consumption with the net effect being an increase in the exchange current density and hence the rate of corrosion. Active path SCC should follow a time-to-failure dependence on current described by the plot in Fig. 15.72. However, electrochemical dissolution at a crack tip will tend to blunt the crack rather than contribute to its advance. So active path SCC is not a plausible explanation for observed stress corrosion cracks.

It should be noted, however, that active path corrosion can contribute to intergranular separation. The intergranular fracture of Ni–Cr–Fe alloys in sodium

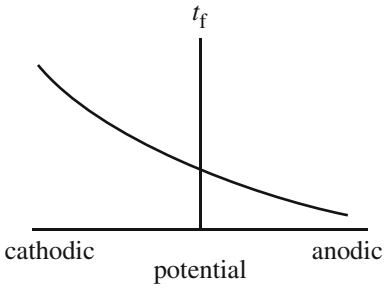

Fig. 15.72 Behavior of time-to-failure for an active path stress corrosion cracking mechanism

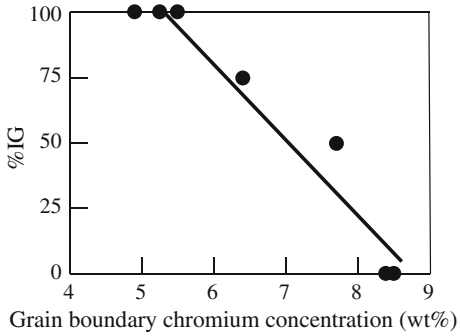

Fig. 15.73 Percent IG fracture versus grain boundary chromium concentration for Ni–16Cr–9Fe stressed in 0.017 M $Na_2S_4O_6$ at 25 °C (after [9])

tetrathionate, $Na_2S_4O_6$ (pH ~ 3–4), depends strongly on the grain boundary chromium level (Fig. 15.73). Cracking is believed to occur by stress-assisted intergranular attack in which the role of stress is to open the crack tip for access by the bulk solution, which then causes preferential dissolution along the grain boundary. This is an example of a stress-assisted anodic dissolution-driven process and is not based on film rupture.

Film Rupture Model

The corrosion resistance of most alloys is attributed to the passive film on the surface. When sufficient stress is applied, the film is ruptured or damaged by shear stresses on properly oriented glide planes (Fig. 15.74). But SCC susceptibility depends on the nature of slip. In alloys with high stacking fault energy (SFE), the separation of total dislocations into partials is unlikely. Since partials must recombine in order to cross-slip, high SFE alloys exhibit easy cross-slip, while low SFE alloys do not exhibit cross-slip. As a result, low SFE alloys exhibit planar slip in which the deformation occurs on relatively few slip planes and is characterized by regularly spaced slip bands, not unlike the morphology of dislocation channels discussed in Chap. 12. Figure 15.75 shows the effect of Ni content in austenitic

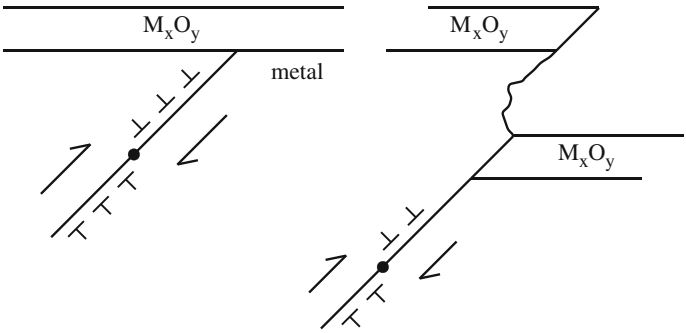

Fig. 15.74 Schematic illustration of the process by which slip can cause rupture of an oxide film, leading to accelerated corrosion before repassivation

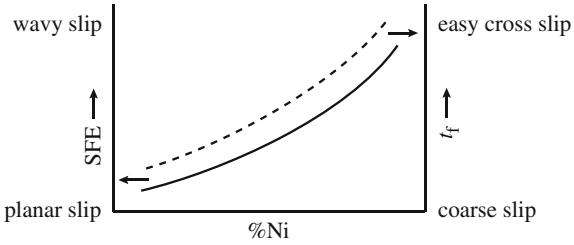

Fig. 15.75 Dependence of stacking fault energy (which determines the slip character) and time to failure on the nickel content in an austenitic, Fe–Cr–Ni alloy

alloys on the SFE and time to failure along with the role of the nature of slip. Low SFE alloys (low Ni content) exhibit coarse or *planar* slip and low time to failure, while high SFE alloys (higher Ni content) can cross-slip exhibiting *wavy* slip and a longer time to failure.

Repassivation of the exposed surface will likely occur, but the rate of repassivation will control the rate of crack propagation. If repassivation occurs too quickly, the corrosion attack causes only a very small increment of crack growth. If repassivation occurs too slowly, corrosion blunts the crack tip. Hence, there is an intermediate rate at which corrosion occurs to maximize growth crack without blunting it. Figure 15.76 shows how the rate of repassivation at a potential, and E_1 can vary with the environment. Chloride ions are effective in slowing repassivation. So while SCC of stainless steels does not occur in sulfuric acid at room temperature, the addition of Cl^- to sulfuric acid induces susceptibility to SCC, presumably by reducing the repassivation rate. In fact, alloy composition can strongly affect repassivation rate as well. Figure 15.77 shows that increasing Cr in a Ni–Cr–Fe alloy substantially increases the repassivation rate, which leads to a reduction in the SCC susceptibility.

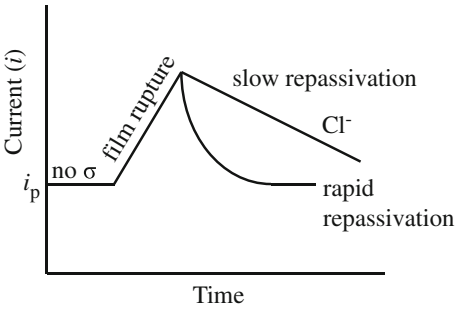

Fig. 15.76 Behavior of the corrosion current in a repassivation test in which an applied stress results in film rupture and repassivation. Aggressive species in the solution can cause slow repassivation, allowing for a greater amount of corrosion

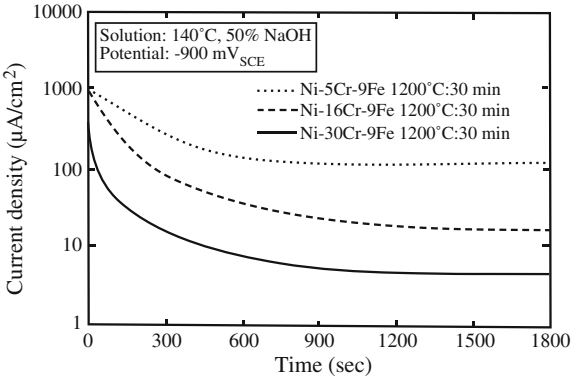

Fig. 15.77 Current decay or repassivation rate of Ni–Cr–Fe alloys as a function of chromium content, showing that repassivation occurs much more quickly with higher alloy chromium contents (after [10])

15.7.8 Predictive Model for Crack Propagation

Structural components manufactured from stainless steels, nickel-base alloys, and ferritic steels are all susceptible to environmentally assisted cracking in light water reactor environments. The phenomenology of cracking in these environments is well-recognized in terms of the effect that various material, stress, and environmental parameters have on the cracking susceptibility. For these systems, Ford and Andresen [11–14] have developed a working hypothesis for the cracking mechanism that is based on the slip oxidation/film rupture model (Fig. 15.64(d)) and the relevant crack tip environment. In this model, crack advance is related to the oxidation reactions that occur at the crack tip as the protective film is ruptured by increasing strain in the underlying matrix. Rupture events occur with a periodicity, t_f, which is determined by the fracture strain of the oxide and the strain rate at the

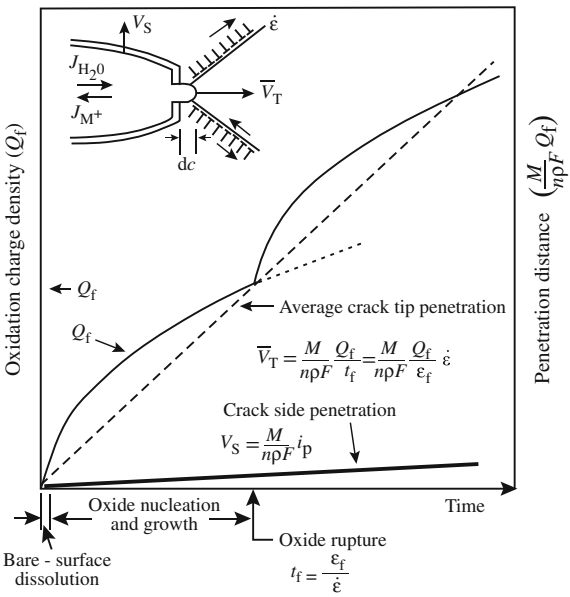

Fig. 15.78 Schematic of the oxidation charge density versus time relationship for a strained crack tip and unstrained crack sides obeying the film rupture model (after [11])

crack tip. The extent of crack advance is related (by Faraday's law) to the oxidation charge density associated with dissolution and oxide growth (passivation) on the bare metal surface, similar to that described by Eq. (15.65):

$$\dot{a} = \frac{M}{nF\rho}\frac{Q_f}{t_f}, \tag{15.66}$$

where

$$t_f = \frac{\varepsilon_f}{\dot{\varepsilon}_{ct}}, \tag{15.67}$$

giving the average crack velocity in terms of the crack tip strain rate:

$$\bar{v}_T = \dot{a} = \frac{M}{nF\rho}\frac{Q_f}{\varepsilon_f}\dot{\varepsilon}_{ct}, \tag{15.68}$$

where Q_f is the charge transfer at fracture, ε_f is the fracture strain, and $\dot{\varepsilon}_{ct}$ is the crack tip strain rate and embodies the mechanical contribution to cracking. The oxidation charge density and crack penetration rate are shown as a function of time in the schematic diagram of Fig. 15.78. Note that the oxidation charge density varies in a parabolic fashion with time according to a solid-state oxidation model [15], and the velocity of crack propagation is an average over time. The reactions at the crack tip vary with time in a complex manner for different environments and material

chemistries, and the resultant average crack growth rate, $\bar{v}_T$, is restated in a general form:

$$\bar{v}_T = \frac{M}{nF\rho}\frac{i_a t_0^m}{(1-m)\varepsilon_f^m}\dot{\varepsilon}_{ct} \tag{15.69}$$

$$= f(m)\dot{\varepsilon}_{ct}^m, \tag{15.70}$$

where i_a is the bare surface dissolution current, and t_0 and m are repassivation parameters that represent the effects of the environment and material chemistries on environmentally assisted crack growth.

The model is composed of three primary conceptual and predictive elements: (1) the rate of film rupture (proportional to the crack tip strain rate), (2) the solution chemistry at the crack tip, and (3) the resultant kinetics of oxidation/repassivation in the crack tip environment following a film rupture event. Most of the parameters that comprise the water and material chemistry effects distill into a single parameter, m, that represents the slope of the repassivation current on a log–log plot. The crack tip strain rate formulations then permit the calculation of the frequency of film rupture *events* and in turn the prediction of the environmental crack growth rate over a continuum of loading, water, and material characteristics. For example, the function, *f,* in Eq. (15.70) may be of the form, $f(m) \sim Am^{3.6}$, where m is a function of water chemistry and material chemistry and is an indicator of the level of susceptibility, where $m \rightarrow 0.3$ for high susceptibility and $m \rightarrow 1$ for low susceptibility. The crack tip strain rate is a function of the stress intensity of the crack tip and may be expressed in the form $\dot{\varepsilon}_{ct} = BK^4$. So the crack growth rate is then as follows:

$$\bar{v}_T = Am^{3.6}(BK^4)^m \tag{15.71}$$

15.7.9 Mechanical Fracture Models

Cracks occur as a result of corrosion reactions, but when their behavior is driven by the stress rather than corrosion reactions, they are considered to fail by mechanical fracture. Several models exist to explain cracking by mechanical fracture processes.

Under certain conditions, a fine array of corrosion-induced tunnels are observed at the point where slip steps emerge on the sample surface. The tunnels grow in diameter and length until stress in the remaining ligaments rises to the point where the load can no longer be sustained with the reduced cross section and fracture occurs by overload. According to the *corrosion tunnel model*, cracks propagate by alternate tunnel growth and ductile fracture. Cracks propagating by this mechanism should result in grooved fracture surfaces with evidence of microvoid coalescence. That this morphology is generally not observed suggests that the application of a

tensile stress results in thin, flat slots instead of tunnels. This morphology is very consistent with transgranular SCC fracture morphology.

Based on fractographic studies, it was concluded that cleavage fracture is not an atomically brittle process, but occurs by alternate slip at the crack tip in conjunction with formation of very small voids ahead of the crack. It was also proposed that chemisorption of environmental species facilitated the nucleation of dislocations at the crack tip, promoting shear processes responsible for brittle cleavage-like fracture. The *adsorption-enhanced plasticity* mechanism relies on adsorption of aggressive species to promote cleavage fracture.

In the *tarnish rupture* model, a brittle surface forms on the metal and fractures under an applied stress. Fracture exposes bare metal, which rapidly reacts with the environment to reform the film. The crack propagates by successive cycles of film growth and fracture. Assuming that the film penetrates along the grain boundary ahead of the crack tip, the model has been applied to intergranular cracking. The key feature of this mechanism is that fracture occurs entirely within the oxide film and not in the metal.

The *film-induced cleavage* mechanism (Fig. 15.64(e)) holds that a thin surface film or layer forms on the surface, followed by the formation of a brittle crack in the layer. The crack crosses the film–matrix interface without loss of velocity and continues to propagate in the ductile matrix along a particular crystallographic direction. The crack eventually blunts and arrests, and the cycle then repeats. This model can also explain crack arrest markings, cleavage-like facets on the fracture surface, and the discontinuous nature of crack propagation. The assumption that a brittle crack continues to propagate in a ductile matrix can be justified if the crack is sharp and propagates at high velocities.

First proposed by Uhlig, the *adsorption*(*stress-sorption*) mechanism (Fig. 15.64(b)) is related to the Griffith criterion for crack formation in glass and other brittle solids. It holds that adsorption of a species of any kind that reduces surface energy should favor crack formation. Recalling the expression for fracture stress, σ_f, from Chap. 14:

$$\sigma_f = \left(\frac{2E\gamma}{\pi c}\right)^{1/2}, \tag{15.72}$$

where E is Young's modulus, γ is the surface energy, and 2c is the crack length, then a reduction in the surface energy, e.g., as might occur by adsorption of Cl^- on a stainless steel surface, results in a lowering in the stress required for fracture. Unfortunately, the plausibility of this model is hard to establish because of the difficulty of determining the energy in the environment.

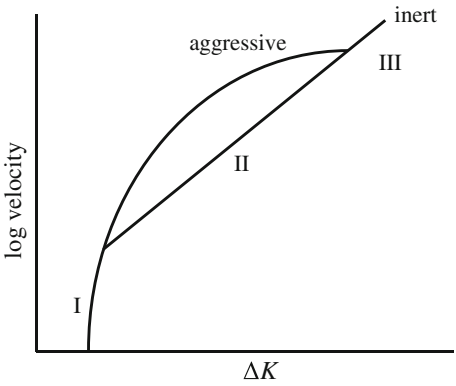

Fig. 15.79 Effect of an aggressive environment on the behavior of crack velocity with ΔK in a corrosion fatigue test

15.7.10 Corrosion Fatigue

Damage by corrosion fatigue is a conjoint action of corrosion and fatigue that is greater than that caused by the sum of both processes acting separately. In air, fatigue proceeds by localized slip within grains of the metal caused by alternating stress, resulting in slip steps at the metal surface. Adsorption of air on the exposed metal surfaces prevents rewelding on the reverse cycle (slip irreversibility). Continued application of stress produces protrusions above the metal surface (extrusions) and intrusions below. Corrosion accelerates plastic deformation by the formation of surface lattice vacancies, in particular, divacancies that rapidly diffuse into the metal at room temperature and accelerate plastic deformation by facilitating dislocation climb. The higher the rate of corrosion, the greater is the availability of divacancies, and the more pronounced is the formation of intrusions and extrusions. Lower frequencies produce greater degradation since more time is available per cycle for corrosion to occur. Figure 15.79 shows that the effect of the environment is greatest at intermediate values of ΔK.

15.7.11 Hydrogen Embrittlement

Hydrogen embrittlement is caused by the entry of hydrogen into the alloy by the corrosion process, cathodic protection, or high hydrogen overpressures. A common characteristic of hydrogen cracking is a specific delay in time for appearance of cracks after stress is applied. This is due to the time required for hydrogen to diffuse to a specific area near a crack nucleus and reach a critical concentration. Hydrogen embrittlement usually results in intergranular fracture and tends to be greatest at low strain rates.

There are several mechanisms by which hydrogen is believed to cause embrittlement. The *decohesion mechanism* (Fig. 15.64(a)) holds that atomic hydrogen

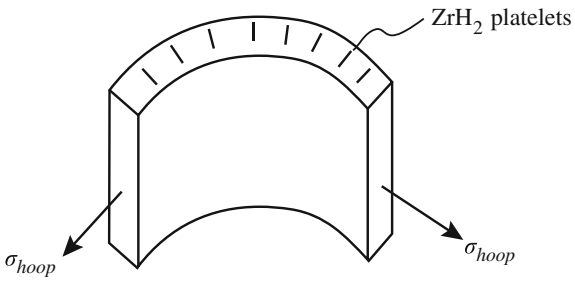

Fig. 15.80 Orientation of ZrH_2 platelets in Zircaloy fuel cladding under the application of a hoop stress

lowers or reduces the metal–metal bond strength. The *pressure theory* is based on precipitation of hydrogen as a gas at internal defects. The pressure developed by precipitation is added to the applied stress to lower the apparent fracture stress. Blisters can form if the process occurs close enough to the surface to deform the thin layer of metal above it.

A variation of the pressure theory is the *hydrogen attack* mechanism, which is due to the reaction between hydrogen and carbon to form methane. In addition to the formation of high-pressure methane gas bubbles, the reaction causes de-carburization and a weakening of the metal. Uhlig proposed that *direct adsorption* of hydrogen reduces the surface energy required to form a crack, thus lowering the fracture stress. The formation of a brittle *hydride* phase, e.g., ZrH_2 or TiH_2, can also induce embrittlement of the metal. The specific volume of the hydride is greater than the metal from which it came. Combined with the plate-like morphology of the hydride, the metal at the edge of the hydride platelet experiences a high tensile stress if the applied stress is perpendicular to the plane of the platelet. In zirconium alloys, platelets form on basal planes that are aligned in the radial direction of fuel cladding, causing a high tensile stress in the metal at the edges of the platelet due to the pressure in the cladding (Fig. 15.80). Hydrogen also interacts with dislocations. A high hydrogen fugacity at the metal surface and along grain boundaries can induce plasticity by activation of dislocation sources. The chemical driving force is responsible for the formation of dislocations, which then spread additional hydrogen into the lattice and exert a large stress intensity factor at the crack tip. This *hydrogen-induced localized plasticity* (HELP) mechanism (Fig. 15.64(f)) can explain high-temperature effects of hydrogen. Hydrogen-induced cracking is an important mechanism in ferritic steels, nickel-base alloys, and titanium and aluminum alloys.

Nomenclature

A	Atomic mass, or electron acceptor, or area
a_k	Activity of substance k
$\dot{a}$	Crack growth rate
$\mathrm{d}a/\mathrm{d}n$	Crack growth per cycle
$\mathrm{d}a/\mathrm{d}t$	Crack growth rate
c	Crack length
C_k	Concentration of substance k
D	Electron donor
i_{corr}	Corrosion current
$i_{0,\mathrm{a,c}}$	Current: exchange, anodic, cathodic
E	Electrode potential
E^e	Equilibrium electrode potential
E^0	Standard equilibrium electrode potential (at STP)
E_{corr}	Corrosion potential
E_{x}	Galvani or electrochemical potential in the phase x
F	Faraday's constant, 96,500 Coulombs/charge
G	Gibbs energy of the system
ΔG	Free energy change for a reaction
I	Current
i	Current density
K	Stress intensity
ΔK	Stress intensity range
K_{Ic}	Mode I fracture toughness
K_{th} or K_{SCC}	Threshold stress intensity for SCC
L	Path length through which a current is passed
m	Repassivation parameter
M	Atomic mass
n	Charge transfer, or number of equivalents exchanged in oxidation/reduction reaction
Q_{f}	Charge transfer at fracture
R	Gas constant or resistance
t	Time
T	Temperature
t_0	Repassivation parameter
$\bar{v}_{\mathrm{T}}$	Average crack velocity
B	Symmetry factor in expression for corrosion current
ε_{f}	Fracture strain
$\dot{\varepsilon}_{\mathrm{ct}}$	Crack tip strain rate
γ	Surface energy, or activity coefficient
h	Overpotential
μ_k^0	Standard chemical potential of species k
$(\mu_k)_x$	Electrochemical potential for the kth particle type in phase x
$(\tilde{\mu}_k)_x$	Electrochemical potential for the kth particle type in phase x

ν_i	Stoichiometric coefficients for substance i in a corrosion reaction
ρ	Density, or solution resistance
σ_f	Fracture stress
σ_{th} or σ_{SCC}	Threshold stress for SCC

Subscripts

A	Anodic
c	Chemical driving force
crit	Critical (refers to current density)
C	Cathodic
e	Reaction under an electric field
fail	Fail (refers to current density)
F	Flade
g	Gas
init	Initiation (refers to current density)
k	Substance
l	Liquid
L	Limiting
m	Metal
p, prod	Product
pp	Primary passive (refers to potential)
prop	Crack propagation (refers to current density)
r, react	Reactant, or reduction reaction designation
R	Resistance
s	Solution
tip	Tip (refers to current density)
trans	Transpassive (refers to potential)
walls	Walls (refers to current density)
x	Phase or oxidation reaction designation

Superscripts

e	Equilibrium condition
r	Reduction
x	Oxidation
0	Standard condition

Acronyms

AGR	Advanced gas reactor
AcSCC	Acidic-induced SCC
AkICG	Alkaline-induced intergranular corrosion
AkSCC	Alkaline-induced SCC

BWR	Boiling water reactor
CT	Compact tension
CERT	Constant extension rate test
DCB	Double cantilever beam
EFPY	Effective full power years
EMF	Electromotive force
ESEP	Equilibrium standard electrode potential
HPSCC	High-potential-induced SCC
HWC	Hydrogen water chemistry
IASCC	Irradiation-assisted stress corrosion cracking
IG	Intergranular
IGSCC	Intergranular stress corrosion cracking
LET	Linear energy transfer
LPSCC	Low-potential-induced SCC
LWR	Light water reactor
MSEP	Measured single electrode potential
NWC	Normal water chemistry
PbSCC	Lead-induced SCC
PWR	Pressurized water reactor
RH	Radiation hardening
RIS	Radiation-induced segregation
SCC	Stress corrosion cracking
SFE	Stacking fault energy
SHE	Standard hydrogen electrode
SGHWR	Steam-generating heavy water reactor
SSEP	Standard single electrode potential
SSRT	Slow strain rate test
STP	Standard temperature and pressure
SySCC	Sulfide-induced SCC
TG	Transgranular
TGSCC	Transgranular stress corrosion cracking

Problems

15.1 (a) Iron in an NaCl solution, pH = 1, shows a potential of +0.2 V_{SHE}. What are the possible anodic and cathodic reactions, assuming that the Pourbaix diagram in Fig. 15.7 applies.

(b) It was suggested that two possible reactions are as follows:

$$Cl_2 + 2e^- = 2Cl^-$$
$$Na = Na^+ + e^-$$

Do you agree with either or both? If so, what assumptions must you make?

15.2 Determine the equations describing the lines ① through ⑨ of the Pourbaix diagram for Ni given below and the following information.

$\mu^0_{NiO} = -51{,}610$ cal/mole
$\mu^0_{Ni_3O_4} = -170{,}150$ cal/mole
$\mu^0_{Ni_2O_3} = -112{,}270$ cal/mole
$\mu^0_{NiO_2} = -51{,}420$ cal/mole

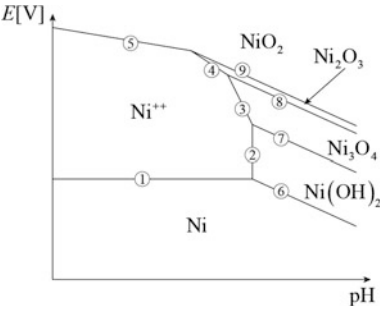

15.3 A zinc specimen exposed to an acid solution loses 25 mg during a 12 h exposure.

(a) What is the equivalent current flowing due to corrosion?
(b) If the specimen area is 200 cm^2, what is the corrosion rate in $mg/dm^2/d$ due to this current?
(c) What is the corrosion rate in mpy? μm/year?

15.4 Using appropriate polarization diagrams, determine the effect of the following parameters on the corrosion potential and corrosion rate of a metal, M, corroding to dissolved M^+ in an acid solution:

(a) Increasing i_0 of the anodic reaction;
(b) Increasing i_0 of the cathodic reaction;
(c) Increasing the concentration of dissolved H^+; and
(d) Increasing the Tafel constant of the anodic reaction.

15.5 (a) Plot the appropriate polarization curves for the following half-cell reactions and determine the corrosion potential and corrosion rate (current density) assuming activation control of both the anodic and cathodic processes. Determine the corrosion potential and corrosion rate from your plot.

$$M = M^+ + e^-, \quad E = -0.7\ V, \quad i_0 = 10^{-8}\ A/cm^2, \quad \beta_A = +0.1\ V$$
$$2H^+ + 2\ e^- = H_2, \quad E = +0.1\ V, \quad i_0 = 10^{-6}\ A/cm^2 \quad \beta_C = -0.1\ V$$

(b) Same as (a), but assume that the limiting current density for the reduction reaction is 10^{-5} A/cm^2. Again, determine the corrosion potential and corrosion rate from your plot.

15.6 Plot the following cathodic polarization data for carbon steel in 0.5 N H_2SO_4 on linear coordinates and determine the polarization resistance. From the shape of the plot, would you estimate that the absolute value of β_A is greater than or less than β_C?

Current density (μA/cm^2)	40	100	160	240	300
Cathodic overvoltage (mV)	1.0	2.5	4.1	6.3	9.0

15.7 With the following anodic and cathodic polarization data—the same conditions as Problem 15.6, but larger currents—plot the polarization curves on semilog coordinates and determine β_A, β_C, E_{corr}, and i_{corr}.

Current density, μA anodic or cathodic	Potential anode, mV_{SHE}	Potential cathode, mV_{SHE}
1.01×10^{-4}	−266	−276
2×10^{-4}	−264	−278
3×10^{-4}	−259	−286
5×10^{-4}	−255	−296
7×10^{-4}	−250	−305
1×10^{-3}	−246	−318
2×10^{-3}	−233	−341
3×10^{-3}	−226	−358
5×10^{-3}	−214	−383
7×10^{-3}	−204	−400
1×10^{-2}	−193	−416
2×10^{-2}	−176	−444

15.8 Plot schematically the polarization curve for anodic dissolution for the metal M that has the following electrochemical parameters:
$E_{corr} = -0.500\,V_{SCE}$, $i_{corr} = 10^{-4}\,A/cm^2$, $E_{pp} = 0.400\,V_{SCE}$,
$\beta_a = +0.05\,V, i_{pass} = 10^{-5}\,A/cm^2, E_{tr} = 1.000\,V.$
From the plot, determine the critical current density for passivation, i_{crit}

15.9 For the case shown in Fig. 15.43 (borderline passivity), draw the potentiostatic polarization curve ascending to higher (more noble) potentials from the corrosion potential. Carefully note changes in direction of current from anodic to cathodic.

15.10 Given active–passive alloys A and B having the following electrochemical parameters:

	E_{corr}, V	I_{corr}, A	β_a, V	E_{pp}, V	i_{pass}, A	E_{tr}, V
Alloy A	−0.400	1×10^{-6}	+0.1	0.0	1×10^{-5}	+0.7
Alloy B	−0.200	7×10^{-7}	+0.1	+0.3	1×10^{-6}	+1.2

(a) Which will be the more corrosion resistant in reducing condition (active state)? Why?
(b) Which will be the more corrosion resistant in the passive state? Why?
(c) Which is more easily passivated by dissolved oxidizers? Why?
(d) Which is more corrosion resistant in strongly oxidizing solutions? Why?
(e) Which would be more easily protected by anodic protection? Why?

15.11 Consider a 304 stainless steel pipe put into service in a boiling water reactor in 1983. The BWR used NWC (ECP = + 150 mV_{SHE}, conductivity = 0.1 μS/cm) for the first 16 years of service and then switched to HWC (ECP = −220 mV_{SHE}, conductivity = 0.1 μS/cm). The pipe was exposed to the standard water chemistry and was 6″ ID and 2″ wall thickness. The pipe experienced a constant stress and no fatigue loading (i.e., it is well supported). In 1991, a small crack was identified in the pipe during routine inspection. Given the water chemistry history of this reactor, should you expect water on the floor of this BWR?

15.12 Discuss the relative advantages and disadvantages of constant load, constant deflection, and CERT tests for assessing:

(a) The relative susceptibility of a variety of alloys to stress corrosion cracking
(b) The susceptibility of one alloy to stress corrosion cracking in several environments; and
(c) The stress and strain dependence of stress corrosion cracking.

15.13 (a) Calculate the minimum specimen width necessary for a valid fracture mechanics test of a steel of yield strength 700 MPa and fracture toughness of 170 $MPa\sqrt{m}$.
(b) Would it be practical to measure the fracture toughness of this sample?
(c) If a corrosive environment makes hydrogen embrittlement possible with K_{Ihic} of 23 $MPa\sqrt{m}$, what is the minimum specimen thickness?
(d) Would it be practical to measure the fracture toughness of this sample?

15.14 Plot the crack growth rate of an alloy over the range $10 \leq K \leq 60\,MPa\sqrt{m}$, for a crack tip strain rate given by BK^4, where B is 2×10^{-22} $MPa^{-1/4}$ $m^{-1/8}$ and A = 10 m/s for values of m = 0.1, 0.5, and 1.0.

References

1. Pourbaix M (1974) Atlas of electrochemical equilibria in aqueous solutions. NACE, Houston, TX
2. Jones DA (1996) Principles and prevention of corrosion, 2nd edn. Prentice-Hall, Upper Saddle River
3. Fontana MG (1986) Corrosion engineering, 3rd edn. McGraw-Hill, New York
4. Uhlig HH, Reive RW (2008) Corrosion and Corrosion Control: an introduction to corrosion science and engineering. Wiley-Interscience, Hoboken
5. Jones RH, Ricker RE (1992) Mechanisms of stress corrosion cracking. In: Jones RH (ed) Stress-corrosion cracking materials performance and evaluation. ASM International, Metals Park
6. Staehle RW, Personal communication
7. Staehle RW (1977) In: Staehle RW (ed) Stress Corrosion and Hydrogen Embrittlement of Iron Base Alloys, NACE-5. NACE, Houston, p 193
8. Staehle RW, Gorman JA (2002) In: Proceedings of the 10th international conference on environmental degradation of materials in nuclear power systems: water reactors. NACE International, Houston, TX, bonus paper
9. Was GS, Rajan VB (1987) Metal Trans A 18A:1313–1323
10. Sung JK, Koch J, Angeliu T, Was GS (1992) Metal Trans A 23A:2804–2887
11. Ford FP, Andresen PL, Solomon HD, Gordon GM, Ranganath S, Weinstein D, Pathania R (1990) In: Proceedings of the 4th international symposium on environmental degradation of materials in nuclear power systems: water reactors. NACE, Houston, TX, pp 4–26 to 4–51
12. Ford FP, Andresen PL (1994) Corrosion in nuclear systems: environmentally assisted cracking in light water reactors. In: Marcus P, Oudar J (eds) Corrosion mechanisms. Dekker, New York, pp 501–546
13. Ford FP, Andresen PL (1988) In: Theus GJ, Weeks JR (eds) Proceedings of the 3rd international symposium on environmental degradation of materials in nuclear power systems: water reactors. The Metallurgical Society of AIME, Warrendale, p 789
14. Andresen PL, Ford FP (1988) Mat Sci Eng vol A 1103:167
15. Wagner C (1959) Z Electrochem 63:772–782